INVESTIGATION OF THE ATMOSPHERIC OZONE FORMATION POTENTIAL OF ACETYLENE

Final Report to
Carbide Graphite Corporation

by
William P. L. Carter, Dongmin Luo, and Irina L. Malkina

August 29, 1997

College of Engineering
Center for Environmental Research and Technology
University of California
Riverside, California 92521

97-AP-RT8D-001-FR

ABSTRACT

Environmental chamber experiments and computer model calculations were carried out to assess the atmospheric ozone formation potential of acetylene. The experiments consisted of irradiations, using a xenon arc light source simulating ground-level sunlight, of acetylene - NO_x - air mixtures and simulated photochemical smog mixtures with and without added acetylene. The latter employed two different reactive organic gas surrogate mixtures to represent other organic pollutants in the atmosphere, and used different surrogate/NO_x levels. Acetylene was found to enhance both ozone formation and OH radical levels to a much greater extent than predicted by the previously assumed atmospheric reaction mechanism for acetylene. The data could be satisfactorily simulated by model calculations only it was assumed that the photolysis of glyoxal, acetylene's major photooxidation product, involved significantly more radical formation than previously assumed, that the overall glyoxal photodecomposition quantum yield in simulates sunlight is almost a factor of 2 higher than previously reported, and that most of the glyoxal formation in the OH + acetylene reaction comes from the decomposition of the OH + acetylene + O_2 adduct to glyoxal + OH radicals.

The modified acetylene and glyoxal mechanisms were then used to estimate ozone impacts of acetylene in one-day box model simulations of a variety of urban ozone pollution episodes. It was found that acetylene caused ~20-25% as much ozone formation on a per gram basis as the sum of all measured VOCs in urban atmospheres, and that acetylene caused somewhere between 25% to three times more ozone formation than an equal mass of ethane, the compound the EPA has been using as the standard to determine VOC exemption. The impact of acetylene relative to ethane tending to be highest in the higher NO_x scenarios representing maximum incremental reactivity (MIR) conditions, while the impact of acetylene relative to the total of all emissions tending to be much less variable. It is concluded that while acetylene has a much lower ozone impact than average, its ozone impact should be considered to be somewhat higher than that of ethane.

ACKNOWLEDGEMENTS

The authors gratefully acknowledge Dr. Roger Atkinson for helpful discussions, Mr. Dennis Fitz for assistance in administering this program, and Carbide Graphite Corporation for funding this project and for assistance with the acetylene preparation method. Although this work was funded by Carbide Graphite Co, the opinions and conclusions expressed in this report are entirely those of the primary author, Dr. William P. L. Carter. Mention of trade names or commercial products do not constitute endorsement or recommendation for use.

TABLE OF CONTENTS

Section	Page
LIST OF TABLES	v
LIST OF FIGURES	v
INTRODUCTION	1
EXPERIMENTAL AND DATA ANALYSIS METHODS	3
Overall Experimental Approach	3
Environmental Chamber	4
Experimental Procedures	5
Analytical Methods	6
Characterization Methods	7
Reactivity Data Analysis Methods	8
CHEMICAL MECHANISMS AND MODELING METHODS	10
Chemical Mechanism	10
General Atmospheric Photooxidation Mechanism	10
Atmospheric Reactions of Acetylene	11
Atmospheric Reactions of Glyoxal	13
Alternative Mechanisms Used for Acetylene Modeling	15
Modeling Methods	16
Environmental Chamber Simulations	16
Atmospheric Reactivity Simulations	17
RESULTS AND DISCUSSION	18
Summary of Experiments	18
Results of The Reactivity Experiments and Mechanism Evaluations	18
ATMOSPHERIC REACTIVITY CALCULATIONS	29
Scenarios Used for Reactivity Assessment	29
Base Case Scenarios	30
Adjusted NO_x scenarios	32
NO_x Conditions in the Base Case Scenarios	32
Incremental and Relative Reactivities	33
Reactivity Scales	34
Calculated Relative Reactivities of Acetylene	35
CONCLUSIONS	37
REFERENCES	39
APPENDIX A. LISTING OF THE CHEMICAL MECHANISM	A-1

LIST OF TABLES

Number page

1. Chronological listing of all the chamber experiments carried out for this program. 19
2. Summary of conditions and selected results of the incremental reactivity experiments. . . . 21
3. Summary of conditions of base case scenarios used for atmospheric reactivity assessment. 31
4. Summary of calculated relative incremental reactivities (gram basis) for acetylene, ethane, and the total of all emitted VOCs. 36

A-1. List of species in the chemical mechanism used in the model simulations for this study. A-1

A-2. List of reactions in the chemical mechanism used in the model simulations for this study. A-4

A-3. Absorption cross sections and quantum yields for photolysis reactions. A-10

A-4. Values of chamber-dependent parameters used in the model simulations of the environmental chamber experiments for this study. A-15

LIST OF FIGURES

Number page

1. Absorption cross sections and quantum yields for radical formation for glyoxal as a function of wavelength, and relative spectral distributions of sunlight and the light source used in the environmental chamber experiments. 14
2. Experimental and calculated concentration-time plots for selected species in the acetylene - NO_x experiment. 22
3. Plots of selected results of the mini-surrogate + acetylene experiment CTC-184. 23
4. Plots of selected results of the mini-surrogate + acetylene experiment CTC-185. 23
5. Plots of selected results of the mini-surrogate + acetylene experiment CTC-185. 24
6. Plots of selected results of the full surrogate + acetylene experiment CTC-186. 25
7. Plots of selected results of the full surrogate + acetylene experiment CTC-193. 25
8. Plots of selected results of the low NO_x full surrogate + acetylene experiment CTC-187. 26
9. Plots of selected results of the low NO_x full surrogate + acetylene experiment CTC-194. 26

INTRODUCTION

Ozone in photochemical smog is formed from the gas-phase reactions of volatile organic compounds (VOCs) and oxides of nitrogen (NO_x) in sunlight. Although Los Angeles has the worst ozone problem in the United States, other areas of the country also have episodes where ozone exceeds the federal air quality standard of 0.12 ppm. Ozone control strategies in the past have focused primarily on VOC controls, though the importance of NO_x control has become recognized in recent years. VOC and NO_x controls have differing effects on ozone formation. NO_x is required for ozone formation, and if the levels of NO_x are low compared to the levels of reactive VOCs, then changing VOC emissions will have relatively little effect on ozone. Since NO_x is removed from the atmosphere more rapidly than VOCs, ozone in areas far downwind from the primary sources tend to be more NO_x limited, and thus less responsive to VOC controls. VOC controls tend to reduce the rate that O_3 is formed when NO_x is present, so VOC controls are the most beneficial in reducing O_3 in the urban source areas, where NO_x is relatively plentiful, and where O_3 yields are determined primarily by how rapidly it is being formed. Because of this, any comprehensive ozone control strategy must involve reduction of emissions of both NO_x and VOCs.

Many different types of VOC compounds are emitted into the atmosphere, each reacting at different rates and having different mechanisms for their reactions. Because of this, they can differ significantly in their effects on ozone formation, or their "reactivity". Some compounds, such as CFCs, do not react in the lower atmosphere at all, and thus make no contribution to ground-level ozone formation. Others, such as methane, react and contribute to ozone formation, but react so slowly that their practical effect on ozone formation is negligible. Obviously, it does not make sense to regulate such compounds as ozone precursors. In recognition of this, the EPA has exempted certain compounds from such regulations on the basis of having "negligible" effects on ozone formation. Although the EPA has no formal policy on what constitutes "negligible" reactivity, in practice it has used the ozone formation potential of ethane as the standard in this regard. This is because ethane is the most reactive of the compounds that the EPA has exempted to date. Therefore, the ozone formation potential of a compound relative to ethane is of particular interest when assessing whether it might be a likely candidate for exemption from regulation as an ozone precursor.

Acetylene is a gaseous compound whose use in a number of processes may results in its being emitted into the atmosphere, where it might contribute to ozone formation. However, it reacts relatively slowly (Atkinson, 1989; Atkinson et al. 1992, 1997), suggesting that it might be of sufficiently low reactivity to qualify for VOC exemption under the EPA's present standards. Carter (1994a) calculated that the ozone impact of acetylene is approximately 2-3 times greater than that of ethane on a per-gram basis, which would disqualify it under this standard. However, the mechanism assumed by Carter (1994a)

has significant uncertainties and its ability to correctly predict acetylene's ozone impact had not been adequately evaluated, so this prediction may well be incorrect. To assess this, Carbide Graphite Corporation contracted the College of Engineering Center for Environmental Research and Technology (CE-CERT) to carry out the environmental chamber experiments to needed to provide an experimental basis to support the chemical mechanism used to calculate acetylene's atmospheric ozone impacts. The results of this program are documented in this report.

EXPERIMENTAL AND DATA ANALYSIS METHODS

Overall Experimental Approach

Most of the environmental chamber experiments for this program consisted of measurements of "incremental reactivities" of acetylene under various conditions. These involve two types of irradiations of model photochemical smog mixtures. The first is a "base case" experiment where a mixture of reactive organic gases (ROGs) representing those present in polluted atmospheres (the "ROG surrogate") is irradiated in the presence of oxides of nitrogen (NO_x) in air. The second is the "test" experiment which consists of repeating the base case irradiation except that the VOC whose reactivity is being assessed is added. The differences between the results of these experiments provide a measure of the atmospheric impact of the test compound, and the difference relative to the amount added is a measure of its reactivity.

To provide data concerning the reactivities of the test compound under varying atmospheric conditions, three types of base case experiments were carried out:

1. Mini-Surrogate Experiments. This base case employed a simplified ROG surrogate and relatively low ROG/NO_x ratios. Low ROG/NO_x ratios represent "maximum incremental reactivity" (MIR) conditions, which are most sensitive to VOC effects. This is useful because it provides a sensitive test for the model, and also because it is most important that the model correctly predict a VOC's reactivity under conditions where the atmosphere is most sensitive to the VOCs. The ROG mini-surrogate mixture employed consisted of ethene, n-hexane, and m-xylene. This same surrogate was employed in our previous studies (Carter et al, 1993a,b; 1995a.), and was found to provide a more sensitive test of the mechanism than the more complex surrogates which more closely represent atmospheric conditions (Carter et al, 1995a). This high sensitivity to mechanistic differences makes the mini-surrogate experiments most useful for mechanism evaluation.

2. Full Surrogate Experiments. This base case employed a more complex ROG surrogate under somewhat higher, though still relatively low, ROG/NO_x conditions. While less sensitive to the mechanism employed, experiments with a more representative ROG surrogate are needed to evaluate the mechanism under conditions that more closely resembling the atmosphere. The ROG surrogate employed was the same as the 8-component "lumped molecule" surrogate as employed in our previous study (Carter et al. 1995a), and consists of n-butane, n-octane, ethene, propene, trans-2-butene, toluene, m-xylene, and formaldehyde. Calculations have indicated that use of this 8-component mixture will give essentially the same results in incremental reactivity experiments as actual ambient mixtures (Carter et al. 1995a).

3. Full Surrogate, low NO_x Experiments. This base case employing the same 8-component lumped molecule surrogate as the full surrogate experiments described above, except that lower NO_x levels (higher

ROG/NO_x ratios) were employed to represent NO_x-limited conditions. Such experiments are necessary to assess the ability of the model to properly simulate reactivities under conditions where NO_x is low. The initial ROG and NO_x reactant concentrations were comparable to those employed in our previous studies (Carter et al. 1995a).

Two acetylene - NO_x irradiation experiment was also carried out to evaluate the predictions of the acetylene photooxidation mechanism under chemically simpler conditions. Although this does not represent a realistic simulation of the chemical characteristics of the atmosphere, it can provide a straightforward test for mechanisms for compounds which involve radical initiation processes. Such experiments are only useful for evaluating mechanisms for compounds which involve radical initiating processes, since otherwise the results are dominated by chamber artifacts (Carter and Lurmann, 1990, 1991). Once it was determined that acetylene reactions tended to enhance radical levels, experiments of this type were included as part of this study. Irradiations were conducted with two different concentrations of acetylene and the same concentration of NO_x.

An appropriate set of control and characterization experiments necessary for assuring data quality and characterizing the conditions of the runs for mechanism evaluation were also carried out. These are discussed where relevant in the results or modeling methods sections.

Environmental Chamber

The environmental chamber system employed in this study was the CE-CERT dual-reactor Xenon Arc Teflon Chamber (CTC). This consists of two 4' x 4' x 8' FEP Teflon reaction bags located adjacent to each other at one end of an 8' x 12' room with reflective aluminum paneling on all surfaces. The two reactors are referred to as the two "sides" of the chamber (Side A and Side B) in the subsequent discussion. Four 6.5 KW xenon arc are lights were mounted on the wall opposite the reaction bags, all in a room with walls and ceiling covered with reflective aluminum paneling to maximize light intensity and homogeneity. The reaction bags were interconnected with two ports, each containing a fan to exchange the contents of the bags to assure that the reactants were adequately mixed. This was important in order to evaluate the effect of adding a test compound to a standard mixture. Two separate fans were also employed to mix the contents within each chamber. As discussed elsewhere (Carter et al. 1995b,c), and shown in a in figure later in this report, this light source gives the closest approximation available of the ground-level solar spectrum for an indoor chamber. The chamber was very similar to the Statewide Air Pollution Research Center's Xenon arc Teflon Chamber (SAPRC XTC) which is described in detail elsewhere (Carter et al. 1995b,c).

Experimental Procedures

The reaction bags were flushed with dry air produced by an AADCO air purification system for 14 hours (6pm-8am) on the nights before experiments. The continuous monitors were connected prior to reactant injection and the data system began logging data from the continuous monitoring systems. The reactants were injected as described below (see also Carter et al, 1993b,, 1995b). The common reactants were injected in both sides simultaneously using a three-way (one inlet and two outlets connected to side A and B respectively) bulb of 2 liters in the injection line and were well mixed before the chamber was divided. The contents of each side were blown into the other using two box fans located between them. Mixing fans were used to mix the reactants in the chamber during the injection period, but these were turned off prior to the irradiation. The sides were then separated by closing the ports which connected them, after turning all the fans off to allow their pressures to equalize. After that, reactants for specific sides (the test compound in the case of reactivity experiments) were injected and mixed. The lights are turned on after lowering a metal baffle between the lights and the reactors, and the lights are allowed to warm up for at least 30 minutes. Irradiation in the chamber is begun by raising the baffle between the lights and the reactors, and the irradiation proceeds for 6 hours. After the run, the contents of the chamber were emptied by allowing the bags to collapse, and then was flushed with purified air. The contents of the reactors were vented into a fume hood.

The procedures for injecting the various types of reactants were as follows. The NO and NO_2 were prepared for injection using a high vacuum rack. Known pressure of NO, measured with MKS Baratron capacitance manometers, were expanded into Pyrex bulbs with known volumes, which were then filled with nitrogen (for NO) or oxygen (for NO2). The contents of the bulbs were then flushed into the chamber with AADCO air. Acetylene usually prepared from CaC_2 as discussed below. The other gas reactants (and, for one experiment, acetylene) were prepared for injection either using a high vacuum rack or a gas-tight syringes whose amounts were calculated. The gas reactants in a gas-tight syringe was usually diluted to 100-ml with nitrogen in a syringe. The volatile liquid reactants were injected, using a micro syringe, into a 1-liter Pyrex bulb equipped with stopcocks on each end and a port for the injection of the liquid. The port was then closed and one end of the bulb was attached to the injection port of the chamber and the other to a dry air source. The stopcocks were then opened, and the contents of the bulb were flushed into the chamber with a combination of dry air and heat gun for approximately 5 minutes. Formaldehyde was prepared in a vacuum rack system by heating paraformaldehyde in an evacuated bulb until the pressure corresponded to the desired amount of formaldehyde. The bulb was then closed and detached from the vacuum system and its contents were flushed into the chamber with dry air through the injection port.

Although acetylene is commercially available in gas cylinders, it needs to be stabilized by dissolving in acetone, and may contain other reactive impurities. Therefore, for most experiments the acetylene was prepared by reacting water with Calcium Carbide. It was done by placing a small amount of Calcium Carbide into an 125 ml flask containing deionized water which was previously flushed with

nitrogen for 10 minutes. The acetylene generated by this reaction is then bubbled first through concentrated sulfuric acid and then through aqueous sodium hydroxide. The desired amount of the purified acetylene is then withdrawn using a glass syringe and flushed into the chamber. This process resulted in no impurities being detected by GC.

For one experiment, acetylene was taken from an acetylene tank (Matheson Co., 99.6% stated purity) and injected into the chamber using a high vacuum system. Some acetone impurity was observed in this experiment (see Results).

Analytical Methods

Ozone and nitrogen oxides (NO_x) were continuously monitored using commercially available continuous analyzers with Teflon sample lines inserted directly into the chambers. The sampling lines from each side of the chamber were connected to solenoids which switched from side to side every 10 minutes, so the instruments alternately collected data from each side. Ozone was monitored using a Dasibi 1003AH UV photometric ozone analyzer and NO and total oxides of nitrogen (including HNO_3 and organic nitrates) were monitored using a Teco Model 14B chemiluminescent NO/NO_x monitor. The output of these instruments, along with that from the temperature sensors and the and formaldehyde instrument, were attached to a computer data acquisition system, which recorded the data at 10 minutes intervals for ozone, NO and temperature (and at 15 minutes for formaldehyde), using 30 second averaging times. This yielded a sampling interval of 20 minutes for taking data from each side.

The Teco instrument and Dasibi CO analyzer were calibrated with a certified NO and CO source and CSI gas-phase dilution system. It was done prior to chamber experiment for each run. The NO_2 converter efficiency check was carried out in regular intervals. Dasibi ozone analyzer was calibrated against transfer standard ozone analyzer using transfer standard method in a interval of three months and was check with CSI ozone generator (set to 400 ppb) for each experiment to assure that the instrument worked properly. The details were discussed elsewhere (Carter et al, 1995b)

Organic reactants other than formaldehyde were measured by gas chromatography with FID and ECD detections as described elsewhere (Carter et al. 1993a; 1995b). GC samples were taken for analysis at intervals from 20 minutes to 30 minutes either using 100 ml gas-tight glass syringes or by collecting the 100 ml sample from the chamber onto Tenax-GC solid adsorbent cartridge. These samples were taken from ports directly connected to the chamber after injection and before irradiation and at regular intervals after irradiation. The sampling method employed for injecting the sample onto the GC column depended on the volatility or "stickiness" of the compound. For analysis of the more volatile species, which includes all the organic compounds monitored in this study, the contents of the syringe were flushed through a 2 ml or 3 ml stainless steel or 1/8’ Teflon tube loop and subsequently injected onto the column by turning a gas sample valve.

The calibrations for the GC analyses for most compounds were carried out by sampling from chambers or vessels of known volume into which known amounts of the reactants were injected, as described previously (Carter et al, 1995b).

Characterization Methods

Three temperature thermocouples for each chamber were used to monitor the chamber temperature, two of which were located in the sampling line of continuous analyzers to monitor the temperature in each side. The third one was located in the chamber to monitor chamber temperature. The temperature in these experiment were typically 25-30° C.

The spectrum of the xenon arc light source was measured several times during each experiment using a LiCor LI-1800 spectraradiometer. (A plot of a representative spectrum, and a comparison with the spectrum of sunlight, is given later in this report.) The absolute light intensity in this chamber was measured by "photostationary state" NO_2 actinometry experiments and by Cl_2 actinometry. The photostationary state experiments (which were carried out prior to the period of the experiments for this report) consisted of simultaneous measurements of photostationary state concentrations of NO, NO_2, and O_3 in otherwise pure air, with the NO_2 photolysis rate being calculated from the $[NO][O_3]/[NO_2]$ ratio (Carter et al. 1997). The Cl_2 actinometry experiments consisted of photolyzing ~0.1 ppm of Cl_2 in ~1 ppm of n-butane, calculating the Cl_2 photolysis rate from the rate of consumption of n-butane, and then calculating the corresponding NO_2 photolysis rate from the absorption cross sections and quantum yields for NO_2 and Cl_2 (assuming unit quantum yields for Cl_2) and the spectral distribution of the light source (Carter et al, 1997). The results of these two methods are generally in good agreement, and were used to place the somewhat more precise data of the relative light intensity methods, discussed below, on an absolute basis (Carter et al, 1997).

Relative trends in light intensity with time are obtained using the quartz tube method of (Zafonte et al. 1977), modified as discussed by Carter et al. (1995b; 1997), and from absolute intensities of spectra taken three or more times during each run using a Li-Cor LI-1800 spectraradiometer. Because the quartz tube during the actinometry experiments was located closer to the lights than the reaction bags, the NO_2 photolysis rates obtained using this method were corrected by multiplying them by a factor of 0.79 to make them consistent with the absolute values obtained using the steady state or Cl_2 actinometry methods (Carter et al, 1997). The LiCor data gave the most precise indication of the relative trend in light intensity, and NO_2 photolysis rates calculated using it (and NO_2 absorption cross sections and quantum yields) were used as the primary method for determining how the light intensity varied with time. These data indicated that the NO_2 photolysis rates declined slowly with time, with the data being fit by a curve giving an NO_2 photolysis rates of 0.183 - 0.178 min^{-1} during the period of this study.

The dilution of the CTC chamber due to sampling is expected to be small because the flexible reaction bags can collapse as samples are withdrawn for analysis. Also, the chamber was designed to

operate under slightly positive pressure, so any small leaks would result in reducing the bag volume rather than diluting the contents of the chamber. Information concerning dilution in an experiment can be obtained from relative rates of decay of added VOCs which react with OH radicals with differing rate constants (Carter et al. 1993a; 1995b). Most experiments had a more reactive compounds such as m-xylene and n-octane present either as a reactant or added in trace amounts to monitor OH radical levels. Trace amounts (~0.1 ppm) of n-butane were also added to experiments if needed to provide a less reactive compound for monitoring dilution. In addition, specific dilution check experiments such as CO irradiations were carried out. Based on these results, the dilution rate was found to be negligible in this chamber during this period, being less than 0.3% per hour in all runs, and usually less than 0.1% per hour.

Reactivity Data Analysis Methods

As indicated above, most of the experiments for this program consisted of simultaneous irradiation of a "base case" reactive organic gas (ROG) surrogate - NO_x mixture in one of the dual reaction chambers, together with an irradiation, in the other reactor, of the same mixture with added. The results are analyzed to yield two measures of VOC reactivity: the effect of the added VOC on the amount of NO reacted plus the amount of ozone formed, and integrated OH radical levels. These are discussed in more detail below.

The first measure of reactivity is the effect of the VOC on the change in the quantity $[O_3]$-[NO], or $([O_3]_t$-$[NO]_t)$-$([O_3]_0$-$[NO]_0)$, which is abbreviated as $d(O_3$-NO) in the subsequent discussion. As discussed elsewhere (e.g., Johnson, 1983; Carter and Atkinson, 1987; Carter and Lurmann, 1990, 1991, Carter et al, 1993a, 1995a,d), this gives a direct measure of the amount of conversion of NO to NO_2 by peroxy radicals formed in the photooxidation reactions, which is the process that is directly responsible for ozone formation in the atmosphere. (Johnson calls it "smog produced" or "SP".) The incremental reactivity of the VOC relative to this quantity, which is calculated for each hour of the experiment, is given by

$$IR[d(O_3\text{-NO})]_t^{VOC} = \frac{d(O_3\text{-NO})_t^{test} - d(O_3\text{-NO})_t^{base}}{[VOC]_0} \qquad (I)$$

where $d(O_3\text{-NO})_t^{test}$ is the $d(O_3$-NO) measured at time t from the experiment where the test VOC was added, $d(O_3\text{-NO})_t^{base}$ is the corresponding value from the corresponding base case run, and $[VOC]_0$ is the amount of test VOC added. An estimated uncertainty for IR[$d(O_3$-NO)] is derived based on assuming an ~3% uncertainty or imprecision in the measured $d(O_3$-NO) values. This is consistent with the results of the side equivalency test, where equivalent base case mixtures are irradiated on each side of the chamber.

Note that reactivity relative to $d(O_3$-NO) is essentially the same as reactivity relative to O_3 in experiments where O_3 levels are high, because under such conditions $[NO]_t^{base} \approx [NO]_t^{test} \approx 0$, so a change $d(O_3$-NO) caused by the test compound is due to the change in O_3 alone. However, $d(O_3$-NO) reactivity has the advantage that it provides a useful measure of the effect of the VOC on processes responsible for O_3 formation even in experiments where O_3 formation is suppressed by relatively high NO levels.

The second measure of reactivity is the effect of the VOC on integrated hydroxyl (OH) radical concentrations in the experiment, which is abbreviated as "IntOH" in the subsequent discussion. This is an important factor affecting reactivity because radical levels affect how rapidly all VOCs present, including the base ROG components, react to form ozone. If a compound is present in the experiment which reacts primarily with OH radicals, then the IntOH at time t can be estimated from

$$\text{IntOH}_t = \int_0^t [\text{OH}]_\tau \, d\tau = \frac{\ln \left(\frac{[\text{tracer}]_0}{[\text{tracer}]_t}\right) - D\,t}{k\text{OH}^{\text{tracer}}}, \qquad \text{(II)}$$

where $[\text{tracer}]_0$ and $[\text{tracer}]_t$ are the initial and time=t concentrations of the tracer compound, $k\text{OH}^{\text{tracer}}$ its OH rate constant, and D is the dilution rate in the experiments. The latter was found to be small and was neglected in our analysis. The concentration of tracer at each hourly interval was determined by linear interpolation of the experimentally measured values. M-xylene was used as the OH tracer in these experiments because it is a surrogate component present in all experiments, its OH rate constant is known (the value used was 2.36×10^{-11} cm^3 molec^{-1} s^{-1} [Atkinson, 1989]), and it reacts relatively rapidly.

The effect of the VOC on OH radicals can thus be measured by its IntOH incremental reactivity, which is defined as

$$\text{IR}[\text{IntOH}]_t = \frac{\text{IntOH}_t^{\text{test}} - \text{IntOH}_t^{\text{base}}}{[\text{VOC}]_0} \qquad \text{(III)}$$

where $\text{IntOH}_t^{\text{test}}$ and $\text{IntOH}_t^{\text{base}}$ are the IntOH values measured at time t in the added VOC and the base case experiment, respectively. The results are reported in units of 10^6 min. The uncertainties in IntOH and IR[IntOH] are estimated based on assuming an ~2% imprecision in the measurements of the m-xylene concentrations. This is consistent with the observed precision of results of replicate analyses of this compound.

CHEMICAL MECHANISMS AND MODELING METHODS

Chemical Mechanism

General Atmospheric Photooxidation Mechanism

The chemical mechanism used in the environmental chamber and atmospheric model simulations in this study is given in Appendix A to this report. This mechanism is based on that documented by Carter (1990), with a number of updates as discussed below. It can explicitly represent a large number of different types of organic compounds, but it lumps together species reacting with similar rate constants and mechanisms in simulations of atmospheric mixtures, and it uses a condensed representation for many of the reactive organic products. The reactions of inorganics, CO, formaldehyde, acetaldehyde, peroxyacetyl nitrate, propionaldehyde, peroxypropionyl nitrate, glyoxal and its PAN analog, methylglyoxal and several other product compounds are represented explicitly. In addition, the reactions of unknown photoreactive products formed in the reactions of aromatic hydrocarbons are represented by model species whose yields and photolysis parameters are adjusted based on fits of model simulations to environmental chamber experiments. A chemical operator approach is used to represent peroxy radical reactions, as discussed in detail by Carter (1990). Generalized reactions with variable rate constants and product yields are used to represent the primary emitted alkane, alkene, aromatic and other VOCs, with rate constants and product yields appropriate for the individual compounds being represented in each simulation). The tables in the Appendix list only those VOCs (or groups of VOCs) used in the simulations in this work. Most of the higher molecular weight oxygenated product species are represented using the "surrogate species" approach, where simpler molecules such as propionaldehyde or 2-butanone are used to represent the reactions of higher molecular weight analogues that are assumed to react similarly.

Several aspects of the Carter (1990) mechanism were updated prior to this work to account for new kinetic and mechanistic information for certain classes of compounds as described by Carter et. al. (1993b) and Carter (1995), and further modifications were made to the uncertain portions of the mechanisms for the aromatic hydrocarbons to satisfactorily simulate results of experiments carried out using differing light sources (Carter et al. 1997). The latest version of the general mechanism is discussed by Carter et al. 1997).

The reactions of toluene and m-xylene also involve the formation of glyoxal, although in this mechanism it contributes relatively little to their overall reactivity. As discussed below, glyoxal is the major reactive product formed from acetylene, and adjustments were made to the its mechanism to improve the fits of the model simulations to the results of the acetylene experiments. However, to preserve the reactivity characteristics the previously optimized mechanisms for toluene and m-xylene, the mechanism for the glyoxal formed from these compounds were not modified. Therefore, a separate model species was used to represent the glyoxal formed from acetylene for those calculations where its

mechanism was changed relative to that used in the standard mechanism. This is discussed in more detail below.

Atmospheric Reactions of Acetylene

The only significant atmospheric removal process for acetylene is believed to be reaction with OH radicals (Atkinson, 1989, and references therein). The latest evaluation of the available kinetic information for this reaction is given in the IUPAC evaluations (Atkinson et al, 1992, 1996). The rate constant is temperature and pressure dependent, since it is believed to involve primarily OH addition to the double bond, forming an energy-rich adduct which can decompose back to the reactants at sufficiently low pressures, though it is at ~90% of its high pressure limit under atmospheric conditions (Atkinson et al, 1996). The abstraction reaction, forming H_2O and $HC_2\cdot$, is important only at elevated temperatures (Atkinson, 1989; Atkinson et al. 1992), and can be neglected in simulations of atmospheric conditions. The rate constant for the addition reaction is both temperature and pressure dependent, but the rate constant expression given in the most recent IUPAC evaluations (Atkinson et al, 1992, 1997) can be approximated by

$$k_{OH + Acetylene} = 5.0 \times 10^{-13} e^{-545/T} \text{ cm}^3 \text{ molec}^{-1} \text{ s}^{-1}$$

at 1 atm. total pressure, which yields

$$k_{OH + Acetylene} = 8.2 \times 10^{-13} \text{ cm}^3 \text{ molec}^{-1} \text{ s}^{-1}$$

at 300K. This expression was used in the model simulations for this work. Most of the recent kinetic data concerning this reaction under atmospheric conditions appear to be in reasonably good agreement, so the kinetics of this reaction does not appear to be a significant uncertainty.

Studies of the reactions of OH radicals with acetylene under low pressure and atmospheric conditions indicate a fairly complex mechanism, and although fairly extensive data are available (Schmidt et al. 1985; Hatakeyama et al, 1986; Atkinson, 1989 and references therein; Siese and Zetzsch, 1995; Bohn et al. 1996), it may not be completely characterized. The possible processes following OH addition to acetylene are as follows (where "*" denotes vibrational excitation):

$$OH + HC{\equiv}CH \rightarrow [HOCH{=}CH\cdot]^* \quad (1)$$

$$[HOCH{=}CH\cdot]^* + M \rightarrow HOCH{=}CH\cdot + M \quad (2)$$

$$HOCH{=}CH\cdot + O_2 \rightarrow [\ HOCH(\dot{O}\cdot)\text{-}(\dot{O}\cdot)CH\ ] \rightarrow HC(O)OH + HCO\cdot \quad (3)$$

$$\rightarrow OH + HCO\text{-}CHO \quad (4)$$

$$HCO\cdot + O_2 \rightarrow HO_2 + CO \quad (5)$$

$$[HOCH{=}CH\cdot]^* \rightarrow [H_2C{=}CHO\cdot]^* \quad (6)$$

$$[H_2C{=}CHO\cdot]^* \rightarrow H_2C{=}CO + H \quad (7)$$

$$[H_2C{=}CHO\cdot]^* + M \rightarrow H_2C{=}CHO\cdot \leftrightarrow \cdot CH_2CHO \quad (8)$$

$$\cdot CH_2CHO + O_2 \rightarrow \cdot OOCH_2CHO \quad (9)$$

$$\cdot OOCH_2CHO \rightarrow OH + HCO\text{-}CHO \quad (10)$$

$$\cdot OOCH_2CHO + NO \rightarrow NO_2 + \cdot OCH_2CHO \quad (11)$$

$$\cdot OCH_2CHO + O_2 \rightarrow HCO\text{-}CHO + HO_2 \quad (12)$$

Although the available data are insufficient to unambiguously characterize this system under low pressure conditions (Siese and Zetzsch, 1995; Bohn et al, 1996), the overall processes under atmospheric conditions appear to be reasonably well established. Hatakeyema et al. (1986) observed that the products of the OH + acetylene reaction under atmospheric conditions were glyoxal (70 ± 30% yield) and formic acid (40 ± 10% yield), with the methyl acetylenes forming products suggesting they react analogously. The source of the formic acid is most likely reaction (3), with glyoxal being formed from either Reactions (4), (10), or, in the presence of NO, Reaction (12). Hatakeyama et al. (1986) also found that the glyoxal / formic acid yield ratio was independent of added NO. This means either that the reaction (3) dominates over Reaction (2) and the glyoxal is formed primarily from reaction (5) (i.e., the reactions shown in bold), or, if vinoxy radical formation is important, that reaction (10) dominates under NO_x-free conditions, and that Reactions (11-12), which also form glyoxal, become important when NO is present. Although ketene, via Reaction (6), is observed in low pressure systems (Hack et al, 1983), it was not observed by Hatakeyama et al. (1986), and its formation is probably not important under atmospheric conditions. Therefore, Reaction (7) is assumed to be negligible in the subsequent discussion.

Kinetic studies of the OH + acetylene system where OH radicals are monitored indicate that regeneration of OH radicals, such as via Reaction (4), occurs to a significant extent. The yield of OH radicals depended on the pressure, temperature and buffer gas, as might be expected given the relatively complex mechanism (Siese and Zetzsch, 1995 and references therein; Bohn et al, 1996). However, Bohn et al. (1996) observed a ~70% yield of OH radicals in synthetic air, in excellent agreement with the glyoxal yield observed by Hatakeyama et al. (1986).

Although the overall processes under atmospheric conditions appear to be reasonably well established, there is some ambiguity whether the observed formation of glyoxal results to any extent from reactions of vinoxy radicals, either via Reaction 9 in the absence of NO or via Reactions 10-11 when NO_x is present (as would be the case in photochemical smog systems). Previously we had assumed that the latter was the major process responsible for glyoxal formation, and that assumption was the basis of the mechanism used in our current mechanism (Carter, 1990). This was based on the observation of vinoxy radicals as an intermediate in this system (Schmidt et al. 1985). However, Siese and Zetzsch (1995) noted that the vinoxy yield at ~1 atm. is minor (<10%), and the intermediacy of vinoxy in the OH regeneration process is probably not consistent with the available data concerning the time, temperature, and pressure dependencies of OH generation in this system (Siese and Zetzsch, 1995; Bohn et al, 1996). Both mechanistic options will be considered for mechanism evaluation purposes.

Based on these considerations, the possible overall processes involved in the reactions of OH with acetylene under atmospheric conditions in the presence of NO_x are as follows:

$$\text{OH + Acetylene} \xrightarrow{2\ O_2} HO_2 + CO + HC(O)OH \qquad \text{(I: 1-3,5)}$$

$$\text{OH + Acetylene} \xrightarrow{O_2} \text{OH + HCO-CHO} \qquad \text{(II: 1,2,4)}$$

$$\text{OH + Acetylene} \xrightarrow{O_2,\ NO,\ O_2} NO_2 + HO_2 + \text{HCO-CHO} \qquad \text{(III: 1,6,8,9,11,12)}$$

with process I occurring ~30% of the time, and processes II or III occurring the remaining 70% of the time. In terms of SAPRC model species, these correspond to:

$$\text{HO. + Acetylene} \rightarrow 0.3\ \{\text{Inert + HO2. + CO}\} + 0.7\ \{\text{GLY + (1-}\alpha\text{) OH + }\alpha\ \text{RO2-R.}\}$$

where "Inert" represents formic acid, whose subsequent reactions are ignored, "GLY" represents glyoxal, "RO2-R." is a chemical "operator" which represents the net effect of the NO to NO_2 conversion and HO_2 generation in Reactions 11 and 12 (see Carter, 1990, for a discussion of these chemical operators), and α is the fraction of glyoxal formation which occurs via Process III (i.e., via Reaction 12).

Atmospheric Reactions of Glyoxal

As discussed above, Glyoxal is the major oxidation product in the atmospheric oxidation of acetylene, being formed ~70% of the time. Glyoxal is expected to react in the atmosphere primarily with OH radicals or by photolysis. The mechanism of the OH radical reaction appears to be reasonably well characterized, and are discussed in recent evaluations (Atkinson et al, 1992, 1997; Atkinson, 1989). The rate and mechanisms for its photolysis reaction is much more uncertain, and as shown later, alternative assumptions can have significant effects on model simulations of the ozone impacts of acetylene.

The absorption cross sections for glyoxal (Plum et al, 1983) are shown on Figure 1, where they are compared with the spectral distribution for the light source of the chamber used in this study and with that for ambient sunlight. It can be seen that there is a significant overlap, and the atmospheric photolysis rate can be significant if the quantum yields are sufficiently high. Glyoxal can photolyze via three possible primary processes,

$$\text{HCOCHO} + h\nu \rightarrow 2\ \text{HCO} \qquad (\Phi_1)$$

$$\text{HCOCHO} + h\nu \rightarrow \text{HCHO} + \text{CO} \qquad (\Phi_2)$$

$$\text{HCOCHO} + h\nu \rightarrow H_2 + 2\ \text{CO} \qquad (\Phi_3)$$

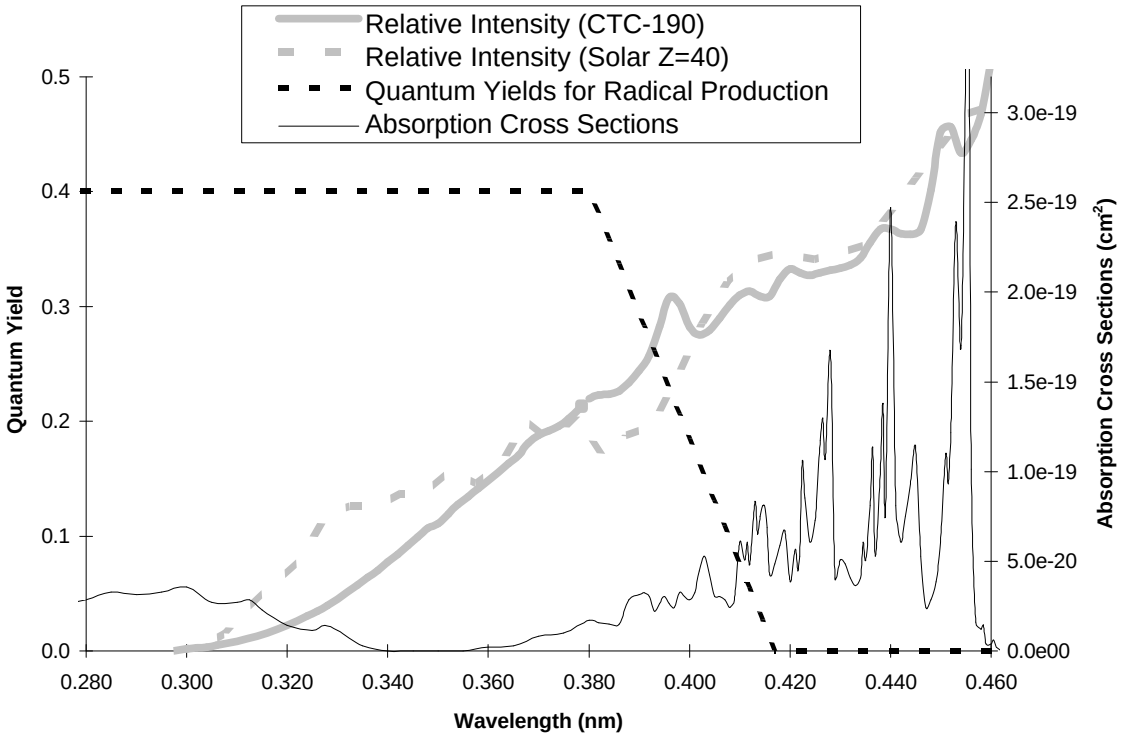

Figure 1. Absorption cross sections and quantum yields for glyoxal (optimized for model C) as a function of wavelength. Also shown are the relative spectral distributions of sunlight and the light source used in the environmental chamber experiments.

Figure 1. Absorption cross sections and quantum yields for radical formation for glyoxal as a function of wavelength, and relative spectral distributions of sunlight and the light source used in the environmental chamber experiments. (The quantum shown are optimized for Model C, see text.)

though the energetics for the radical formation route (Reaction 12) is such that it can only occur at wavelengths less than 418 nm (Atkinson et al, 1992, 1997). The limited information given in Calvert and Pitts (1966) suggests that the quantum yields may be pressure dependent, and the data there are inconclusive concerning the quantum yields and relative importances of these processes under atmospheric conditions. The only quantitative information concerning quantum yields at atmospheric pressure comes from Langford and Moore (1984) and Plum et al. (1983). Langford and Moore (1984) observed that Φ_2=0.4±0.2 at λ=308 nm. Note that this is only applicable to the lower wavelength (λ<340 nm) absorption band (see Figure 1), and the quantum yields at the λ>360 nm band are much more important in affecting atmospheric photolysis rates. The only information concerning glyoxal photolysis at this higher wavelength band comes from Plum et al. (1983), who observed that the overall quantum yield of glyoxal consumption ($\Phi_1+\Phi_2+\Phi_3$) was 0.029, when photolyzed using a xenon arc solar simulator filtered such that $\lambda\geq$320 nm, and that the relative yield of formaldehyde, $\Phi_2/(\Phi_1+\Phi_2+\Phi_3)$, was ~13%. This means that, for the light source used by Plum et al. (1983), the overall Φ_2=0.004 and $\Phi_1+\Phi_2$=0.025. No information is available concerning how these quantum yields depend on wavelength.

Model simulations of systems containing glyoxal are highly sensitive to the assumed overall Φ_1, since this is a radical initiating process. In the SAPRC-90 and SAPRC-93 mechanisms (Carter, 1990),

based on qualitative information given by Calvert and Pitts (1966), and the fact that energetics prevent radical formation being important at λ>418 nm, it was assumed that Φ_1=0 in the high wavelength band. Since photolysis in the low wavelength band is relatively minor under atmospheric conditions, overall quantum yields of Φ_2=0.004 and Φ_3=0.025, independent of wavelength, were assumed to be consistent with the overall quantum yield and relative formaldehyde formation yields reported by Plum et al. (1983). The model calculations where this is assumed are labeled "SAPRC-93" in the presentation of the results.

However, as shown later in this reports, the results of the environmental chamber experiments carried out for this program could not be fit by model simulations unless it was assumed that most of the photolysis of glyoxal involves radical formation, i.e., that $\Phi_1 \gg \Phi_3$. Therefore, this is assumed in most of the model calculations shown in this report. However, since photolysis to form radicals cannot occur at wavelengths lower than 418 nm, and since glyoxal has significant absorption bands at higher wavelengths (see Figure 1), a wavelength-independent overall quantum yield was not used in the model simulations. Instead, we assume that Φ_1 was constant at the low wavelength value of 0.4 (Langford and Moore, 1984) up to a certain wavelength (referred to as λ_1^{gly} in the subsequent discussion), and then decreasing linearly between that wavelength and λ=418 nm, where it was assumed to be zero. (See Figure 1 for an example of an assumed wavelength dependence for Φ_1.) The data of plum et al. (1983) yield an upper limit for Φ_1 of 0.025 for their light source. Using the spectral distribution for the by Plum et al. (1983) light source[1], we calculate that this corresponds to $\lambda_1^{gly} \leq 354$ nm. Lower values of λ_1^{gly} would yield lower values of overall Φ_1, and thus higher values of Φ_3, if the $\Phi_1+\Phi_3$ = 0.025 value of Plum et al. (1983) is assumed. However, as discussed below, the environmental chamber data are better fit by models assuming higher values of λ_1^{gly}, and thus higher overall quantum yields, than are consistent with the data reported by Plum et al. (1983).

Alternative Mechanisms Used for Acetylene Modeling

As indicated above, there are two uncertain aspects of the acetylene and glyoxal mechanisms which are potentially significant in affecting model predictions of acetylene reactivity. These are (1) the relative importance of Process II vs Process III in the OH + acetylene reactions, and (2) the overall quantum yield for radical production in the photolysis of glyoxal. These are represented by the parameters α and λ_1^{gly}, respectively. Four alternative mechanisms, using differing assumptions concerning these uncertain parameters, are considered for mechanism evaluation purposes:

The SAPRC-90 Model uses the same representation of acetylene and glyoxal as used in the SAPRC-90 mechanism (Carter, 1990). In this mechanism it is assumed that Process III dominates over

[1]Plum et al (1983) carried out their experiments in the Statewide Air Pollution Research Center Evacuable Chamber (EC) using its solar simulator light source. The spectra of that light source, which varied over time, can be derived as described by Carter et al (1995b). Based on the times these experiments were carried out, it was assumed that the spectrum of the light source when used by Plum et al (1983) was similar to those derived for EC runs around the time of run EC-900.

Process II (α=1), and that there is no radical formation in the photolysis of glyoxal in the high wavelength band (λ_1^{gly}=340 nm, with Φ_1 going to zero by λ=360 nm).

Model A is similar to the SAPRC-90 model in that it assumes that Process III dominates over Process II (α=1), but differs in that it assumes that glyoxal photolysis forms radicals with the highest overall quantum yields which are consistent with the data of Plum et al. (1983) (λ_1^{gly}=354 nm).

Model B assumes that Process II dominates over Process III (α=0), and the value the overall radical quantum yield from glyoxal photolysis, or λ_1^{gly}, is adjusted to yield best fits of model simulations to the results of the chamber experiments. The optimizations use a nonlinear algorithm to minimize the sum of squares difference between results of model simulations and the experimentally measured values of d(O_3-NO) in the acetylene - NO_x experiments, and of d(O_3-NO) and m-xylene in selected incremental reactivity runs. The specific experiments used in the optimization calculations are indicated in Results section.

In Model C the values of α and λ_1^{gly} are both optimized to yield the best fits between model simulations and experimental results. Other than optimizing α as well as λ_1^{gly}, the optimization method was the same as used when deriving Model B.

A third optimized mechanism, involving deriving an optimum λ_1^{gly} when α=1 is assumed, was not considered separately because it is evident from the results, discussed below, that it would not perform significantly better than Model A in simulating the experimental results.

Modeling Methods

Environmental Chamber Simulations

The ability of the chemical mechanisms to appropriately simulate the atmospheric impacts of acetylene was evaluated by conducting model simulations of the environmental chamber experiments from this study. This requires including in the model appropriate representations of chamber-dependent effects such as wall reactions and characteristics of the light source. The methods used are based on those discussed in detail by Carter and Lurmann (1990, 1991), updated as discussed by Carter et al. (1995b,c; 1997). The photolysis rates were derived from results of NO_2 actinometry experiments and measurements of the relative spectra of the light source. In the case of the xenon arc lights used in the CTC, the spectra were derived from those measured during the individual experiments, assuming continuous linear changes in relative intensity at the various wavelengths, as discussed by Carter et al. (1997). The thermal rate constants were calculated using the temperatures measured during the experiments, with the small variations in temperature with time during the experiment being taken into account. The computer programs and modeling methods employed are discussed in more detail elsewhere (Carter et al, 1995b). The specific values of the chamber-dependent parameters used in the model simulations of the experiments for this study are given in Table A-4 in Appendix A. Various alternative assumptions were made

concerning the OH + acetylene and the glyoxal photolysis reactions, as indicated above and discussed later.

Atmospheric Reactivity Simulations

To estimate its effects on ozone formation under conditions more representative of polluted urban atmospheres, incremental reactivities, defined as the change in O_3 caused by adding small amounts of a compound to the emissions, were calculated for ethane, acetylene, and the mixture representing the VOCs emitted from all sources, for various simulated atmospheric pollution scenarios. Carter (1994a) used a series of single-day EKMA box model scenarios (EPA, 1984) derived by the EPA to represent 39 different urban ozone exceedence areas around the United States (Baugues, 1990), to develop various reactivity scales to quantify impacts of VOCs on ozone formation in various environments. It was found that NO_x levels are the most important factor affecting differences in relative ozone impacts among VOCs, and that the ranges of relative reactivities in the various scales can be reasonably well represented by ranges in relative reactivities in three "averaged conditions" scenarios representing three different NO_x conditions. These scenarios were derived by averaging the inputs to the 39 EPA scenarios, except for the NO_x emissions. In the "maximum reactivity" scenario, the NO_x inputs were adjusted such that the final O_3 level is most sensitive to changes in VOC emissions; in the "maximum ozone" scenario the NO_x inputs were adjusted to yield the highest maximum O_3 concentration; and in the "equal benefit" scenario the NO_x inputs were adjusted such that relative changes in VOC and NO_x emissions had equal effect on ozone formation. As discussed by Carter (1994a), there represent respectively the high, medium and low ranges of NO_x conditions which are of relevance when assessing VOC control strategies for reducing ozone.

The chemical mechanisms used for these atmospheric simulations were the same as used to simulate the chamber experiments, except that the reactions representing chamber effects were removed, and the reactions for the full variety of VOCs emitted into the scenarios (Carter, 1994a) were represented (see Appendix A). Most of the emitted VOCs (other than the test compound whose reactivity is being calculated) are not represented in the model explicitly, but are represented using lumped model species whose rate constants and product yield parameters are derived based on the mixture of compounds they represent. The rate constants and mechanistic parameters for the emitted species in the scenarios were the same as those used previously (Carter et al, 1993b), except for the aromatics, whose unknown photoreactive product yields were reoptimized in a manner analogous to that discussed above for toluene and m-xylene (Carter et al. 1997). The listings on Appendix A give the lumped model species used to represent the emissions into the scenarios, indicate the types of species each is used to represent, and give their rate constants and product yield parameters.

RESULTS AND DISCUSSION

Summary of Experiments

Table 1 gives a chronological listing of all the experiments carried out for this program. These consisted primarily of incremental reactivity experiments, whose conditions and selected results are summarized in more detail on Table 2. Also, as indicated on Table 2, one dual-chamber acetylene - NO_x experiment (CTC-188) was carried out. Control experiments were conducted to assure consistency with previous results, and side equivalency tests were conducted to assure that essentially equivalent results were obtained when equal mixtures were simultaneously irradiated in each of the dual reaction bags. Table 1 summarizes relevant results from these characterization and control runs.

The results of the characterization and control runs were generally as expected based on our previous experience with these and similar chambers in our laboratories (Carter et al. 1995b and references therein). Good side equivalency was observed when equivalent surrogate - NO_x (not shown on Table 1), propene - NO_x, CO - NO_x, or n-butane - NO_x mixtures were simultaneously irradiated in the dual reactors. The results of the CO - NO_x and n-butane - NO_x experiments, which are highly sensitive to the magnitude of the chamber radical source assumed in the model (see Table A-4 in Appendix A), were sufficiently well simulated by the model to indicate that the model was appropriately representing this effect for these runs. The actinometry results agreed with the extrapolated values based on results of previous determinations, to within the variability of these determinations.

Results of The Reactivity Experiments and Mechanism Evaluations

Figure 2 shows concentration-time plots for ozone, NO, acetylene, and formaldehyde in the two acetylene - NO_x experiments, along with results of several model simulations of those runs. Significant ozone formation is seen to occur in both experiments, with more ozone formation occurring on the side with the greater amount of acetylene, as expected. Very small amounts of formaldehyde, approximately 1 ppb on the 10 ppm acetylene side and 2 ppb on the 20 ppm acetylene side, are observed. The analytical methods employed in these experiments could not detect glyoxal and formic acid, the major expected products. The fractions of acetylene reacting in these experiments was small, as expected given its relatively low rate of reaction.

Summaries of the conditions and results of the incremental reactivity experiments are given on Table 2, and Figures 3 through 9 give time series plots for relevant measurements used for mechanism evaluation. These include concentrations of d(O_3-NO) and m-xylene in the base case and test experiments, concentrations of acetylene in the test experiment, and the d(O_3-NO) and IntOH incremental reactivities derived from the differences between the two sides. Results of model calculations, discussed below, are also shown in these figures.

Table 1. Chronolological listing of the environmental chamber experiments carried out for this program.

RunID	Date	Title	Comments
CTC170	11/15/96	Propene + NOx	Control run for comparison with other propene runs carried out in this and other chambers. Good side equivalency was observed. The results were in good agreement with model predictions.
CTC174	11/22/96	Pure air irradiation	After 6 hours of irriadiation, approximately 22 ppb O_3 formed on side A and 24 on side B. Results are within the normal range, and were consistent with the predictions of the chamber effects model.
CTC175	11/25/96	n-Butane + NOx	Control run to measure the chamber radical source. NO consumption rate well fit by predictions of the chamber model.
CTC177	11/27/96	NO2 and Chlorine Actinometry.	In-chamber NO_2 photolysis rates from the NO_2/N_2 tube and the n-butane - Cl_2 method were calculated to be 0.185 and 0.174 min^{-1}, respectively. These are in reasonably good agreement with other actinometry measurements in this chamber.
CTC184	12/13/96	Mini surrogate + Acetylene (B)	Acetylene made from CaC_2. The addition of acetylene had a large positive effect on O3 formation and m-xylene consumption rates. See Table 2 and Figure 2.
CTC185	12/17/96	Mini surrogate + Acetylene (from tank)	Repeat of run CTC185 except with acetylene from a tank. Acetone impurity ~ 9 ppb. Results similar to run CTC184, with a slightly greater O_3 formation rate attributed to the slightly greater amount of acetylene injected. See Table 2 and Figure 3.
CTC186	12/18/96	Full Surrogate + Acetylene	Acetylene made from CaC_2. The addition of acetylene had a moderate positive effect on O_3 formation and m-xylene consumption rates. See Table 2 and Figure 5.
CTC187	12/19/96	Low NOx full surrogate + Acetylene	Acetylene made from CaC_2. The addition of acetylene had a moderate positive effect on O_3 formation and m-xylene consumption rates, but final O_3 about the same on both sides. See Table 2 and Figure 7.

Table 1 (continued)

RunID	Date	Title	Comments
CTC188	12/20/96	Acetylene + NOx	Acetylene made from CaC_2. Equal amounts on NOx on both sides, with acetylene varied. Significant O_3 formation on both sides, with O_3 nearing its maximum on the high acetylene side. See Table 2 and Figure 1.
CTC189	12/23/96	n-Butane + NOx	Control run to measure the chamber radical source. NO consumption rate was slightly slower than predictions of the chamber model, but within the expected range.
CTC190	1/3/97	n-Butane + chlorine Actinometry	NO_2 photolysis rates from the NO_2/N_2 tube and the n-butane - Cl_2 method were calculated to be 0.160 and 0.107 min^{-1}, respectively. The latter is anomalously low, but the former is within the range observed in other actinometry experiments.
CTC191	1/7/97	Propene + NOx	Control run for comparison with other propene runs carried out in this and other chambers. Good side equivalency was observed. The ozone formation rate was slightly slower than predicted by the model, but within the expected range.
CTC192	1/8/97	Mini surrogate + acetylene (A)	Repeat of run CTC184 with about half the amount of acetylene added. Consistent results obtained. See Table 2 and Figure 4.
CTC193	1/9/97	Full surrogate + acetylene (B)	Repeat of run CTC186 with about 50% more acetylene added. Consistent results obtained. See Table 2 and Figure 6.
CTC194	1/14/97	Low NOx full surrogate + Acetylene	Repeat of run CTC187 with about 75% more acetylene added. Consistent results obtained. See Table 2 and Figure 8.
CTC200	1/24/97	CO + NOx	Control run to measure the chamber radical source. NO consumption rate well fit by predictions of the chamber model. CO data indicated that dilution was negligible.
CTC207	2/7/97	NO2 and Chlorine Actinometry.	In-chamber NO_2 photolysis rates from the NO_2/N_2 tube and the n-butane - Cl_2 method were calculated to be 0.156 and 0.175 min^{-1}, respectively. These are in reasonably good agreement with other actinometry measurements in this chamber.

Table 2. Summary of conditions and results of the environmental chamber experiments.

Run	Initial Reactants (ppm)			t=6 d(O_3-NO) (ppm)			t=6 IntOH (10^{-6} min)		
	NOx	Surg [a]	Acetylene	Base	Test	IR [b]	Base	Test	IR
Incremental Reactivity: Mini-Surrogate									
CTC-184 (B) [c]	0.25	4.9	17.0	0.60	0.81	0.0122	20	33	0.8
CTC-185 (A) [d]	0.30	5.0	17.8	0.60	0.92	0.0178	22	38	0.9
CTC-192 (A)	0.24	4.9	8.3	0.57	0.77	0.0233	20	31	1.3
Incremental Reactivity: Full Surrogate - High NOx									
CTC-186 (B)	0.39	5.4	8.5	0.70	0.89	0.0229	26	37	1.2
CTC-193 (B) [c]	0.39	5.4	12.6	0.72	0.93	0.0165	25	37	1.0
Incremental Reactivity: Full Surrogate - Low NOx									
CTC-187 (A)	0.17	5.7	9.3	0.44	0.47	0.0028	26	27	0.1
CTC-194 (A)	0.16	5.7	16.2	0.44	0.48	0.0025	24	26	0.1
Acetylene - NOx									
CTC-188 (A) [e]	0.15	-	10.5	-	0.46	-	-	-	-
CTC-188 (B) [e]	0.15	-	20.1	-	0.68 [f]	-	-	-	-

Notes

[a] Total base ROG surrogate in ppmC.

[b] Incremental reactivity

[c] d(O_3-NO) and m-xylene data used in optimization calculations.

[d] Acetylene from tank used. Approximately 9 ppb acetone impurity observed.

[e] d(O_3-NO) data used in optimization calculations.

[f] T = 349 minute value.

Table 2. Summary of conditions and selected results of the incremental reactivity experiments.

The additions of 8-17 ppm of acetylene to the mini-surrogate and the higher NO_x full surrogate experiments caused significant increases in the rates of ozone formation and NO oxidation, though the magnitudes of the incremental reactivities were relatively low because of the large amounts of acetylene which were added. The effects on $d(O_3\text{-NO})$ tended to increase with time in the experiments up to the time that the ozone on the added acetylene side approached a maximum, after which the $d(O_3\text{-NO})$ incremental reactivities began to decline. The effects of acetylene on $d(O_3\text{-NO})$ were much smaller in the low NO_x full surrogate experiments, with final $d(O_3\text{-NO})$ incremental reactivities being ~6-8 times lower in the low NO_x full surrogate runs compared with the higher NO_x runs with the same ROG surrogate.

The addition of acetylene also caused increased the m-xylene consumption rates in all the incremental reactivity experiments, which indicates that acetylene has positive reactivities relative to integrated OH radical levels (IntOH). This means that significant radical initiation processes are involved in its photooxidation mechanism. Positive effects on radicals is consistent with the observation that the ozone impact decreases with decreasing NO_x levels, since radical initiation processes have the greatest impact on ozone formation under conditions where NO_x is relatively high (Carter and Atkinson, 1989).

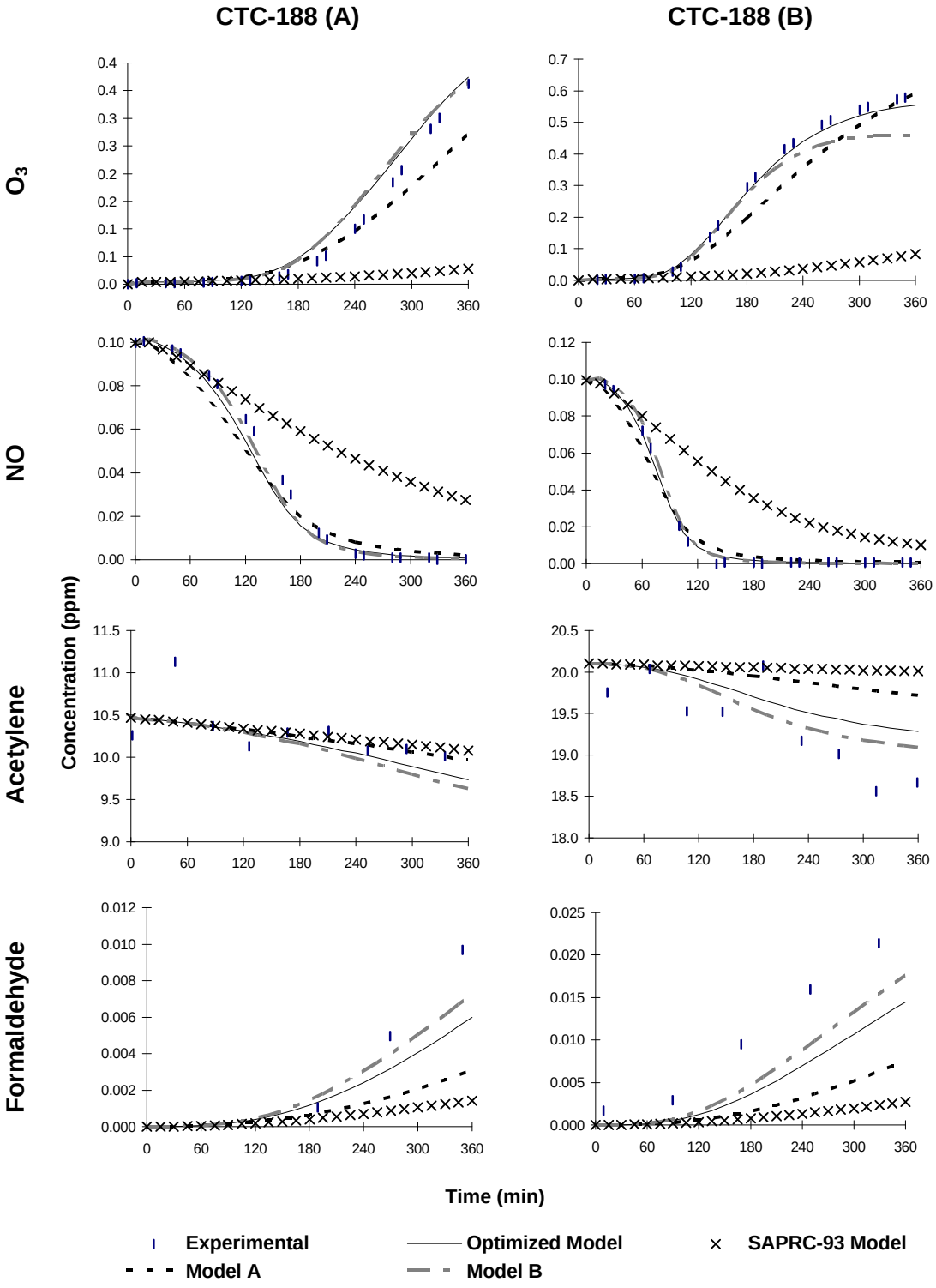

Figure 2. Experimental and calculated concentration - time plots for selected species in the acetylene - NOx experiment.

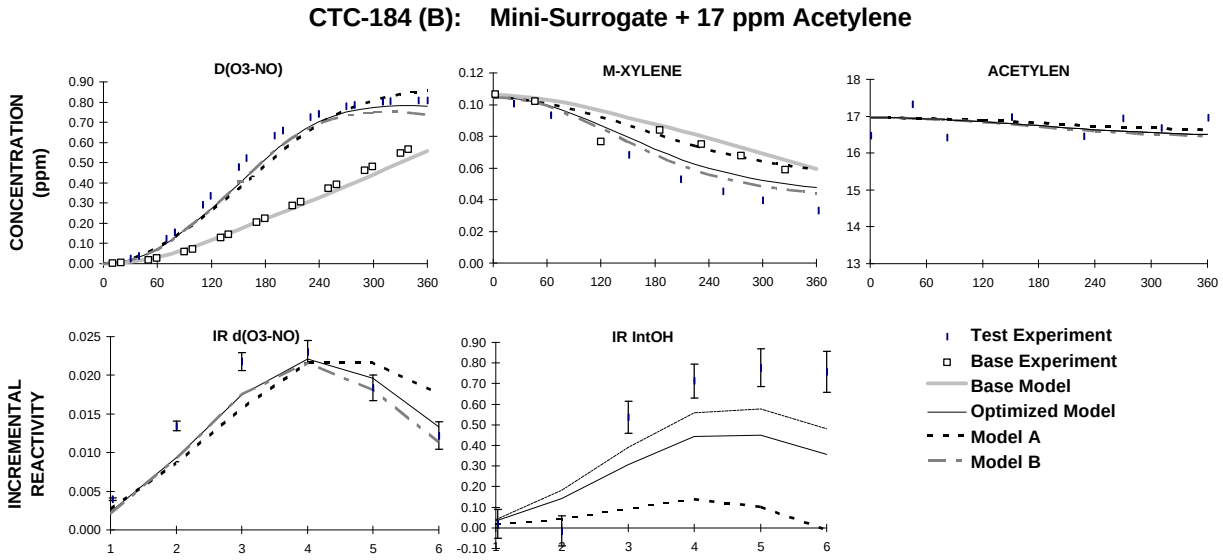

Figure 3. Plots of selected results of the mini-surrogate +acetylene experiment CTC-184.

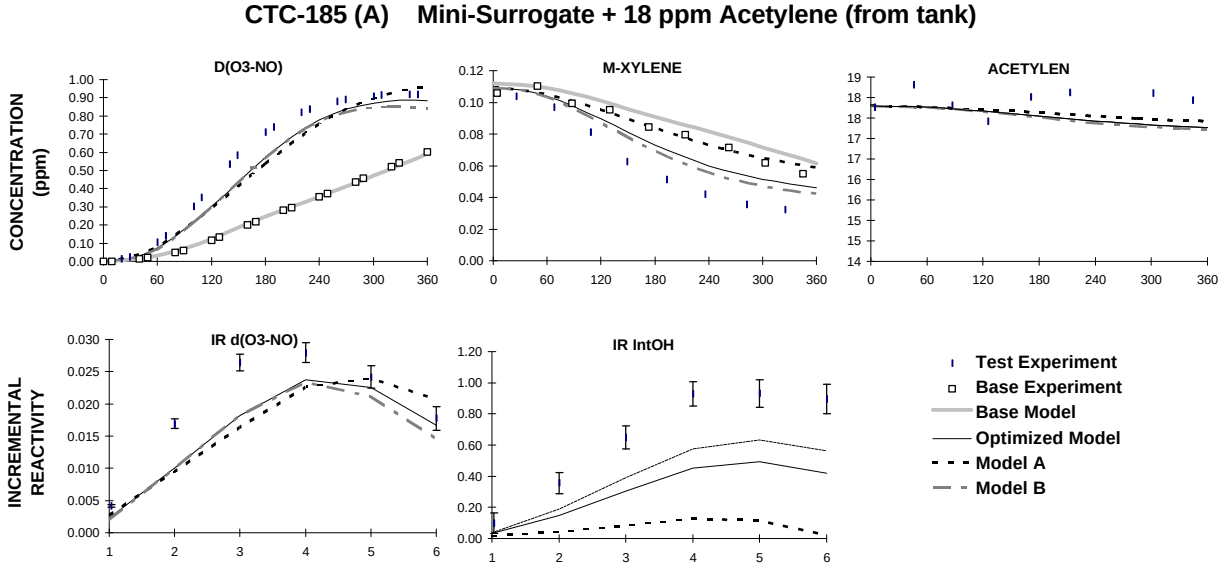

Figure 4. Plots of selected results of the mini-surrogate + acetylene experiment CTC-185.

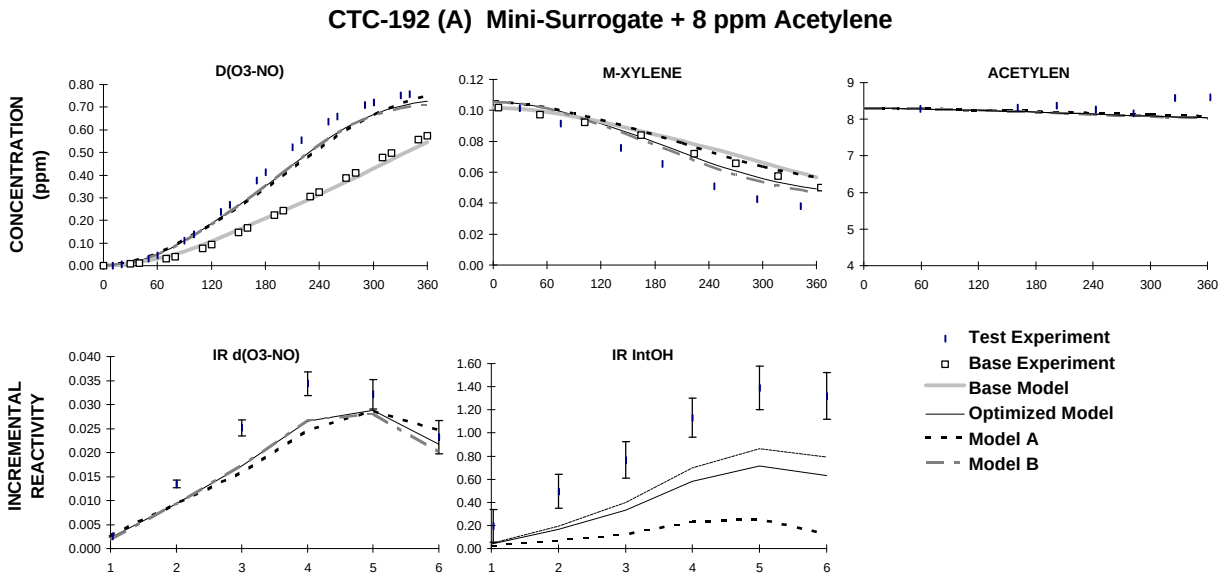

Figure 5. Plots of selected results of the mini-surrogate +acetylene experiment CTC-192.

Figure 5. Plots of selected results of the mini-surrogate + acetylene experiment CTC-185.

Note that the mini-surrogate + acetylene run CTC-185 was essentially a duplicate of run CTC-184, except the acetylene used was from a commercially-obtained lecture bottle instead of being prepared from the reaction of CaC_2 with water. Other than the observations of a small amount of acetone impurity in the run using acetylene from the lecture bottle, the results of the two experiments were very similar. This indicates no significant effects of impurity species in the commercially-obtained acetylene (or vise-versa). The slightly higher final ozone observed in the added acetylene side of run CTC-185 can be attributed to the slightly higher initial NO_x levels, and is predicted by the results of the model simulations (discussed below). The model predicted that the 9 ppb acetone impurity would have a negligible effect on the results of these experiments. Nevertheless, because it produces no measurable impurities, the CaC_2 method was used to prepare the acetylene for all the other experiments in this program.

The results of the model simulations of the acetylene - NO_x and acetylene reactivity experiments are shown on Figures 2-9, where they can be compared with the experimental data. Figure 2 shows that the model simulations using the SAPRC-90 representation of acetylene and glyoxal reactions significantly underpredict the ozone formation and NO oxidation rates. Simulations of the reactivity experiments using that mechanism (not shown) were also unsatisfactory, with the model, contrary to the observations, predicting negative effects on IntOH in all experiments, and also predicting significantly lower effects on $d(O_3\text{-NO})$ in the mini-surrogate experiments than were observed experimentally. On the other hand, this model gave fair fits to the $d(O_3\text{-NO})$ reactivities in the high NO_x full surrogate experiments, and actually overpredicted the $d(O_3\text{-NO})$ reactivities in the low NO_x full surrogate runs.

Figure 2 shows that the simulations with acetylene Model A performs much better in simulating the results of the acetylene - NO_x experiments. This differs from the SAPRC-90 acetylene model only

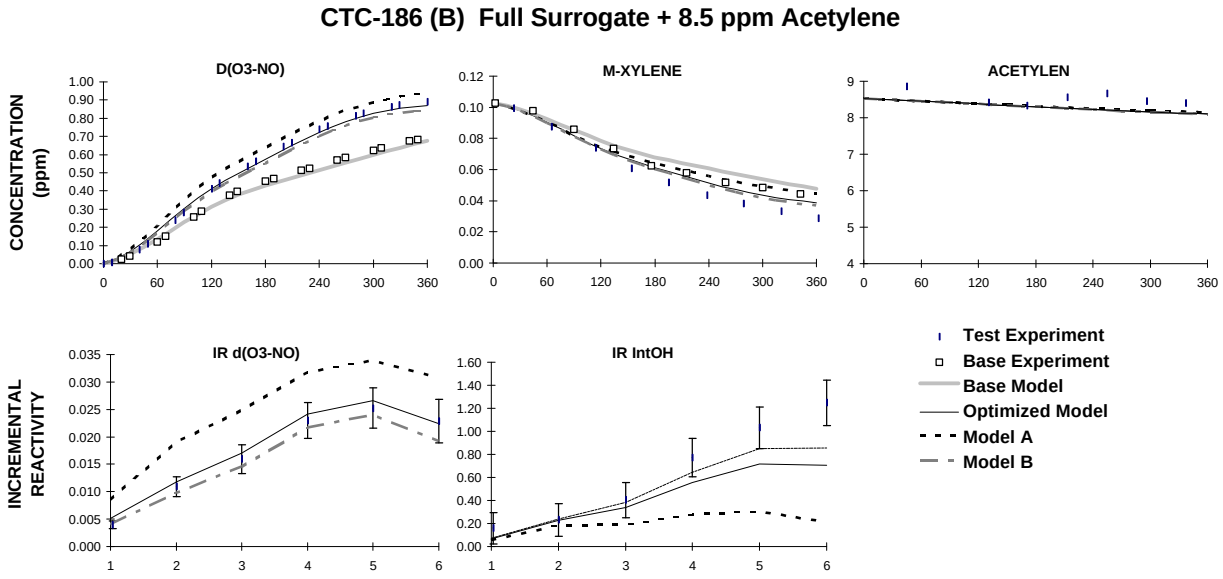

Figure 6. Plots of selected results of the full surrogate +acetylene experiment CTC-186.

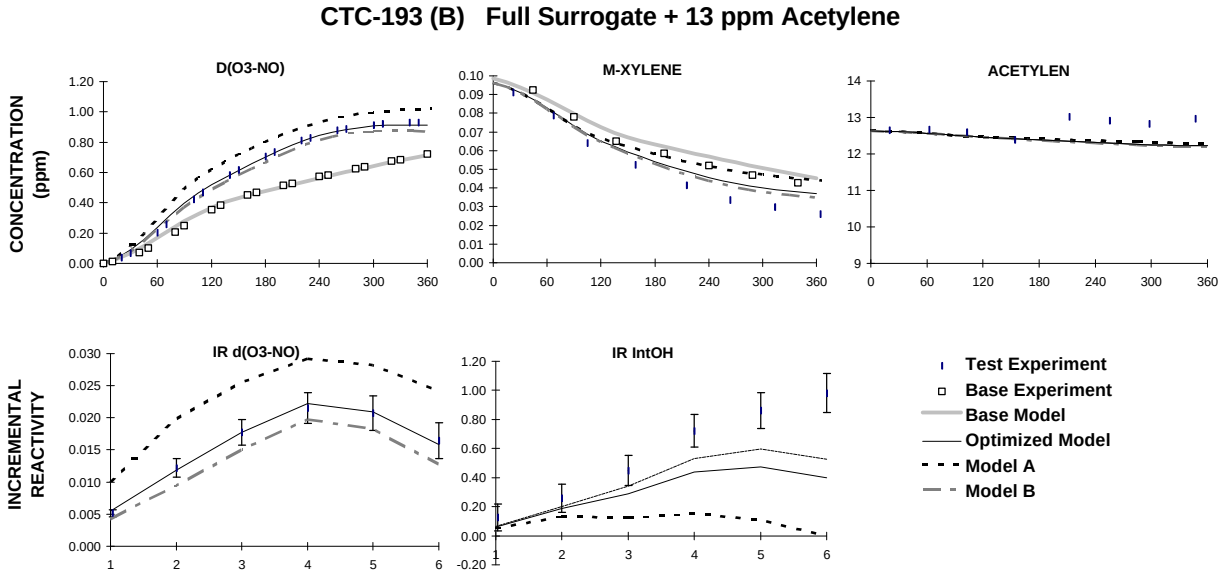

Figure 7. Plots of selected results of the full surrogate + acetylene experiment CTC-193.

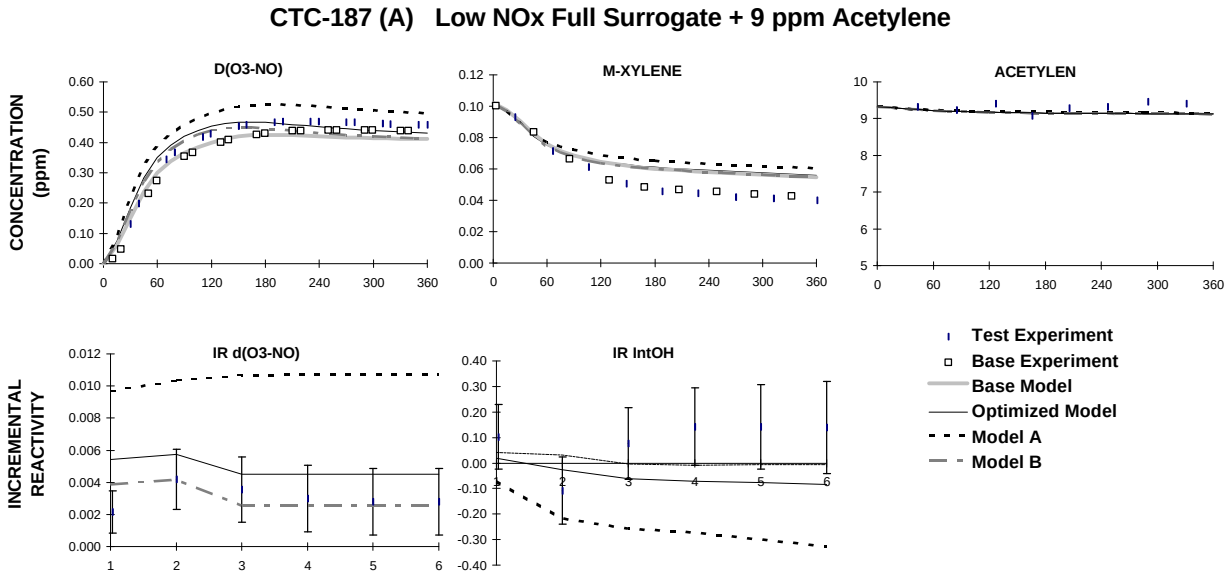

Figure 8. Plots of selected results of the low NOx full surrogate + acetylene experiment CTC-187.

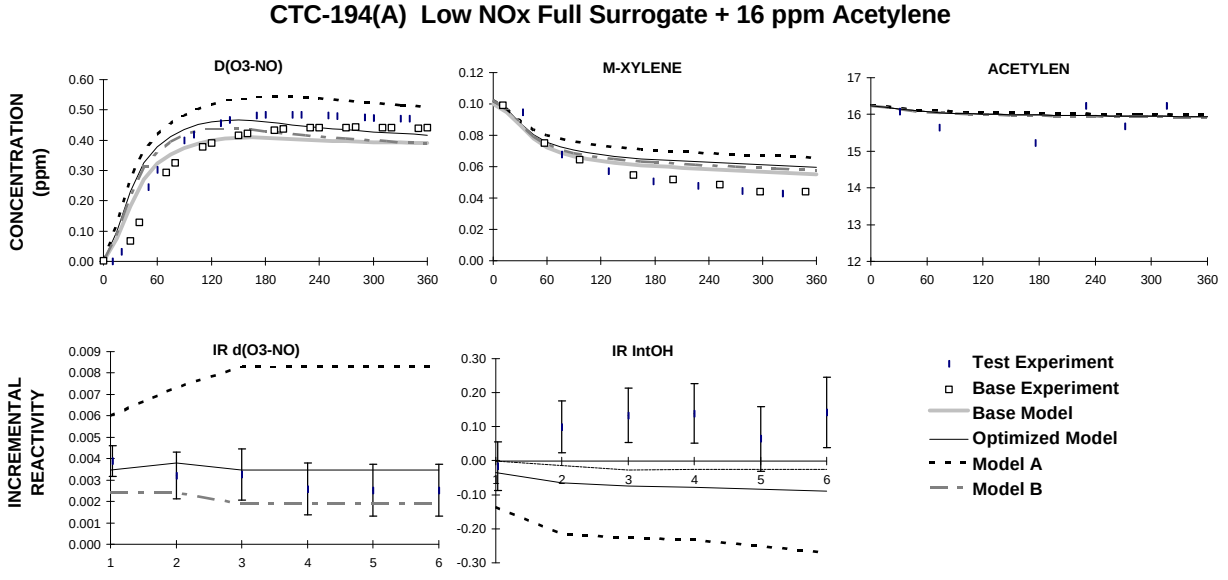

Figure 9. Plots of selected results of the low NOx full surrogate + acetylene experiment CTC-194.

in that it assumes that most of the glyoxal consumption observed by Plum et al. (1983), other than that involving formaldehyde formation, is due to formation of 2 HCO, rather than H_2 + CO. This indicates the results of the acetylene - NO_x experiments can only be explained if significant radical formation from glyoxal photolysis is assumed. Indeed, the data suggest that the overall radical yields from glyoxal photolysis may be somewhat higher than the upper limit indicated by the overall glyoxal quantum yields of Plum et al. (1983), since Model A, which uses this upper limit, slightly underpredicts O_3 formation in these experiments. Note that Model A assumes the maximum possible number of NO to NO_2 conversions in the acetylene + OH reaction (α=1), so making alternative assumptions concerning this reaction would result in even lower predicted O_3 yields in these experiments. This suggests that the actual quantum yields for radical production in glyoxal photolysis may be higher than the overall quantum yields reported by Plum et al. (1983).

The performance of Model A in simulating the incremental reactivity experiments are shown in Figures 3-9. Although this model gives reasonably good predictions of the effects of acetylene on d(O_3-NO) in the mini-surrogate experiments, it underpredicts the effects of acetylene on IntOH in all the runs, and significantly overpredicts its effects on d(O_3-NO) in the full surrogate runs. The consistent underprediction of IntOH by Model A is further evidence that the upper limit quantum yields reported by Plum et al. (1983) may be low. We can propose no other reasonable mechanism to explain this apparent excess radical initiation in this system, nor are there termination processes in our assumed acetylene or glyoxal which are of sufficient magnitude to account for this underprediction of the IntOH reactivities.

The overprediction of the d(O_3-NO) reactivities in the full surrogate experiments by Model A is also significant, and can be explained by the model overpredicting the number of NO to NO_2 conversions involved in the acetylene photooxidation process. As discussed elsewhere (Carter et al. 1993a, 1995a,d, d(O_3-NO) reactivities are affected both by the numbers of NO to NO_2 conversions in the photooxidation process, ad by the effects of the test compound on radical levels. In previous studies, we have found that the effects on radical levels are much less important in determining d(O_3-NO) reactivities in the full surrogate experiments than they are in the mini-surrogate runs (Carter et al. 1995a). The fact that Model A can approximately simulate the d(O_3-NO) reactivities in the mini-surrogate experiments while significantly underpredicting IntOH reactivities is explained by overprediction of NO to NO_2 conversions compensating for an underprediction of effects on radical levels. In the full surrogate runs, the underprediction of radicals is much less important in affecting the d(O_3-NO) reactivities, and thus the overprediction caused by the excess NO to NO_2 conversions becomes evident.

Most of the NO to NO_2 conversions predicted by Model A (and the SAPRC-90 model) is due to the assumed importance of vinoxy radical formation in the OH + acetylene system, via Pathway III, above. If the alternative mechanism, involving direct OH + glyoxal formation from the OH + acetylene + O_2 adduct, is assumed (Pathway II), then significantly fewer NO to NO_2 conversions are involved. This is assumed in Model B. However, in order to account for the observed ozone formation in the acetylene -

NO_x and mini-surrogate reactivity experiments, both of which are highly sensitive to radical initiation, it is necessary to assume higher quantum yields for radical formation from glyoxal photolysis than are consistent with the data from Plum et al. (1983). In the case of Model B, these data can only be fit if λ_1^{gly} = 385 nm, which gives a calculated overall Φ_1 of 0.056 for the spectral distribution of the light source used by Plum et al. (1983), a factor of 1.8 higher than their reported $\Phi_1+\Phi_3$ of 0.025.

Figures 2-9 show that Model B preforms significantly better in simulating the results of the acetylene - NO_x and all three types of incremental reactivity experiments. The ozone yields and NO oxidation rates in the acetylene - NO_x experiments are predicted quite well, except that Model B tends to slightly underpredict the maximum ozone in the higher acetylene run, where a true O_3 maximum was attained. The d(O_3-NO) reactivities are predicted reasonably well in both the mini-surrogate and full surrogate runs, in the latter case both under high and low NO_x conditions. The model performs much better in simulating the IntOH reactivities, though there is still a slight tendency for underprediction.

In Model C, the extent of NO to NO_2 conversion, controlled by α, the relative importance of the vinoxy vs the direct OH pathways in the acetylene + OH mechanism, is optimized along with the glyoxal radical quantum yields. Best fits are obtained with α = 0.21 (i.e, 55% direct OH route and 15% vinoxy route) and λ_1^{gly} = 380 nm. Note that this λ_1^{gly} value gives a calculated overall Φ_1 of 0.042 for the conditions of Plum et al. (1983), which is still a factor of ~1.7 higher than their reported upper limit. The occurrence of a small extent of vinoxy formation is consistent with the data of Schmidt et al. (1985), as noted above, with the fact that it is not the dominant route being consistent with the observations of Siese and Zetzsch (1995).

The performance of Model C in simulating the chamber data is shown on Figures 2-9. Figure 2 shows that it performs somewhat better than model B in simulating O_3 formation in the acetylene - NO_x run with the higher acetylene, and Figures 3-9 show that it preforms about equally well in simulating the d(O_3-NO) data in the reactivity runs. However, this model has a somewhat greater tendency to underpredict the IntOH reactivities than does Model B, though the difference between the two models is probably not significant given the experimental uncertainties. Overall, the fit to CTC-188(B) is the only experiment where there is a difference between the models which is greater than experimental uncertainty, with model C preforming somewhat better in this case.

In view of these results, we conclude that Models B and C perform sufficiently well in simulating the results of the chamber experiments to be suitable for estimating ozone impacts of acetylene in the atmosphere. Although the performance of Model C is slightly better in some (though not all) regards, given the uncertainties involved — both in modeling and measurements — these data cannot be considered to be definitive in choosing between these two alternatives. Therefore, the atmospheric ozone impact calculations, discussed in the following section, will be carried out using both Models B and C.

ATMOSPHERIC REACTIVITY CALCULATIONS

Incremental reactivities of VOCs have been shown to be highly dependent on environmental conditions, so reactivities measured in environmental chamber experiments cannot necessarily be assumed to be exactly the same as those under atmospheric conditions (Carter and Atkinson, 1989; Carter et al, 1995a). The only method available to obtain quantitative estimates of incremental reactivities of VOCs in ambient air pollution episodes is to conduct airshed model simulations of the episodes. Since these simulations cannot be any more reliable than the chemical mechanisms used, the major objective of this program was to assess the reliability of the acetylene mechanism for use in such simulations. This was discussed in the previous sections. In this section, we discuss the results of model simulations of its incremental reactivities in a variety of model scenarios representing ozone exceedence episodes in various areas in the United States (Baugues, 1990), and compare the results to incremental reactivities calculated for ethane, the compound used by the EPA as the criterion for determining "negligible" reactivity, and for the base ROG, the mixture representing total ROG emissions from all sources. Because the data from these experiments are insufficient to distinguish between models B and C, which are both reasonably consistent with most of the data, both models will be used in the atmospheric reactivity calculations for acetylene.

Scenarios Used for Reactivity Assessment

The set of airshed scenarios employed to assess the acetylene reactivity for this study is the same as those used for calculating the MIR and other reactivity scales (Carter, 1994a; Carter et al, 1993b). The objective is to use a set of scenarios which represents, as much as possible, a comprehensive distribution of the environmental conditions where unacceptable levels of ozone are formed. Although a set of scenarios has not been developed for the specific purpose of VOC reactivity assessment, the EPA developed an extensive set of scenarios for conducting analyses of effects of ROG and NO_x controls on ozone formation using the EKMA modeling approach (Gipson et al. 1981; Gipson and Freas, 1983; EPA, 1984; Gery et al. 1987; Baugues, 1990). The EKMA approach involves the use of single-cell box models to simulate how the ozone formation in one day episodes is affected by changes in ROG and NO_x inputs. Although single-cell models cannot represent realistic pollution episodes in great detail, they can represent dynamic injection of pollutants, time-varying changes of inversion heights, entrainment of pollutants from aloft as the inversion height raises, and time-varying photolysis rates, temperatures, and humidities (Gipson and Freas, 1981; EPA, 1984; Gipson, 1984; Hogo and Gery, 1988). Thus, they can be used to simulate a wide range of the chemical conditions which affect ozone formation from ROG and NO_x, and which affect VOC reactivity. Therefore, at least to the extent they are suitable for their intended purpose, an appropriate set of EKMA scenarios should also be suitable for assessing reactivities over a wide range of conditions.

Base Case Scenarios

The set of EKMA scenarios used in this study were developed by the United States EPA for assessing how various ROG and NO_x control strategies would affect ozone nonattainment in various areas of the country (Baugues, 1990). The characteristics of these scenarios and the methods used to derive their input data are described in more detail elsewhere (Baugues, 1990; Carter, 1994b). Briefly, 39 urban areas in the United States were selected based on geographical representativeness of ozone nonattainment areas and data availability, and a representative high ozone episode was selected for each. The initial non-methane organic carbon (NMOC) and NO_x concentrations, the aloft O_3 concentrations, and the mixing height inputs were based on measurement data for the various areas, the hourly emissions in the scenarios were obtained from the National Acid Precipitation Assessment Program emissions inventory (Baugues, 1990), and biogenic emissions were also included. Table 3 gives a summary of the urban areas represented and other selected characteristics of the scenarios.

Several changes to the scenario inputs were made based on discussions with the California ARB staff and others (Carter, 1994b). Two percent of the initial NO_x and 0.1% of the emitted NO_x in all the scenarios was assumed to be in the form of HONO. The photolysis rates were calculated using solar light intensities and spectra calculated by Jeffries (1991) for 640 meters, the approximate mid-point of the mixed layer during daylight hours. The composition of the NMOCs entrained from aloft was based on the analysis of Jeffries et al. (1989). The composition of the initial and emitted reactive organics was derived as discussed below. Complete listings of the input data for the scenarios are given elsewhere (Carter, 1994b).

This set of 39 EKMA scenarios are referred to as "base case" to distinguish them from the scenarios derived from them by adjusting NO_x inputs to yield standard conditions of NO_x availability as discussed below. No claim is made as to the accuracy of these scenarios in representing any real episode, but they are a result of an effort to represent, as accurately as possible given the available data and the limitations of the formulation of the EKMA model, the range of conditions occurring in urban areas throughout the United States. When developing general reactivity scales it is more important that the scenarios employed represent a realistic distribution of chemical conditions than accurately representing the details of any one particular episode.

The Base ROG mixture is the mixture of reactive organic gases used to represent the chemical composition of the initial and emitted anthropogenic reactive organic gases from all sources in the scenarios. Consistent with the approach used in the original EPA scenarios, the same mixture was used for all scenarios. The speciation for this mixture was derived by Croes (1991) based on an analysis of the EPA database (Jeffries et al. 1989) for the hydrocarbons and the 1987 Southern California Air Quality Study (SCAQS) database for the oxygenates (Croes et al. 1994; Lurmann et al. 1992). This mixture consists of 52% (by carbon) alkanes, 15% alkenes, 27% aromatics, 1% formaldehyde, 2% higher aldehydes, 1% ketones, and 2% acetylene. (Because the small amount of acetylene in the base ROG

Table 3. Summary of conditions of base case scenarios used for atmospheric reactivity assessment.

City, State	Calc. Max O_3 (ppb)	ROG /NO_x	NO_x /NO_x^{MOR}	Final Height (km)	Init.+Emit Base ROG (mmol m^{-2})	Aloft O_3 (ppb)
Atlanta, GA	174	7.3	0.7	2.1	12	63
Austin, TX	171	9.3	0.5	2.1	11	85
Baltimore, MD	304	5.2	1.1	1.2	17	84
Baton Rouge, LA	235	6.8	1.0	1.0	11	62
Birmingham, AL	233	6.9	0.6	1.8	13	81
Boston, MA	191	6.5	0.6	2.6	14	105
Charlotte, NC	142	7.8	0.3	3.0	7	92
Chicago, IL	273	11.6	0.5	1.4	25	40
Cincinnati, OH	192	6.4	0.8	2.8	17	70
Cleveland, OH	239	6.6	1.0	1.7	16	89
Dallas, TX	192	4.7	1.3	2.3	18	75
Denver, CO	195	6.3	1.2	3.4	29	57
Detroit, MI	229	6.8	0.8	1.8	17	68
El Paso, TX	177	6.6	1.1	2.0	12	65
Hartford, CT	166	8.4	0.5	2.3	11	78
Houston, TX	291	6.1	1.0	1.7	25	65
Indianapolis, IN	201	6.6	0.9	1.7	12	52
Jacksonville, FL	152	7.6	0.7	1.5	8	40
Kansas City, MO	151	7.1	0.6	2.2	9	65
Lake Charles, LA	282	7.4	0.7	0.5	7	40
Los Angeles, CA	546	7.6	1.0	0.5	23	100
Louisville, KY	203	5.5	0.9	2.5	14	75
Memphis, TN	218	6.8	0.7	1.8	15	58
Miami, FL	131	9.6	0.4	2.7	9	57
Nashville, TN	163	8.1	0.5	1.6	7	50
New York, NY	350	8.1	0.8	1.5	39	103
Philadelphia, PA	230	6.2	1.0	1.8	19	53
Phoenix, AZ	258	7.6	1.0	3.3	40	60
Portland, OR	161	6.5	0.7	1.6	6	66
Richmond, VA	225	6.2	0.8	1.9	16	64
Sacramento, CA	194	6.6	0.9	1.1	7	60
St Louis, MO	301	6.1	1.1	1.6	26	82
Salt Lake City, UT	179	8.5	0.6	2.2	11	85
San Antonio, TX	126	3.9	1.1	2.3	6	60
San Diego, CA	186	7.1	1.0	0.9	8	90
San Francisco, CA	222	4.8	1.8	0.7	25	70
Tampa, FL	217	4.4	1.1	1.0	8	68
Tulsa, OK	216	5.3	0.9	1.8	15	70
Washington, DC	268	5.3	0.9	1.4	13	99

mixture was lumped with other VOCs, the parameters used to derive its contribution to the total mixture were the same as in the base mechanism.) The detailed composition of this mixture is given elsewhere (Carter, 1994b).

Adjusted NO_x scenarios

Incremental reactivities in the base case scenarios would be expected to vary widely, since incremental reactivities depend on the ROG/NO_x ratio, and that ratio varies widely among the base case scenarios. To obtain reactivity scales for specified NO_x conditions, separate sets of scenarios, designated MIR (for maximum incremental reactivity), MOR (for maximum ozone reactivity), and Equal Benefit Incremental Reactivity (EBIR) were developed (Carter, 1994a). In the MIR scenarios, the NO_x inputs were adjusted so the base ROG mixture (and most other VOCs) have their highest incremental reactivity. This is representative of the highest NO_x conditions of relevance to VOC reactivity assessment because at higher NO_x levels O_3 yields become significantly suppressed, but is also the condition where O_3 is most sensitive to VOC emissions. In the MOR scenarios, the NO_x inputs were adjusted to yield the highest ozone concentration. In the EBIR scenarios, the NO_x inputs were adjusted so that the relative effects of NO_x reductions and total ROG reductions on peak ozone levels were equal. This represents the lowest NO_x condition of relevance for VOC reactivity assessment, because O_3 formation becomes more sensitive to NO_x emissions than VOC emissions at lower NO_x levels. The changes in the base case ROG/NO_x ratios which yielded the MOR scenarios are given in Table 3. As discussed by Carter (1994a) the MIR and EBIR ROG/NO_x ratios are respectively ~1.5 and ~0.7 times those for the MOR scenarios in all cases.

For this study, the MIR, MOIR, and EBIR reactivities were calculated using the "averaged conditions" scenarios with the corresponding adjusted NO_x conditions. As discussed by Carter (1994a), averaged conditions scenarios have all inputs derived by averaging the corresponding inputs of the base case scenarios, except that the NO_x inputs were adjusted to yield the specified NO_x conditions as discussed above. This is slightly different than the approach used by Carter (1994a) to derive the MIR, MOIR, and EBIR scales, which involved adjusting NO_x conditions separately for each of the 39 base case scenarios, and then averaging the reactivities derived from them. Since Carter (1994a) showed that both approaches yield essentially the same result. For this work use of the averaged conditions approach was preferred because it is computationally much more straightforward, and gives an equally a good indication of how the relative reactivities of compounds vary with varying NO_x conditions.

NO_x Conditions in the Base Case Scenarios

The variability of ROG/NO_x ratios in the base case scenarios suggest a variability of reactivity characteristics in the base case scenarios. However, as discussed previously (Carter, 1994a), the ROG/NO_x ratio is also variable in the MIR or MOR scenarios, despite the fact that the NO_x inputs in these scenarios are adjusted to yield a specified reactivity characteristic. Thus, the ROG/NO_x ratio, by itself, is not necessarily a good predictor of reactivity characteristics of a particular scenario. The NO_x/NO_x^{MOR} ratio is a much better predictor of this, with values greater than 1 indicating relatively high NO_x conditions

where ozone formation is more sensitive to VOCs, and values less than 1 indicating NO_x-limited conditions. NO_x/NO_x^{MOR} ratios less than 0.7 represent conditions where NO_x control is a more effective ozone control strategy than ROG control (Carter, 1994a). Note that more than half of the base case scenarios represent NO_x-limited conditions, and ~25% of them represent conditions where NO_x control is more beneficial than VOC control. A relatively small number of scenarios represent MIR or near MIR conditions. However, as discussed elsewhere (Carter, 1994a), this set of scenarios is based on near-worst-case conditions for ozone formation in each of the airsheds. Had scenarios representing less-than-worst-case conditions been included, one might expect a larger number of MIR or near MIR scenarios. This is because NO_x is consumed more slowly on days with lower light intensity or temperature, and thus the scenario is less likely to become NO_x-limited.

Incremental and Relative Reactivities

The incremental reactivity of a VOC in an airshed scenario is the change in ozone caused by adding the VOC to the emissions, divided by the amount of VOC added, calculated for sufficiently small amounts of added VOC that the incremental reactivity is independent of the amount added. The procedure used to calculate incremental reactivities in a scenario was as discussed in detail elsewhere (Carter, 1994a,b). The incremental reactivities depend on how the amount of VOC added are quantified. In this work, the added VOC was quantified on a mass basis, since this is how VOCs are regulated. In addition, the incremental reactivities also depend on how ozone impacts are quantified (Carter, 1994a). In this work, two different ozone quantifications were used, resulting in two different incremental reactivities being calculated for a VOC in a scenario. These are discussed below.

The "Ozone Yield" incremental reactivities measure the effect of the VOC on the total amount of ozone formed in the scenario at the time of its maximum concentration. In this work, this is quantified as grams O_3 formed per gram VOC added. This gives the same ratios of incremental reactivities as reactivities calculated from peak ozone concentrations, but is preferred because it permits magnitudes of reactivities in scenarios with differing dilutions to be compared on the same basis. Most previous recent studies of incremental reactivity (Dodge, 1984; Carter and Atkinson, 1987, 1989, Chang and Rudy, 1990; Jeffries and Crouse, 1991) have all been based on ozone yield or peak ozone concentration reactivities.

The ozone yield incremental reactivities do not necessarily measure the effect of the VOC on exposure to unacceptable levels of ozone because it does not measure how long high levels of ozone are present. A quantification which reflects this is integrated ozone over the standard, which is defined as the sum of the hourly ozone concentrations for the hours when ozone exceeds the standard in the base case scenarios (Carter 1994a). In the previous work (Carter, 1994a), we used the California ozone standard of 90 ppb, but in this work we will use the national standard of 0.12 ppm. Reactivities relative to this quantification of ozone are referred to by the abbreviation "$IntO_3$>0.12" reactivities.

Relative reactivities are ratios of incremental reactivities to incremental reactivities of some standard VOC or mixture. Since these are the quantities which usually are the most relevant to control strategy applications, the results in this work will be given in terms of relative reactivities. In our previous work (Carter 1991, 1994a), we used the incremental reactivity of the base ROG mixture, i.e., the mixture representing ROG pollutants from all sources, as the standard to define relative reactivities. However, because of the tendency within the EPA to consider ethane as the standard to define exempt vs controlled VOCs, in this work we will present reactivity ratios where ethane is used as the standard.

Reactivity Scales

A reactivity scale is a set of incremental or relative reactivities for a particular scenario or group of scenarios. Two types of reactivity scales will be discussed here, "base case" scales and adjusted NO_x scales. Base case scales are simply the set of incremental or relative reactivities in the 39 base case scenarios. Two sets of scales are derived — those based ozone yield reactivities and those based on $Int O_3$>0.12 reactivities. In the previous work (Carter, 1991, 1994a) we derived various multi-scenario scales from the individual base case scales by averaging or other procedures, to evaluate alternative approaches for developing single reactivity scales for applications requiring single scales. However, the decision of whether to exempt a VOC should not be made based on relative reactivities of a single scale, but on a knowledge of the range of relative reactivities for a variety of conditions. Thus in this work we present the distribution of base case relative reactivities for the 39 individual scenarios rather than developing aggregated or optimum scales which represent the distribution by single numbers.

The adjusted NO_x incremental reactivity scales refer to the MIR (maximum incremental reactivity), MOIR (maximum ozone incremental reactivity), or the EBIR (Equal Benefit Incremental Reactivity) scales. These consist of reactivities in averaged conditions scenarios where NO_x inputs were adjusted to yield MIR, MOR or EBIR conditions, respectively. Reactivities in the MIR scale are of interest because the California Air Resources Board utilized an MIR scale to calculate reactivity adjustment factors in its clean fuels/low emissions vehicle regulations (CARB, 1993). The justification for using this scale in applications requiring a single scale (such as the CARB vehicle regulations) is that it reflects conditions where ozone is most sensitive to changes in VOC emissions, and complements NO_x control, which is most effective for reducing ozone under conditions where the MIR scale is least applicable (Carter, 1994a). The MOIR scale is preferred by many as an alternative for such applications because it reflects conditions which are most favorable for ozone, and is more representative of the distribution of conditions in the base case scenarios (Carter 1994a). Most other alternative reactivity scales which might be appropriate for assessing VOC control strategies (i.e., excluding scales representing highly NO_x-limited conditions where ozone is more sensitive to NO_x than VOCs) tend to fall in the range defined by the MIR and MOIR scales. Since the EBIR scale represents lower NO_x conditions where O_3 is less sensitive to VOCs, its use in applications requiring a single scale has not been considered. However, it is useful for assessing how reactivities depend on NO_x conditions.

Note that the MIR, MOIR, EBIR and base case scales derived in this work are somewhat different from those calculated previously (Carter, 1994a; Carter et al, 1993b) because an updated chemical mechanism was used. In addition, as indicated above, for computational efficiency the MIR, MOIR and EBIR scales were calculated using a single averaged conditions scenario, rather than the average of the adjusted NO_x base case scenarios as done previously (Carter, 1994a).

Calculated Relative Reactivities of Acetylene

Table 4 lists the ozone yield and $Int O_3$>0.12 reactivities calculated for acetylene relative to ethane and relative to the total of all emitted VOCs for the base case and the adjusted NO_x averaged conditions scenarios. Both mechanisms predict that the ozone forming potential of acetylene (on a gram basis) is ~20-25% that of the average of all emitted VOCs, regardless of whether ozone is quantified by ozone yield or integrated O_3 over the standard. Model C tends to predict slightly higher ozone impacts than model B under relatively low NO_x conditions (by ~20% in the EBIR scales), though the two model give very similar reactivity predictions under the relatively high NO_x MIR conditions. Model C has somewhat more NO to NO_2 conversions in the acetylene mechanism, but slightly less radical input from glyoxal photolysis, relative to Model B. Under MIR conditions these two opposing factors apparently tend to cancel out, yielding similar net reactivities for both mechanisms. The differences in radical inputs tend to become less important as NO_x is reduced, resulting in the differences in numbers of NO to NO_x becoming relatively more important. For that reason, Model C tends to predict somewhat greater ozone impacts than Model B in the lower NO_x scenarios. However, given the other and variabilities involved in reactivity assessment, the differences between the predictions of these models is relatively small.

Table 4 shows that the reactivity of acetylene relative to ethane varies somewhat depending on the scenario, model, and ozone quantification method. As was the case with acetone (Carter et al. 1993b), this variability is due more to variability in the relative reactivity of ethane than that for acetylene. The reactivity of acetylene relative to ethane is the highest under high NO_x, MIR conditions, where it is calculated to cause approximately three times more O_3 formation than ethane on a per gram basis. Under lower NO_x or base case conditions, the reactivity relative to ethane ranges from ~1.25 to 2, depending on the scenario, mechanism, and how ozone is quantified. The reactivities relative to ethane in the lower NO_x scenarios tend to be higher with Model C, and also tend to be higher when O_3 is quantified by integrated ozone over the standard. If Model C is assumed, there are no scenarios where acetylene is calculated to have a lower ozone impact per gram than ethane. If Model B is assumed, then acetylene is calculated to have a lower ozone yield reactivity than ethane in 36% of the base case scenarios but to have lower integrated ozone reactivities in only 3% of these scenarios. Therefore, Model C predicts that acetylene is always more reactive than ethane, while Model B predicts that acetylene usually is. Overall, regardless of what model is assumed, it appears that acetylene is somewhat more reactive than ethane, though not by a large margin.

Table 4. Summary of calculated relative incremental reactivities (gram basis) for acetylene, ethane, and the total of all emitted VOCs.

Scenario	Relative to the Total of Emitted VOCS (Base ROG)						Reactivity Relative to Ethane				
	O_3 Yield Reactivity			$IntO_3$ >0.12 Reactivity			O_3 Yield			$IntO_3$ >0.12	
	Acetylene		Ethane	Acetylene		Ethane	Acetylene			Acetylene	
	C	B		C	B		C	B		C	B
Averaged Conditions											
Max React	0.24	0.23	0.08	0.22	0.21	0.07	3.08	2.99		3.10	3.01
Max Ozone	0.24	0.21	0.15	0.22	0.20	0.10	1.64	1.45		2.25	2.07
Equal Benefit	0.23	0.19	0.19	0.21	0.18	0.12	1.24	1.01		1.73	1.47
Base Case											
Average	**0.24**	**0.20**	**0.17**	**0.22**	**0.19**	**0.11**	**1.50**	**1.28**		**2.00**	**1.77**
St.Dev	**0.12**	**0.15**	**0.23**	**0.10**	**0.12**	**0.25**	**0.36**	**0.44**		**0.27**	**0.33**
ATL GA	0.25	0.22	0.17	0.23	0.20	0.12	1.53	1.31	#	1.94	1.70
AUS TX	0.24	0.19	0.19	0.21	0.17	0.14	1.23	1.00	#	1.55	1.24
BAL MD	0.21	0.18	0.15	0.19	0.18	0.09	1.39	1.18	#	2.24	2.06
BAT LA	0.30	0.26	0.15	0.26	0.23	0.10	1.94	1.72	#	2.51	2.26
BIR AL	0.24	0.19	0.23	0.20	0.17	0.13	1.03	0.82	#	1.55	1.32
BOS MA	0.22	0.18	0.20	0.19	0.16	0.12	1.12	0.89	#	1.56	1.31
CHA NC	0.21	0.16	0.20	0.20	0.15	0.16	1.04	0.79	#	1.22	0.93
CHI IL	0.32	0.22	0.27	0.25	0.19	0.14	1.17	0.83	#	1.79	1.37
CIN OH	0.20	0.17	0.19	0.19	0.17	0.12	1.08	0.88	#	1.56	1.36
CLE OH	0.23	0.19	0.15	0.20	0.19	0.09	1.53	1.32	#	2.31	2.10
DAL TX	0.27	0.26	0.12	0.24	0.22	0.09	2.33	2.22	#	2.73	2.60
DEN CO	0.23	0.21	0.11	0.22	0.20	0.07	2.17	1.92	#	3.00	2.80
DET MI	0.21	0.17	0.20	0.19	0.17	0.11	1.09	0.88	#	1.73	1.52
ELP TX	0.26	0.24	0.11	0.23	0.22	0.08	2.27	2.09	#	2.94	2.76
HAR CT	0.21	0.16	0.20	0.20	0.16	0.15	1.03	0.80	#	1.39	1.13
HOU TX	0.24	0.20	0.18	0.21	0.19	0.11	1.32	1.11	#	1.89	1.67
IND IN	0.23	0.20	0.16	0.22	0.20	0.11	1.49	1.28	#	2.11	1.92
JAC FL	0.27	0.23	0.16	0.25	0.21	0.13	1.66	1.40	#	1.89	1.59
KAN MO	0.21	0.16	0.19	0.20	0.16	0.14	1.06	0.84	#	1.40	1.15
LAK LA	0.32	0.25	0.22	0.28	0.22	0.14	1.44	1.12	#	2.03	1.65
LOS CA	0.21	0.18	0.15	0.20	0.18	0.08	1.43	1.21	#	2.34	2.08
LOU KY	0.25	0.21	0.19	0.24	0.21	0.13	1.34	1.15	#	1.78	1.57
MEM TN	0.24	0.19	0.20	0.22	0.18	0.13	1.19	0.96	#	1.64	1.39
MIA FL	0.24	0.18	0.18	0.23	0.18	0.17	1.31	1.01	#	1.35	1.03
NAS TN	0.27	0.22	0.23	0.24	0.20	0.19	1.14	0.95	#	1.27	1.04
NEW NY	0.23	0.14	0.17	0.20	0.16	0.09	1.37	0.85	#	2.30	1.84
PHI PA	0.22	0.19	0.17	0.21	0.18	0.11	1.34	1.12	#	1.88	1.66
PHO AZ	0.22	0.19	0.16	0.20	0.19	0.09	1.38	1.20	#	2.13	1.96
POR OR	0.23	0.19	0.17	0.23	0.20	0.14	1.33	1.12	#	1.64	1.40
RIC VA	0.20	0.16	0.18	0.19	0.17	0.12	1.08	0.87	#	1.66	1.45
SAC CA	0.25	0.23	0.17	0.24	0.22	0.12	1.50	1.33	#	2.00	1.82
SAI MO	0.22	0.18	0.14	0.19	0.18	0.08	1.55	1.30	#	2.38	2.16
SAL UT	0.22	0.18	0.19	0.20	0.18	0.12	1.18	0.99	#	1.75	1.54
SAN TX	0.26	0.25	0.13	0.25	0.24	0.12	2.10	1.98	#	2.16	2.03
SDO CA	0.23	0.20	0.12	0.22	0.19	0.09	1.97	1.71	#	2.40	2.12
SFO CA	0.21	0.21	0.05	0.20	0.19	0.05	3.91	3.82	#	3.96	3.87
TAM FL	0.27	0.24	0.13	0.24	0.22	0.09	2.03	1.83	#	2.61	2.41
TUL OK	0.22	0.18	0.18	0.20	0.18	0.11	1.26	1.03	#	1.83	1.60
WAS DC	0.23	0.18	0.19	0.20	0.17	0.11	1.18	0.96	#	1.76	1.52

CONCLUSIONS

The decision whether it is appropriate to regulate a compound as an ozone precursor requires a qualitative assessment of its ozone impacts under a variety of environmental conditions. This involves developing a chemical mechanism for the compounds atmospheric reactions which can be reliably used in airshed models to predict its atmospheric reactivity. Until this study, reactivity estimates for acetylene were uncertain because of lack of sufficient data to test model predictions. The objective of this study was to provide the data needed to verify the predictive capabilities of atmospheric photooxidation mechanisms for this compound, and thus allow for more reliable estimates of its atmospheric ozone impacts. We believe this program addressed this objective.

The results of this study clearly show that the mechanism previously assumed for acetylene's atmospheric reactions are incorrect in at least two important respects. First, the data indicate that acetylene has significantly more radical sources in its mechanism than predicted by the previous model. This radical input can only be explained only if glyoxal, its major known product, photolyzes with significantly higher quantum yields for radical formation than has previously been assumed to be the case. Information concerning the quantum yields for glyoxal photolysis under atmospheric conditions is limited to a single study (Plum et al. 1983), which obtained an overall quantum yield for all photodecomposition processes which is a almost a factor of two lower than the radical input required to fit our data. Therefore, there is a inconsistency between our data and the data of Plum et al. (1983). However, the study of Plum et al. (1983) have been shown to give absorption cross sections for methyl glyoxal which are a factor of 2 too high (Atkinson et al. 1992, 1997; Meller et al. 1991), suggesting that there may be problems with the glyoxal data as well. Thus, the factor of ~2 discrepancy may not be outside the uncertainty of their data. However, the method they employed was such that incorrect absorption cross sections would necessarily yield incorrect overall photolysis rates. Clearly, more data are needed concerning the glyoxal photolysis under atmospheric conditions.

This study also showed that the acetylene photooxidation reaction involves significantly fewer NO to NO_2 conversions than had been assumed previously. The chamber experiments can only be simulated if it is assumed that the reaction of OH radicals with acetylene involves direct OH regeneration, without any NO to NO_2 conversions, anywhere between ~50 to ~70% of the time. The available data indicate that ~30% of the time the OH + acetylene adduct reacts to form HCO + formic acid, with the remaining ~70% of the reaction involving glyoxal formation, but it was uncertain whether the glyoxal formation involved the intermediacy of vinoxy radicals, or whether it was formed directly by the OH + acetylene + O_2 adduct decomposing to acetylene + OH. This direct decomposition must be the major process involved in glyoxal formation, though the chamber data are best fit if it is assumed that at least some (~20%) of the glyoxal is also being formed via the vinoxy route. However, modeling chamber data is a highly indirect way to

obtain mechanistic information, and clearly more direct studies are necessary to more clearly indicate the involvement of vinoxy radicals in the reactions of OH radicals with acetylene under *atmospheric* conditions.

If the acetylene mechanism is revised to assume fewer NO to NO_2 conversions and higher radical quantum yields from glyoxal photolysis, then good agreement between model simulations and chamber experiments could be obtained. Two alternative mechanisms were developed which gave satisfactory simulations of the data: One which assumed that all vinoxy radicals were not involved as intermediates, and that the overall radical quantum for glyoxal photolysis in our experiments was 0.044, and the other which assumed that ~20% of the glyoxal was formed via a vinoxy intermediate, and the overall radical quantum yield from glyoxal was 0.040. The conditions of the experiments employed were sufficiently varied to test various aspects of the mechanisms, and although the second mechanism performed slightly better in some respects, the data were insufficient to judge which was necessarily correct.

If these experimentally-verified modified acetylene mechanisms are assumed, the atmospheric ozone impact of acetylene is calculated to have approximately 20% the ozone impact, on a per gram basis, as the average of all VOC emissions, and approximately 1.25 - 3 times the ozone impact of ethane. The ozone impacts relative to ethane appear to be somewhat higher under high NO_x, MIR conditions, and when ozone impacts are quantified by integrated ozone over the standard, as opposed to maximum ozone yields. Alternative acetylene mechanisms which fit the chamber data give slightly different reactivities in the lower NO_x scenarios, but these differences are not significant given the other uncertainties and scenario-to-scenario variabilities involved in VOC reactivity assessment. We conclude that while acetylene is a relatively low reactivity compound, it must be judged to have a somewhat higher ozone impact than does ethane, the compound the EPA uses as the standard to determine VOC exemptions.

REFERENCES

Atkinson, R. (1989): "Kinetics and Mechanisms of the Gas-Phase Reactions of the Hydroxyl Radical with Organic Compounds," J. Phys. Chem. Ref. Data, Monograph no 1.

Atkinson, R., D. L. Baulch, R. A. Cox, R. F. Hampson, Jr., J. A. Kerr, and J. Troe (1992): "Evaluated Kinetic and Photochemical Data for Atmospheric Chemistry. Supplement IV. IUPAC Subcommittee on Gas Kinetic Data Evaluation for Atmospheric Chemistry," J. Phys. Chem. Ref. Data 21, 1125-1568.

Atkinson, R., D. L. Baulch, R. A. Cox, R. F. Hampson, Jr., J. A. Kerr, M. J. Rossi, and J. Troe (1997): "Evaluated Kinetic, Photochemical and Heterogeneous Data for Atmospheric Chemistry: Supplement V., IUPAC Subcommittee on Gas Kinetic Data Evaluation for Atmospheric Chemistry," J. Phys. Chem. Ref. Data, in press.

Baugues, K. (1990): "Preliminary Planning Information for Updating the Ozone Regulatory Impact Analysis Version of EKMA," Draft Document, Source Receptor Analysis Branch, Technical Support Division, U. S. Environmental Protection Agency, Research Triangle Park, NC, January.

Bohn, B., M. Seise and C. Zetzsch (1996): "Kinetics of the OH + C_2H_2 Reaction in the Presence of O_2," J. Chem. Soc. Faraday Trans. 92, 1459-1466.

CARB (1993): "Proposed Regulations for Low-Emission Vehicles and Clean Fuels — Staff Report and Technical Support Document," California Air Resources Board, Sacramento, CA, August 13, 1990. See also Appendix VIII of "California Exhaust Emission Standards and Test Procedures for 1988 and Subsequent Model Passenger Cars, Light Duty Trucks and Medium Duty Vehicles," as last amended September 22, 1993. Incorporated by reference in Section 1960.1 (k) of Title 13, California Code of Regulations.

Calvert, J. G., and J. N. Pitts, Jr. (1966): Photochemistry, John Wiley and Sons, New York.

Carter, W. P. L. (1990): "A Detailed Mechanism for the Gas-Phase Atmospheric Reactions of Organic Compounds," Atmos. Environ., 24A, 481-518.

Carter, W. P. L. (1991): "Development of Ozone Reactivity Scales for Volatile Organic Compounds", EPA-600/3-91/050, August.

Carter, W. P. L. (1994a): "Development of Ozone Reactivity Scales for Volatile Organic Compounds," J. Air & Waste Manage. Assoc., 44, 881-899.

Carter, W. P. L. (1994b): "Calculation of Reactivity Scales Using an Updated Carbon Bond IV Mechanism," Draft Report Prepared for Systems Applications International Under Funding from the Auto/Oil Air Quality Improvement Research Program, April 12.

Carter, W. P. L. (1995): "Computer Modeling of Environmental Chamber Measurements of Maximum Incremental Reactivities of Volatile Organic Compounds," Atmos. Environ., 29, 2513-2517.

Carter, W. P. L. and R. Atkinson (1987): "An Experimental Study of Incremental Hydrocarbon Reactivity," Environ. Sci. Technol., 21, 670-679

Carter, W. P. L. and R. Atkinson (1989): "A Computer Modeling Study of Incremental Hydrocarbon Reactivity", Environ. Sci. Technol., 23, 864.

Carter, W. P. L., and F. W. Lurmann (1990): "Evaluation of the RADM Gas-Phase Chemical Mechanism," Final Report, EPA-600/3-90-001.

Carter, W. P. L. and F. W. Lurmann (1991): "Evaluation of a Detailed Gas-Phase Atmospheric Reaction Mechanism using Environmental Chamber Data," Atm. Environ. 25A, 2771-2806.

Carter, W. P. L., J. A. Pierce, I. L. Malkina, D. Luo and W. D. Long (1993a): "Environmental Chamber Studies of Maximum Incremental Reactivities of Volatile Organic Compounds," Report to Coordinating Research Council, Project No. ME-9, California Air Resources Board Contract No. A032-0692; South Coast Air Quality Management District Contract No. C91323, United States Environmental Protection Agency Cooperative Agreement No. CR-814396-01-0, University Corporation for Atmospheric Research Contract No. 59166, and Dow Corning Corporation. April 1.

Carter, W. P. L, D. Luo, I. L. Malkina, and J. A. Pierce (1993b): "An Experimental and Modeling Study of the Photochemical Ozone Reactivity of Acetone," Final Report to Chemical Manufacturers Association Contract No. KET-ACE-CRC-2.0. December 10.

Carter, W. P. L., D. Luo, I. L. Malkina, and J. A. Pierce (1995a): "Environmental Chamber Studies of Atmospheric Reactivities of Volatile Organic Compounds. Effects of Varying ROG Surrogate and NO_x," Final report to Coordinating Research Council, Inc., Project ME-9, California Air Resources Board, Contract A032-0692, and South Coast Air Quality Management District, Contract C91323. March 24.

Carter, W. P. L., D. Luo, I. L. Malkina, and D. Fitz (1995b): "The University of California, Riverside Environmental Chamber Data Base for Evaluating Oxidant Mechanism. Indoor Chamber Experiments through 1993," Report submitted to the U. S. Environmental Protection Agency, EPA/AREAL, Research Triangle Park, NC., March 20..

Carter, W. P. L., D. Luo, I. L. Malkina, and J. A. Pierce (1995c): "Environmental Chamber Studies of Atmospheric Reactivities of Volatile Organic Compounds. Effects of Varying Chamber and Light Source," Final report to National Renewable Energy Laboratory, Contract XZ-2-12075, Coordinating Research Council, Inc., Project M-9, California Air Resources Board, Contract A032-0692, and South Coast Air Quality Management District, Contract C91323, March 26.

Carter, W. P. L., J. A. Pierce, D. Luo, and I. L. Malkina (1995d): "Environmental Chamber Study of Maximum Incremental Reactivities of Volatile Organic Compounds," Atmos. Environ. 29, 2499-2511.

Carter, W. P. L., D. Luo, and I. L. Malkina (1997): "Environmental Chamber Studies for Development of an Updated Photochemical Mechanism for VOC Reactivity Assessment," Draft final report to California Air Resources Board Contract 92-345, Coordinating Research Council Project M-9, and National Renewable Energy Laboratory Contract ZF-2-12252-07. March 10.

Chang, T. Y. and S. J. Rudy (1990): "Ozone-Forming Potential of Organic Emissions from Alternative-Fueled Vehicles," Atmos. Environ., 24A, 2421-2430.

Croes, B. E., Technical Support Division, California Air Resources Board, personal communication (1991).

Croes, B. E., et al. (1994): "Southern California Air Quality Study Data Archive," Research Division, California Air Resources Board.

Dodge, M. C. (1984): "Combined effects of organic reactivity and NMHC/NOx ratio on photochemical oxidant formation -- a modeling study," Atmos. Environ., 18, 1657.

EPA (1984): "Guideline for Using the Carbon Bond Mechanism in City-Specific EKMA," EPA-450/4-84-005, February.

Gery, M. W., R. D. Edmond and G. Z. Whitten (1987): "Tropospheric Ultraviolet Radiation. Assessment of Existing Data and Effects on Ozone Formation," Final Report, EPA-600/3-87-047, October.

Gipson, G. L., W. P. Freas, R. A. Kelly and E. L. Meyer (1981): "Guideline for Use of City-Specific EKMA in Preparing Ozone SIPs, EPA-450/4-80-027, March.

Gipson, G. L. and W. P. Freas (1983): "Use of City-Specific EKMA in the Ozone RIA," U. S. Environmental Protection Agency, July.

Gipson, G. L. (1984): "Users Manual for OZIPM-2: Ozone Isopleth Plotting Package With Optional Mechanism/Version 2," EPA-450/4-84-024, August.

Hatakeyama, S., N. Washida, and H. Akimoto, (1986): "Rate Constants and Mechanisms for the Reaction of OH (OD) Radicals with Acetylene, Propyne, and 2-Butyne in Air at 297 ± 2 K," J. Phys Chem. 90, 173-178.

Hack, W., K. Hoyermann, R. Sievert, and H. Gg. Wagner (1983): Oxid. Commun. 5, 101.

Hogo, H. and M. W. Gery (1988): "Guidelines for Using OZIPM-4 with CBM-IV or Optional Mechanisms. Volume 1. Description of the Ozone Isopleth Plotting Package Version 4", Final Report for EPA Contract No. 68-02-4136, Atmospheric Sciences Research Laboratory, Research Triangle Park, NC. January.

Jeffries, H. E., K. G. Sexton, J. R. Arnold, and T. L. Kale (1989): "Validation Testing of New Mechanisms with Outdoor Chamber Data. Volume 2: Analysis of VOC Data for the CB4 and CAL Photochemical Mechanisms," Final Report, EPA-600/3-89-010b.

Jeffries, H. E. and R. Crouse (1991): "Scientific and Technical Issues Related to the Application of Incremental Reactivity. Part II: Explaining Mechanism Differences," Report prepared for Western States Petroleum Association, Glendale, CA, October.

Jeffries, H. E. (1991): "UNC Solar Radiation Models," unpublished draft report for EPA Cooperative Agreements CR813107, CR813964 and CR815779". Undated.

Johnson, G. M. (1983): "Factors Affecting Oxidant Formation in Sydney Air," in "The Urban Atmosphere -- Sydney, a Case Study." Eds. J. N. Carras and G. M. Johnson (CSIRO, Melbourne), pp. 393-408.

Langford, A. O, and C. B. Moore (1984): J. Chem. Phys. 80, 4211.

Lurmann, F. W. and H. H. Main (1992): "Analysis of the Ambient VOC Data Collected in the Southern California Air Quality Study," Final Report to California Air Resources Board Contract No. A832-130, February.

Meller, R., W. Raber, J. N. Crowley, M. E. Jenkin, and G. K. Moortgat (1991): J. Photochem. Photobiol., A: Chemistry 62, 163.

Pitts, J. N., Jr., E. Sanhueza, R. Atkinson, W. P. L. Carter, A. M. Winer, G. W. Harris, and C. N. Plum (1984): "An Investigation of the Dark Formation of Nitrous Acid in Environmental Chambers," Int. J. Chem. Kinet., 16, 919-939.

Plum, C. N., Sanhuesa, E., Atkinson, R., Carter W. P. L. and Pitts, J. N., Jr. (1983): "OH Radical Rate Constants and Photolysis Rates of α-Dicarbonyls," Environ. Sci. Technol. 17, 479-484.

Siese, M. and C. Zetzsch (1995): "The Addition of OH to Acetylene and Consecutive Reactions of the Adduct with O_2," Zeitsch. fur Phys. Chem. 188, 75-89.

Schmidt, V., G. Y. Zhu, K. H. Becker and E. H. Fink (1985): Ber. Bunsenges. Phys. Chem 89 323.

Tuazon, E. C., R. Atkinson, C. N. Plum, A. M. Winer, and J. N. Pitts, Jr. (1983): "The Reaction of Gas-Phase N_2O_5 with Water Vapor," Geophys. Res. Lett. 10, 953-956.

Zafonte, L., P. L. Rieger, and J. R. Holmes (1977): "Nitrogen Dioxide Photolysis in the Los Angeles Atmosphere," Environ. Sci. Technol. 11, 483-487.

APPENDIX A
LISTING OF THE CHEMICAL MECHANISM

The chemical mechanism used in the environmental chamber and atmospheric model simulations discussed in this report is given in Tables A-1 through A-4. Table A-1 lists the species used in the mechanism, Table A-2 gives the reactions and rate constants, Table A-3 gives the parameters used to calculate the rates of the photolysis reactions, and Table A-4 gives the values and derivations of the chamber-dependent parameters used when modeling the environmental chamber experiments. Footnotes to Table A-2 indicate the format used for the reaction listing.

Table A-1. List of species in the chemical mechanism used in the model simulations for this study.

Name	Description
Constant Species.	
O2	Oxygen
M	Air
H2O	Water
Active Inorganic Species.	
O3	Ozone
NO	Nitric Oxide
NO2	Nitrogen Dioxide
NO3	Nitrate Radical
N2O5	Nitrogen Pentoxide
HONO	Nitrous Acid
HNO3	Nitric Acid
HNO4	Peroxynitric Acid
HO2H	Hydrogen Peroxide
Active Radical Species and Operators.	
HO2.	Hydroperoxide Radicals
RO2.	Operator to Calculate Total Organic Peroxy Radicals
RCO3.	Operator to Calculate Total Acetyl Peroxy Radicals
Active Reactive Organic Product Species.	
CO	Carbon Monoxide
HCHO	Formaldehyde
CCHO	Acetaldehyde
RCHO	Lumped C3+ Aldehydes
ACET	Acetone
MEK	Lumped Ketones

Table A-1, (continued)

Name	Description
PHEN	Phenol
CRES	Cresols
BALD	Aromatic aldehydes (e.g., benzaldehyde)
GLY	Glyoxal (formed from aromatics an SAPRC-90 acetylene model)
GLY-A	Glyoxal (formed from acetylene Model A)
GLY-B	Glyoxal (formed from acetylene Model B)
GLY-C	Glyoxal (formed from acetylene Model C)
MGLY	Methyl Glyoxal
AFG1	Reactive Aromatic Fragmentation Products from benzene and naphthalene
AFG2	Other Reactive Aromatic Fragmentation Products
RNO3	Organic Nitrates
NPHE	Nitrophenols
PAN	Peroxy Acetyl Nitrate
PPN	Peroxy Propionyl Nitrate
GPAN	PAN Analogue formed from Glyoxal
PBZN	PAN Analogues formed from Aromatic Aldehydes
-OOH	Operator Representing Hydroperoxy Groups
ISOPROD	Lumped reactive isoprene products
Non-Reacting Species	
CO2	Carbon Dioxide
-C	"Lost Carbon"
-N	"Lost Nitrogen"
H2	Hydrogen
Steady State Species and Operators.	
HO.	Hydroxyl Radicals
O	Ground State Oxygen Atoms
O*1D2	Excited Oxygen Atoms
RO2-R.	Peroxy Radical Operator representing NO to NO_2 conversion with HO_2 formation.
RO2-N.	Peroxy Radical Operator representing NO consumption with organic nitrate formation.
RO2-NP.	Peroxy Radical Operator representing NO consumption with nitrophenol formation
R2O2.	Peroxy Radical Operator representing NO to NO_2 conversion.
CCO-O2.	Peroxy Acetyl Radicals
C2CO-O2.	Peroxy Propionyl Radicals
HCOCO-O2.	Peroxyacyl Radical formed from Glyoxal
BZ-CO-O2.	Peroxyacyl Radical formed from Aromatic Aldehydes
HOCOO.	Intermediate formed in Formaldehyde + HO_2 reaction
BZ-O.	Phenoxy Radicals
BZ(NO2)-O.	Nitratophenoxy Radicals
HOCOO.	Radical Intermediate formed in the HO_2 + Formaldehyde system.
(HCHO2)	Excited Criegee biradical formed from $=CH_2$ groups
(CCHO2)	Excited Criegee biradical formed from $=CHCH_3$ groups
(RCHO2)	Excited Criegee biradicals formed from =CHR groups, where R not CH_3

Table A-1, (continued)

Name	Description
(C(C)CO2)	Excited Criegee biradical formed from $=C(CH_3)_2$ groups
(C(R)CO2)	Excited Criegee biradicals formed from $=C(CH_3)R$ or CR_2 groups
(BZCHO2)	Excited Criegee biradicals formed from styrenes
(C:CC(C)O2)	Excited Criegee biradical formed from ISOPROD
(C:C(C)CHO2)	Excited Criegee biradical formed from ISOPROD
(C2(O2)CHO)	Excited Criegee biradical formed from ISOPROD
(HOCCHO2)	Excited Criegee biradical formed from ISOPROD
Hydrocarbon species represented explicitly	
ETHANE	Ethane
N-C4	n-Butane
N-C6	n-Hexane
N-C8	n-Octane
ETHE	Ethene
PROPENE	Propene
T-2-BUTE	trans-2-Butene
TOLUENE	Toluene
M-XYLENE	m-Xylene
ACETYLEN	Acetylene
Hydrocarbon species represented explicitly in EKMA model simulations	
CH4	Methane (EKMA simulations only)
ISOP	Isoprene (EKMA simulations only)
APIN	α-Pinene (EKMA simulations only)
UNKN	Unknown biogenics (EKMA simulations only)
Lumped species used to represent the Base ROG mixture in the EKMA model simulations.	
ALK1	Alkanes and other saturated compounds with $k_{OH} < 10^4$ ppm^{-1} min^{-1}.
ALK2	Alkanes and other saturated compounds with $k_{OH} \geq 10^4$ ppm^{-1} min^{-1}.
ARO1	Aromatics with $k_{OH} < 2x10^4$ ppm^{-1} min^{-1}.
ARO2	Aromatics with $k_{OH} \geq 2x10^4$ ppm^{-1} min^{-1}.
OLE1	Alkenes (other than ethene) with $k_{OH} < 7x10^4$ ppm^{-1} min^{-1}.
OLE2	Alkenes with $k_{OH} \geq 7x10^4$ ppm^{-1} min^{-1}.

Table A-2. List of reactions in the chemical mechanism used in the model simulations for this study.

Rxn. Label	Kinetic Parameters [a] k(300)	A	Ea	B	Reactions [b]
Inorganic Reactions					
1	(Phot. Set = NO2)				NO2 + HV = NO + O
2	6.00E-34	6.00E-34	0.00	-2.30	O + O2 + M = O3 + M
3A	9.69E-12	6.50E-12	-0.24	0.00	O + NO2 = NO + O2
3B	1.55E-12	(Falloff Kinetics)			O + NO2 = NO3 + M
	k0 =	9.00E-32	0.00	-2.00	
	kINF =	2.20E-11	0.00	0.00	
		F= 0.60	n= 1.00		
4	1.88E-14	2.00E-12	2.78	0.00	O3 + NO = NO2 + O2
5	3.36E-17	1.40E-13	4.97	0.00	O3 + NO2 = O2 + NO3
6	2.80E-11	1.70E-11	-0.30	0.00	NO + NO3 = 2 NO2
7	1.92E-38	3.30E-39	-1.05	0.00	NO + NO + O2 = 2 NO2
8	1.26E-12	(Falloff Kinetics)			NO2 + NO3 = N2O5
	k0 =	2.20E-30	0.00	-4.30	
	kINF =	1.50E-12	0.00	-0.50	
		F= 0.60	n= 1.00		
9	5.53E+10	9.09E+26	22.26	0.00	N2O5 + #RCON8 = NO2 + NO3
10	1.00E-21	(No T Dependence)			N2O5 + H2O = 2 HNO3
11	4.17E-16	2.50E-14	2.44	0.00	NO2 + NO3 = NO + NO2 + O2
12A	(Phot. Set = NO3NO)				NO3 + HV = NO + O2
12B	(Phot. Set = NO3NO2)				NO3 + HV = NO2 + O
13A	(Phot. Set = O3O3P)				O3 + HV = O + O2
13B	(Phot. Set = O3O1D)				O3 + HV = O*1D2 + O2
14	2.20E-10	(No T Dependence)			O*1D2 + H2O = 2 HO.
15	2.92E-11	1.92E-11	-0.25	0.00	O*1D2 + M = O + M
16	4.81E-12	(Falloff Kinetics)			HO. + NO = HONO
	k0 =	7.00E-31	0.00	-2.60	
	kINF =	1.50E-11	0.00	-0.50	
		F= 0.60	n= 1.00		
17	(Phot. Set = HONO)				HONO + HV = HO. + NO
18	1.13E-11	(Falloff Kinetics)			HO. + NO2 = HNO3
	k0 =	2.60E-30	0.00	-3.20	
	kINF =	2.40E-11	0.00	-1.30	
		F= 0.60	n= 1.00		
19	1.03E-13	6.45E-15	-1.65	0.00	HO. + HNO3 = H2O + NO3
21	2.40E-13	(No T Dependence)			HO. + CO = HO2. + CO2
22	6.95E-14	1.60E-12	1.87	0.00	HO. + O3 = HO2. + O2
23	8.28E-12	3.70E-12	-0.48	0.00	HO2. + NO = HO. + NO2
24	1.37E-12	(Falloff Kinetics)			HO2. + NO2 = HNO4
	k0 =	1.80E-31	0.00	-3.20	
	kINF =	4.70E-12	0.00	-1.40	
		F= 0.60	n= 1.00		
25	7.92E+10	4.76E+26	21.66	0.00	HNO4 + #RCON24 = HO2. + NO2
27	4.61E-12	1.30E-12	-0.75	0.00	HNO4 + HO. = H2O + NO2 + O2
28	2.08E-15	1.10E-14	0.99	0.00	HO2. + O3 = HO. + 2 O2
29A	1.73E-12	2.20E-13	-1.23	0.00	HO2. + HO2. = HO2H + O2
29B	5.00E-32	1.90E-33	-1.95	0.00	HO2. + HO2. + M = HO2H + O2
29C	3.72E-30	3.10E-34	-5.60	0.00	HO2. + HO2. + H2O = HO2H + O2 + H2O
29D	2.65E-30	6.60E-35	-6.32	0.00	HO2. + HO2. + H2O = HO2H + O2 + H2O
30A	1.73E-12	2.20E-13	-1.23	0.00	NO3 + HO2. = HNO3 + O2
30B	5.00E-32	1.90E-33	-1.95	0.00	NO3 + HO2. + M = HNO3 + O2
30C	3.72E-30	3.10E-34	-5.60	0.00	NO3 + HO2. + H2O = HNO3 + O2 + H2O
30D	2.65E-30	6.60E-35	-6.32	0.00	NO3 + HO2. + H2O = HNO3 + O2 + H2O
31	(Phot. Set = H2O2)				HO2H + HV = 2 HO.
32	1.70E-12	3.30E-12	0.40	0.00	HO2H + HO. = HO2. + H2O
33	9.90E-11	4.60E-11	-0.46	0.00	HO. + HO2. = H2O + O2
Peroxy Radical Operators					
B1	7.68E-12	4.20E-12	-0.36	0.00	RO2. + NO = NO
B2	2.25E-11	(Falloff Kinetics)			RCO3. + NO = NO
	k0 =	5.65E-28	0.00	-7.10	
	kINF =	2.64E-11	0.00	-0.90	
		F= 0.27	n= 1.00		
B4	1.04E-11	(Falloff Kinetics)			RCO3. + NO2 = NO2
	k0 =	2.57E-28	0.00	-7.10	
	kINF =	1.20E-11	0.00	-0.90	
		F= 0.30	n= 1.00		
B5	4.90E-12	3.40E-13	-1.59	0.00	RO2. + HO2. = HO2. + RO2-HO2-PROD
B6	4.90E-12	3.40E-13	-1.59	0.00	RCO3. + HO2. = HO2. + RO2-HO2-PROD
B8	1.00E-15	(No T Dependence)			RO2. + RO2. = RO2-RO2-PROD
B9	1.09E-11	1.86E-12	-1.05	0.00	RO2. + RCO3. = RO2-RO2-PROD
B10	1.64E-11	2.80E-12	-1.05	0.00	RCO3. + RCO3. = RO2-RO2-PROD

Table A-2 (continued)

Rxn. Label	Kinetic Parameters [a] k(300)	A	Ea	B	Reactions [b]
B11	(Same k as for RO2.)				RO2-R. + NO = NO2 + HO2.
B12	(Same k as for RO2.)				RO2-R. + HO2. = -OOH
B13	(Same k as for RO2.)				RO2-R. + RO2. = RO2. + 0.5 HO2.
B14	(Same k as for RO2.)				RO2-R. + RCO3. = RCO3. + 0.5 HO2.
B19	(Same k as for RO2.)				RO2-N. + NO = RNO3
B20	(Same k as for RO2.)				RO2-N. + HO2. = -OOH + MEK + 1.5 -C
B21	(Same k as for RO2.)				RO2-N. + RO2. = RO2. + 0.5 HO2. + MEK + 1.5 -C
B22	(Same k as for RO2.)				RO2-N. + RCO3. = RCO3. + 0.5 HO2. + MEK + 1.5 -C
B15	(Same k as for RO2.)				R2O2. + NO = NO2
B16	(Same k as for RO2.)				R2O2. + HO2. =
B17	(Same k as for RO2.)				R2O2. + RO2. = RO2.
B18	(Same k as for RO2.)				R2O2. + RCO3. = RCO3.
B23	(Same k as for RO2.)				RO2-XN. + NO = -N
B24	(Same k as for RO2.)				RO2-XN. + HO2. = -OOH
B25	(Same k as for RO2.)				RO2-XN. + RO2. = RO2. + 0.5 HO2.
B26	(Same k as for RO2.)				RO2-XN. + RCO3. = RCO3. + HO2.
G2	(Same k as for RO2.)				RO2-NP. + NO = NPHE
G3	(Same k as for RO2.)				RO2-NP. + HO2. = -OOH + 6 -C
G4	(Same k as for RO2.)				RO2-NP. + RO2. = RO2. + 0.5 HO2. + 6 -C
G5	(Same k as for RO2.)				RO2-NP. + RCO3. = RCO3. + HO2. + 6 -C
Excited Criegee Biradicals					
RZ1	(fast)				(HCHO2) = 0.7 HCOOH + 0.12 "HO. + HO2. + CO" + 0.18 "H2 + CO2"
RZ2	(fast)				(CCHO2) = 0.25 CCOOH + 0.15 "CH4 + CO2" + 0.6 HO. + 0.3 "CCO-O2. + RCO3." + 0.3 "RO2-R. + HCHO + CO + RO2."
RZ3	(fast)				(RCHO2) = 0.25 CCOOH + 0.15 CO2 + 0.6 HO. + 0.3 "C2CO-O2. + RCO3." + 0.3 "RO2-R. + CCHO + CO + RO2." + 0.55 -C
RZ4	(fast)				(C(C)CO2) = HO. + R2O2. + HCHO + CCO-O2. + RCO3. + RO2.
RZ5	(fast)				(C(R)CO2) = HO. + CCO-O2. + CCHO + R2O2. + RCO3. + RO2.
RZ6	(fast)				(CYCCO2) = 0.3 "HO. + C2CO-O2. + R2O2. + RCO3. + RO2." + 0.3 RCHO + 4.2 -C
RZ8	(fast)				(BZCHO2) = 0.5 "BZ-O. + R2O2. + CO + HO."
ISZ1	(fast)				(C:CC(C)O2) = HO. + R2O2. + HCHO + C2CO-O2. + RO2. + RCO3.
ISZ2	(fast)				(C:C(C)CHO2) = 0.75 RCHO + 0.25 ISOPROD + 0.5 -C
MAZ1	(fast)				(C2(O2)CHO) = HO. + R2O2. + HCHO + HCOCO-O2. + RO2. + RCO3.
M1Z1	(fast)				(HOCCHO2) = 0.6 HO. + 0.3 "CCO-O2. + RCO3." + 0.3 "RO2-R. + HCHO + CO + RO2." + 0.8 -C
M2Z1	(fast)				(HCOCHO2) = 0.12 "HO2. + 2 CO + HO." + 0.74 -C + 0.51 "CO2 + HCHO"
M2Z2	(fast)				(C2(O2)COH) = HO. + MGLY + HO2. + R2O2. + RO2.
	(fast)				(C:CC(C)O2) = HO. + R2O2. + HCHO + C2CO-O2. + RO2. + RCO3.
	(fast)				(C:C(C)CHO2) = 0.75 RCHO + 0.25 ISOPROD + 0.5 -C
	(fast)				(C2(O2)CHO) = HO. + R2O2. + HCHO + HCOCO-O2. + RO2. + RCO3.
	(fast)				(HOCCHO2) = 0.6 HO. + 0.3 {CCO-O2. + RCO3.} + 0.3 {RO2-R. + HCHO + CO + RO2.} + 0.8 -C
	(fast)				(HCOCHO2) = 0.12 {HO2. + 2 CO + HO.} + 0.74 -C + 0.51 {CO2 + HCHO}
	(fast)				(C2(O2)COH) = HO. + MGLY + HO2. + R2O2. + RO2.
Organic Product Species					
B7	(Phot. Set = CO2H)				-OOH + HV = HO2. + HO.
B7A	1.81E-12	1.18E-12	-0.25	0.00	HO. + -OOH = HO.
B7B	3.71E-12	1.79E-12	-0.44	0.00	HO. + -OOH = RO2-R. + RO2.
C1	(Phot. Set = HCHONEWR)				HCHO + HV = 2 HO2. + CO
C2	(Phot. Set = HCHONEWM)				HCHO + HV = H2 + CO
C3	9.76E-12	1.13E-12	-1.29	2.00	HCHO + HO. = HO2. + CO + H2O
C4	7.79E-14	9.70E-15	-1.24	0.00	HCHO + HO2. = HOCOO.
C4A	1.77E+02	2.40E+12	13.91	0.00	HOCOO. = HO2. + HCHO
C4B	(Same k as for RO2.)				HOCOO. + NO = -C + NO2 + HO2.
C9	6.38E-16	2.80E-12	5.00	0.00	HCHO + NO3 = HNO3 + HO2. + CO
C10	1.57E-11	5.55E-12	-0.62	0.00	CCHO + HO. = CCO-O2. + H2O + RCO3.
C11A	(Phot. Set = CCHOR)				CCHO + HV = CO + HO2. + HCHO + RO2-R. + RO2.
C12	2.84E-15	1.40E-12	3.70	0.00	CCHO + NO3 = HNO3 + CCO-O2. + RCO3.
C25	1.97E-11	8.50E-12	-0.50	0.00	RCHO + HO. = C2CO-O2. + RCO3.
C26	(Phot. Set = RCHO)				RCHO + HV = CCHO + RO2-R. + RO2. + CO + HO2.

Table A-2 (continued)

Rxn.	Kinetic Parameters [a]				Reactions [b]
Label	k(300)	A	Ea	B	
C27	2.84E-15	1.40E-12	3.70	0.00	NO3 + RCHO = HNO3 + C2CO-O2. + RCO3.
C38	2.23E-13	4.81E-13	0.46	2.00	ACET + HO. = R2O2. + HCHO + CCO-O2. + RCO3. + RO2.
C39	(Phot. Set = ACET-93C)				ACET + HV = CCO-O2. + HCHO + RO2-R. + RCO3. + RO2.
C44	1.16E-12	2.92E-13	-0.82	2.00	MEK + HO. = H2O + 0.5 "CCHO + HCHO + CCO-O2. + C2CO-O2." + RCO3. + 1.5 "R2O2. + RO2."
C57	(Phot. Set = KETONE)				MEK + HV + #0.1 = CCO-O2. + CCHO + RO2-R. + RCO3. + RO2.
C95	2.07E-12	2.19E-11	1.41	0.00	RNO3 + HO. = NO2 + 0.155 MEK + 1.05 RCHO + 0.48 CCHO + 0.16 HCHO + 0.11 -C + 1.39 "R2O2. + RO2."
C58A	(Phot. Set = GLYOXAL1)				GLY + HV = 0.8 HO2. + 0.45 HCHO + 1.55 CO
C58B	(Phot. Set = GLYOXAL2)				GLY + HV + #0.029 = 0.13 HCHO + 1.87 CO
C59	1.14E-11	(No T Dependence)			GLY + HO. = 0.6 HO2. + 1.2 CO + 0.4 "HCOCO-O2. + RCO3."
C60	(Same k as for CCHO)				GLY + NO3 = HNO3 + 0.6 HO2. + 1.2 CO + 0.4 "HCOCO-O2. + RCO3."
C68A	(Phot. Set = MEGLYOX1)				MGLY + HV = HO2. + CO + CCO-O2. + RCO3.
C68B	(Phot. Set = MEGLYOX2)				MGLY + HV + 0.107 = HO2. + CO + CCO-O2. + RCO3.
C69	1.72E-11	(No T Dependence)			MGLY + HO. = CO + CCO-O2. + RCO3.
C70	(Same k as for CCHO)				MGLY + NO3 = HNO3 + CO + CCO-O2. + RCO3.
G7	1.14E-11	(No T Dependence)			HO. + AFG1 = HCOCO-O2. + RCO3.
G8	(Phot. Set = ACROLEIN)				AFG1 + HV + #0.029 = HO2. + HCOCO-O2. + RCO3.
U2OH	1.72E-11	(No T Dependence)			HO. + AFG2 = C2CO-O2. + RCO3.
U2HV	(Phot. Set = ACROLEIN)				AFG2 + HV = HO2. + CO + CCO-O2. + RCO3.
G46	2.63E-11	(No T Dependence)			HO. + PHEN = 0.15 RO2-NP. + 0.85 RO2-R. + 0.2 GLY + 4.7 -C + RO2.
G51	3.60E-12	(No T Dependence)			NO3 + PHEN = HNO3 + BZ-O.
G52	4.20E-11	(No T Dependence)			HO. + CRES = 0.15 RO2-NP. + 0.85 RO2-R. + 0.2 MGLY + 5.5 -C + RO2.
G57	2.10E-11	(No T Dependence)			NO3 + CRES = HNO3 + BZ-O. + -C
G30	1.29E-11	(No T Dependence)			BALD + HO. = BZ-CO-O2. + RCO3.
G31	(Phot. Set = BZCHO)				BALD + HV + #0.05 = 7 -C
G32	2.61E-15	1.40E-12	3.75	0.00	BALD + NO3 = HNO3 + BZ-CO-O2.
G58	3.60E-12	(No T Dependence)			NPHE + NO3 = HNO3 + BZ(NO2)-O.
G59	(Same k as for BZ-O.)				BZ(NO2)-O. + NO2 = 2 -N + 6 -C
G60	(Same k as for RO2.)				BZ(NO2)-O. + HO2. = NPHE
G61	(Same k as for BZ-O.)				BZ(NO2)-O. = NPHE
C13	(Same k as for RCO3.)				CCO-O2. + NO = CO2 + NO2 + HCHO + RO2-R. + RO2.
C14	(Same k as for RCO3.)				CCO-O2. + NO2 = PAN
C15	(Same k as for RCO3.)				CCO-O2. + HO2. = -OOH + CO2 + HCHO
C16	(Same k as for RCO3.)				CCO-O2. + RO2. = RO2. + 0.5 HO2. + CO2 + HCHO
C17	(Same k as for RCO3.)				CCO-O2. + RCO3. = RCO3. + HO2. + CO2 + HCHO
C18	6.50E-04	(Falloff Kinetics)			PAN = CCO-O2. + NO2 + RCO3.
	k0 =	4.90E-03	23.97	0.00	
	kINF =	4.00E+16	27.08	0.00	
		F= 0.30	n= 1.00		
C28	(Same k as for RCO3.)				C2CO-O2. + NO = CCHO + RO2-R. + CO2 + NO2 + RO2.
C29	8.40E-12	(No T Dependence)			C2CO-O2. + NO2 = PPN
C30	(Same k as for RCO3.)				C2CO-O2. + HO2. = -OOH + CCHO + CO2
C31	(Same k as for RCO3.)				C2CO-O2. + RO2. = RO2. + 0.5 HO2. + CCHO + CO2
C32	(Same k as for RCO3.)				C2CO-O2. + RCO3. = RCO3. + HO2. + CCHO + CO2
C33	6.78E-04	1.60E+17	27.97	0.00	PPN = C2CO-O2. + NO2 + RCO3.
C62	(Same k as for RCO3.)				HCOCO-O2. + NO = NO2 + CO2 + CO + HO2.
C63	(Same k as for RCO3.)				HCOCO-O2. + NO2 = GPAN
C65	(Same k as for RCO3.)				HCOCO-O2. + HO2. = -OOH + CO2 + CO
C66	(Same k as for RCO3.)				HCOCO-O2. + RO2. = RO2. + 0.5 HO2. + CO2 + CO
C67	(Same k as for RCO3.)				HCOCO-O2. + RCO3. = RCO3. + HO2. + CO2 + CO
C64	(Same k as for PAN)				GPAN = HCOCO-O2. + NO2 + RCO3.
G33	(Same k as for RCO3.)				BZ-CO-O2. + NO = BZ-O. + CO2 + NO2 + R2O2. + RO2.
G43	3.53E-11	1.30E-11	-0.60	0.00	BZ-O. + NO2 = NPHE
G44	(Same k as for RO2.)				BZ-O. + HO2. = PHEN
G45	1.00E-03	(No T Dependence)			BZ-O. = PHEN
G34	8.40E-12	(No T Dependence)			BZ-CO-O2. + NO2 = PBZN
G36	(Same k as for RCO3.)				BZ-CO-O2. + HO2. = -OOH + CO2 + PHEN
G37	(Same k as for RCO3.)				BZ-CO-O2. + RO2. = RO2. + 0.5 HO2. + CO2 + PHEN

Table A-2 (continued)

Rxn. Label	Kinetic Parameters [a] k(300)	A	Ea	B	Reactions [b]
G38	(Same k as for RCO3.)				BZ-CO-O2. + RCO3. = RCO3. + HO2. + CO2 + PHEN
G35	2.17E-04	1.60E+15	25.90	0.00	PBZN = BZ-CO-O2. + NO2 + RCO3.
	3.36E-11	(No T Dependence)			ISOPROD + HO. = 0.293 CO + 0.252 CCHO + 0.126 HCHO + 0.041 GLY + 0.021 RCHO + 0.168 MGLY + 0.314 MEK + 0.503 RO2-R. + 0.21 CCO-O2. + 0.288 C2CO-O2. + 0.21 R2O2. + 0.713 RO2. + 0.498 RCO3. + -.112 -C
	7.11E-18	(No T Dependence)			ISOPROD + O3 = 0.02 CCHO + 0.04 HCHO + 0.01 GLY + 0.84 MGLY + 0.09 MEK + 0.66 (HCHO2) + 0.09 (HCOCHO2) + 0.18 (HOCCHO2) + 0.06 (C2(O2)CHO) + 0.01 (C2(O2)COH) + -.39 -C
	(Phot. Set = ACROLEIN)				ISOPROD + HV + 0.0036 = 0.333 CO + 0.067 CCHO + 0.9 HCHO + 0.033 MEK + 0.333 HO2. + 0.7 RO2-R. + 0.267 CCO-O2. + 0.7 C2CO-O2. + 0.7 RO2. + 0.967 RCO3. + -.133 -C
	1.00E-15	(No T Dependence)			ISOPROD + NO3 = 0.643 CO + 0.282 HCHO + 0.85 RNO3 + 0.357 RCHO + 0.925 HO2. + 0.075 C2CO-O2. + 0.075 R2O2. + 0.925 RO2. + 0.075 RCO3. + 0.075 HNO3 + -2.471 -C
Hydrocarbon Species Represented Explicitly [c]					
	8.71E-15	6.25E-13	2.55	2.00	CH4 + HO. = HCHO + RO2-R. + RO2.
	2.74E-13	1.28E-12	0.92	2.00	ETHANE + HO. = RO2-R. + CCHO + RO2.
	2.56E-12	1.36E-12	-0.38	2.00	N-C4 + HO. = 0.076 RO2-N. + 0.924 RO2-R. + 0.397 R2O2. + 0.001 HCHO + 0.571 CCHO + 0.14 RCHO + 0.533 MEK + -0.076 -C + 1.397 RO2.
	5.63E-12	1.35E-11	0.52	0.00	N-C6 + HO. = 0.185 RO2-N. + 0.815 RO2-R. + 0.738 R2O2. + 0.02 CCHO + 0.105 RCHO + 1.134 MEK + 0.186 -C + 1.738 RO2.
	8.76E-12	3.15E-11	0.76	0.00	N-C8 + HO. = 0.333 RO2-N. + 0.667 RO2-R. + 0.706 R2O2. + 0.002 RCHO + 1.333 MEK + 0.998 -C + 1.706 RO2.
	5.91E-12	1.81E-12	-0.70	0.00	TOLUENE + HO. = 0.085 BALD + 0.26 CRES + 0.118 GLY + 0.9638 MGLY + 0.259 AFG2 + 0.74 RO2-R. + 0.26 HO2. + 2.486 -C + 0.74 RO2.
	2.36E-11	(No T Dependence)			M-XYLENE + HO. = 0.04 BALD + 0.18 CRES + 0.108 GLY + 1.599 MGLY + 0.4612 AFG2 + 0.82 RO2-R. + 0.18 HO2. + 2.884 -C + 0.82 RO2.
	8.43E-12	1.96E-12	-0.87	0.00	ETHENE + HO. = RO2-R. + RO2. + 1.56 HCHO + 0.22 CCHO
	1.68E-18	9.14E-15	5.13	0.00	ETHENE + O3 = HCHO + (HCHO2)
	2.18E-16	4.39E-13	4.53	2.00	ETHENE + NO3 = R2O2. + RO2. + 2 HCHO + NO2
	7.42E-13	1.04E-11	1.57	0.00	ETHENE + O = RO2-R. + HO2. + RO2. + HCHO + CO
	2.60E-11	4.85E-12	-1.00	0.00	PROPENE + HO. = RO2-R. + RO2. + HCHO + CCHO
	1.05E-17	5.51E-15	3.73	0.00	PROPENE + O3 = 0.6 HCHO + 0.4 CCHO + 0.4 (HCHO2) + 0.6 (CCHO2)
	9.74E-15	4.59E-13	2.30	0.00	PROPENE + NO3 = R2O2. + RO2. + HCHO + CCHO + NO2
	4.01E-12	1.18E-11	0.64	0.00	PROPENE + O = 0.4 HO2. + 0.5 RCHO + 0.5 MEK + -0.5 -C
	6.30E-11	1.01E-11	-1.09	0.00	T-2-BUTE + HO. = RO2-R. + RO2. + 2 CCHO
	1.95E-16	6.64E-15	2.10	0.00	T-2-BUTE + O3 = CCHO + (CCHO2)
	3.92E-13	1.10E-13	-0.76	2.00	T-2-BUTE + NO3 = R2O2. + RO2. + 2 CCHO + NO2
	2.34E-11	2.26E-11	-0.02	0.00	T-2-BUTE + O = 0.4 HO2. + 0.5 RCHO + 0.5 MEK + 0.5 -C
	9.88E-11	2.54E-11	-0.81	0.00	ISOP + HO. = 0.088 RO2-N. + 0.912 RO2-R. + 0.629 HCHO + 0.912 ISOPROD + 0.079 R2O2. + 1.079 RO2. + 0.283 -C
	1.34E-17	7.86E-15	3.80	0.00	ISOP + O3 = 0.4 HCHO + 0.6 ISOPROD + 0.55 (HCHO2) + 0.2 (C:CC(C)O2) + 0.2 (C:C(C)CHO2) + 0.05 -C
	3.60E-11	(No T Dependence)			ISOP + O = 0.75 {ISOPROD + -C }+ 0.25 {C2CO-O2. + RCO3. + 2 HCHO + RO2-R. + RO2.}
	6.81E-13	3.03E-12	0.89	0.00	ISOP + NO3 = 0.8 {RCHO + RNO3 + RO2-R.} + 0.2 {ISOPROD + R2O2. + NO2} + RO2. + -2.2 -C
	1.50E-19	(No T Dependence)			ISOP + NO2 = 0.8 {RCHO + RNO3 + RO2-R.} + 0.2 {ISOPROD + R2O2. + NO} + RO2. + -2.2 -C
	5.31E-11	1.21E-11	-0.88	0.00	APIN + HO. = RO2-R. + RCHO + RO2. + 7 -C
	1.00E-16	9.90E-16	1.37	0.00	APIN + O3 = 0.05 HCHO + 0.2 CCHO + 0.5 RCHO + 0.61 MEK + 0.075 CO + 0.1 O3OL-SB + 0.05 CCO-O2. + 0.05 C2CO-O2. + 0.1 RCO3. + 0.105 HO2. + 0.16 HO. + 0.135 RO2-R. + 0.15 R2O2. + 0.285 RO2. + 5.285 -C

Table A-2 (continued)

Rxn. Label	Kinetic Parameters [a] k(300)	A	Ea	B	Reactions [b]
	6.10E-12	1.19E-12	-0.97	0.00	APIN + NO3 = NO2 + R2O2. + RCHO + RO2. + 7 -C
	3.00E-11	(No T Dependence)			APIN + O = 0.4 HO2. + 0.5 MEK + 0.5 RCHO + 6.5 -C
	6.57E-11	(No T Dependence)			UNKN + HO. = RO2-R. + RO2. + 0.5 HCHO + RCHO + 6.5 -C
	5.85E-17	(No T Dependence)			UNKN + O3 = 0.135 RO2-R. + 0.135 HO2. + 0.075 R2O2. + 0.21 RO2. + 0.025 CCO-O2. + 0.025 C2CO-O2. + 0.05 RCO3. + 0.275 HCHO + 0.175 CCHO + 0.5 RCHO + 0.41 MEK + 0.185 CO + 5.925 -C + 0.11 HO. + 0.192 O3OL-SB
	4.30E-12	(No T Dependence)			UNKN + NO3 = R2O2. + RO2. + 0.5 HCHO + RCHO + 6.5 -C + NO2
	2.90E-11	(No T Dependence)			UNKN + O = 0.4 HO2. + 0.5 RCHO + 0.5 MEK + 6.5 -C
Lumped Species used for Base ROG in EKMA Simulations [c]					
	3.46E-12	2.58E-12	-0.17	1.00	ALK1 + HO. = 0.828 RO2-R. + 0.073 RO2-N. + 0.005 RO2-XN. + 0.011 HO2. + 0.574 R2O2. + 1.48 RO2. + 0.021 HO. + 0.022 HCHO + 0.339 CCHO + 0.176 RCHO + 0.26 ACET + 0.447 MEK + 0.024 CO + 0.026 GLY2 + 0.062 C2(C)-O. + 0.142 -C
	9.14E-12	5.12E-12	-0.35	1.00	ALK2 + HO. = 0.749 RO2-R. + 0.249 RO2-N. + 0.002 RO2-XN. + 0.891 R2O2. + 1.891 RO2. + 0.029 HCHO + 0.048 CCHO + 0.288 RCHO + 0.028 ACET + 1.105 MEK + 0.043 CO + 0.018 CO2 + 1.268 -C
	5.87E-12	(No T Dependence)			ARO1 + HO. = 0.742 RO2-R. + 0.258 HO2. + 0.742 RO2. + 0.015 PHEN + 0.244 CRES + 0.08 BALD + 0.124 GLY + 0.773 MGLY + 0.091 AFG1 + 0.229 AFG2 + 1.665 -C
	3.22E-11	1.20E-11	-0.59	1.00	ARO2 + HO. = 0.82 RO2-R. + 0.18 HO2. + 0.82 RO2. + 0.18 CRES + 0.036 BALD + 0.068 GLY + 1.159 MGLY + 0.49 AFG2 + 2.297 -C
	3.17E-11	2.22E-12	-1.59	1.00	OLE1 + HO. = 0.858 RO2-R. + 0.142 RO2-N. + RO2. + 0.858 HCHO + 0.252 CCHO + 0.606 RCHO + 1.267 -C
	1.08E-17	1.42E-15	2.91	1.00	OLE1 + O3 = 0.6 HCHO + 0.635 RCHO + 0.981 -C + 0.4 (HCHO2) + 0.529 (CCHO2) + 0.071 (RCHO2)
	1.16E-14	1.99E-13	1.69	1.00	OLE1 + NO3 = R2O2. + RO2. + HCHO + 0.294 CCHO + 0.706 RCHO + 1.451 -C + NO2
	4.11E-12	4.51E-12	0.06	1.00	OLE1 + O = 0.4 HO2. + 0.5 RCHO + 0.5 MEK + 1.657 -C
	6.23E-11	4.54E-12	-1.56	1.00	OLE2 + HO. = 0.861 RO2-R. + 0.139 RO2-N. + RO2. + 0.24 HCHO + 0.661 CCHO + 0.506 RCHO + 0.113 ACET + 0.086 MEK + 0.057 BALD + 0.848 -C
	1.70E-16	1.77E-15	1.40	1.00	OLE2 + O3 = 0.203 HCHO + 0.358 CCHO + 0.309 RCHO + 0.061 MEK + 0.027 BALD + 0.976 -C + 0.076 (HCHO2) + 0.409 (CCHO2) + 0.279 (RCHO2) + 0.158 (C(C)CO2 + 0.039 (C(R)CO2 + 0.04 (BZCHO2)
	1.07E-12	3.19E-13	-0.72	1.00	OLE2 + NO3 = R2O2. + RO2. + 0.278 HCHO + 0.767 CCHO + 0.588 RCHO + 0.131 ACET + 0.1 MEK + 0.066 BALD + 0.871 -C + NO2
	2.52E-11	8.66E-12	-0.64	1.00	OLE2 + O = 0.4 HO2. + 0.5 RCHO + 0.5 MEK + 2.205 -C
Acetylene (SAPRC-90 mechanism) [d,e]					
	8.18E-13	5.03E-12	1.08	0.00	ACETYLEN + HO. = 0.3 {HO2. + CO + -C} + 0.7 {RO2-R. + RO2. + GLY}
Acetylene and Glyoxal from Acetylene (Model A) [e]					
	8.18E-13	5.03E-12	1.08	0.00	ACETYLEN + HO. = 0.3 {HO2. + CO + -C} + 0.7 {RO2-R. + RO2. + GLY-A}
	(Phot. Set = GLYR-A)				GLY-A + HV = 2 {HO2. + CO}
	(Phot. Set = GLYM)				GLY-A + HV = HCHO + CO
	1.14E-11	(No T Dependence)			GLY-A + HO. = 0.6 HO2. + 1.2 CO + 0.4 "HCOCO-O2. + RCO3."
	(Same k as for CCHO)				GLY-A + NO3 = HNO3 + 0.6 HO2. + 1.2 CO + 0.4 "HCOCO-O2. + RCO3."
Acetylene and Glyoxal from Acetylene (Model B)					
	8.18E-13	5.03E-12	1.08	0.00	ACETYLEN + HO. = 0.3 {HO2. + CO + -C} + 0.7 {HO. + GLY-B}
	(Phot. Set = GLYR-B)				GLY-B + HV = 2 {HO2. + CO}
	(Phot. Set = GLYM)				GLY-A + HV = HCHO + CO
	1.14E-11	(No T Dependence)			GLY-B + HO. = 0.6 HO2. + 1.2 CO + 0.4 "HCOCO-O2. + RCO3."

Table A-2 (continued)

Rxn. Label	Kinetic Parameters [a] k(300)	A	Ea	B	Reactions [b]
	(Same k as for CCHO)				GLY-B + NO3 = HNO3 + 0.6 HO2. + 1.2 CO + 0.4 "HCOCO-O2. + RCO3."
Acetylene and Glyoxal from Acetylene (Model C)					
	8.18E-13	5.03E-12	1.08	0.00	ACETYLEN + HO. = 0.3 {HO2. + CO + -C} + 0.55 HO. + 0.15 {RO2-R. + RO2.} + 0.7 GLY-C
	(Phot. Set = GLYR-C)				GLY-C + HV = 2 {HO2. + CO}
	(Phot. Set = GLYM)				GLY-A + HV = HCHO + CO
	1.14E-11	(No T Dependence)			GLY-C + HO. = 0.6 HO2. + 1.2 CO + 0.4 "HCOCO-O2. + RCO3."
	(Same k as for CCHO)				GLY-C + NO3 = HNO3 + 0.6 HO2. + 1.2 CO + 0.4 "HCOCO-O2. + RCO3."
Reactions used to Represent Chamber-Dependent Processes [f]					
O3W	k(O3W)	(No T Dependence)			O3 = (loss of O_3)
N25I	k(N25I)	(No T Dependence)			N2O5 = 2 NOX-WALL
N25S	k(N25S)	(No T Dependence)			N2O5 + H2O = 2 NOX-WALL
NO2W	k(NO2W)	(No T Dependence)			NO2 = (yHONO) HONO + (1-yHONO) NOX-WALL
XSHC	k(XSHC)	(No T Dependence)			HO. = HO2.
RSI	(Phot. Set = NO2)				HV + (RS/K1) = HO.
ONO2	(Phot. Set = NO2)				HV + (E-NO2/K1) = NO2 + #-1 NOX-WALL

[a] Except as noted, expression for rate constant is $k = A\ e^{Ea/RT}\ (T/300)^B$. Rate constants and A factor are in ppm, min units. Units of Ea is kcal $mole^{-1}$. "Phot Set" means this is a photolysis reaction, with the absorption coefficients and quantum yields given in Table A-3. In addition, if "#number" or "(parameter)" is given as a reactant, then the value of that number or parameter is multiplied by the result in the "rate constant expression" columns to obtain the rate constant used. Furthermore, "#RCONnn" as a reactant means that the rate constant for the reaction is obtained by multiplying the rate constant given by that for reaction "nn". Thus, the rate constant given is actually an equilibrium constant.
[b] Format of reaction listing same as used in documentation of the SAPRC-90 mechanism (Carter 1990).
[c] Rate constants and product yield parameters based on the mixture of species in the base ROG mixture which are being represented.
[d] Glyoxal reactions are represented as in the general mechanism, as shown with reactions of the other organic product species..
[e] Not used in atmospheric reactivity simulations because of poor performance in simulating the chamber data.
[f] See Table A-4 for the values of the parameters used for the chamber modeled in this study.

Table A-3. Absorption cross sections and quantum yields for photolysis reactions.

WL (nm)	Abs (cm^2)	QY	WL (nm)	Abs (cm^2)	QY	WL (nm)	Abs (cm^2)	QY	WL (nm)	Abs (cm^2)	QY	WL (nm)	Abs (cm^2)	QY
Photolysis File = NO2														
250.0	2.83E-20	1.000	255.0	1.45E-20	1.000	260.0	1.90E-20	1.000	265.0	2.05E-20	1.000	270.0	3.13E-20	1.000
275.0	4.02E-20	1.000	280.0	5.54E-20	1.000	285.0	6.99E-20	1.000	290.0	8.18E-20	0.999	295.0	9.67E-20	0.998
300.0	1.17E-19	0.997	305.0	1.66E-19	0.996	310.0	1.76E-19	0.995	315.0	2.25E-19	0.994	320.0	2.54E-19	0.993
325.0	2.79E-19	0.992	330.0	2.99E-19	0.991	335.0	3.45E-19	0.990	340.0	3.88E-19	0.989	345.0	4.07E-19	0.988
350.0	4.10E-19	0.987	355.0	5.13E-19	0.986	360.0	4.51E-19	0.984	365.0	5.78E-19	0.983	370.0	5.42E-19	0.981
375.0	5.35E-19	0.979	380.0	5.99E-19	0.975	381.0	5.98E-19	0.974	382.0	5.97E-19	0.973	383.0	5.96E-19	0.972
384.0	5.95E-19	0.971	385.0	5.94E-19	0.969	386.0	5.95E-19	0.967	387.0	5.96E-19	0.966	388.0	5.98E-19	0.964
389.0	5.99E-19	0.962	390.0	6.00E-19	0.960	391.0	5.98E-19	0.959	392.0	5.96E-19	0.957	393.0	5.93E-19	0.953
394.0	5.91E-19	0.950	395.0	5.89E-19	0.942	396.0	6.06E-19	0.922	397.0	6.24E-19	0.870	398.0	6.41E-19	0.820
399.0	6.59E-19	0.760	400.0	6.76E-19	0.695	401.0	6.67E-19	0.635	402.0	6.58E-19	0.560	403.0	6.50E-19	0.485
404.0	6.41E-19	0.425	405.0	6.32E-19	0.350	406.0	6.21E-19	0.290	407.0	6.10E-19	0.225	408.0	5.99E-19	0.185
409.0	5.88E-19	0.153	410.0	5.77E-19	0.130	411.0	5.88E-19	0.110	412.0	5.98E-19	0.094	413.0	6.09E-19	0.083
414.0	6.19E-19	0.070	415.0	6.30E-19	0.059	416.0	6.29E-19	0.048	417.0	6.27E-19	0.039	418.0	6.26E-19	0.030
419.0	6.24E-19	0.023	420.0	6.23E-19	0.018	421.0	6.18E-19	0.012	422.0	6.14E-19	0.008	423.0	6.09E-19	0.004
424.0	6.05E-19	0.000	425.0	6.00E-19	0.000									
Photolysis File = NO3NO														
585.0	2.77E-18	0.000	590.0	5.14E-18	0.250	595.0	4.08E-18	0.400	600.0	2.83E-18	0.250	605.0	3.45E-18	0.200
610.0	1.48E-18	0.200	615.0	1.96E-18	0.100	620.0	3.58E-18	0.100	625.0	9.25E-18	0.050	630.0	5.66E-18	0.050
635.0	1.45E-18	0.030	640.0	1.11E-18	0.000									
Photolysis File = NO3NO2														
400.0	0.00E+00	1.000	405.0	3.00E-20	1.000	410.0	4.00E-20	1.000	415.0	5.00E-20	1.000	420.0	8.00E-20	1.000
425.0	1.00E-19	1.000	430.0	1.30E-19	1.000	435.0	1.80E-19	1.000	440.0	1.90E-19	1.000	445.0	2.20E-19	1.000
450.0	2.80E-19	1.000	455.0	3.30E-19	1.000	460.0	3.70E-19	1.000	465.0	4.30E-19	1.000	470.0	5.10E-19	1.000
475.0	6.00E-19	1.000	480.0	6.40E-19	1.000	485.0	6.90E-19	1.000	490.0	8.80E-19	1.000	495.0	9.50E-19	1.000
500.0	1.01E-18	1.000	505.0	1.10E-18	1.000	510.0	1.32E-18	1.000	515.0	1.40E-18	1.000	520.0	1.45E-18	1.000
525.0	1.48E-18	1.000	530.0	1.94E-18	1.000	535.0	2.04E-18	1.000	540.0	1.81E-18	1.000	545.0	1.81E-18	1.000
550.0	2.36E-18	1.000	555.0	2.68E-18	1.000	560.0	3.07E-18	1.000	565.0	2.53E-18	1.000	570.0	2.54E-18	1.000
575.0	2.74E-18	1.000	580.0	3.05E-18	1.000	585.0	2.77E-18	1.000	590.0	5.14E-18	0.750	595.0	4.08E-18	0.600
600.0	2.83E-18	0.550	605.0	3.45E-18	0.400	610.0	1.45E-18	0.300	615.0	1.96E-18	0.250	620.0	3.58E-18	0.200
625.0	9.25E-18	0.150	630.0	5.66E-18	0.050	635.0	1.45E-18	0.000						
Photolysis File = O3O3P														
280.0	3.97E-18	0.100	281.0	3.60E-18	0.100	282.0	3.24E-18	0.100	283.0	3.01E-18	0.100	284.0	2.73E-18	0.100
285.0	2.44E-18	0.100	286.0	2.21E-18	0.100	287.0	2.01E-18	0.100	288.0	1.76E-18	0.100	289.0	1.58E-18	0.100
290.0	1.41E-18	0.100	291.0	1.26E-18	0.100	292.0	1.10E-18	0.100	293.0	9.89E-19	0.100	294.0	8.59E-19	0.100
295.0	7.70E-19	0.100	296.0	6.67E-19	0.100	297.0	5.84E-19	0.100	298.0	5.07E-19	0.100	299.0	4.52E-19	0.100
300.0	3.92E-19	0.100	301.0	3.42E-19	0.100	302.0	3.06E-19	0.100	303.0	2.60E-19	0.100	304.0	2.37E-19	0.100
305.0	2.01E-19	0.112	306.0	1.79E-19	0.149	307.0	1.56E-19	0.197	308.0	1.38E-19	0.259	309.0	1.25E-19	0.339
310.0	1.02E-19	0.437	311.0	9.17E-20	0.546	312.0	7.88E-20	0.652	313.0	6.77E-20	0.743	314.0	6.35E-20	0.816
315.0	5.10E-20	0.872	316.0	4.61E-20	0.916	317.0	4.17E-20	0.949	318.0	3.72E-20	0.976	319.0	2.69E-20	0.997
320.0	3.23E-20	1.000	330.0	6.70E-21	1.000	340.0	1.70E-21	1.000	350.0	4.00E-22	1.000	355.0	0.00E+00	1.000
400.0	0.00E+00	1.000	450.0	1.60E-22	1.000	500.0	1.34E-21	1.000	550.0	3.32E-21	1.000	600.0	5.06E-21	1.000
650.0	2.45E-21	1.000	700.0	8.70E-22	1.000	750.0	3.20E-22	1.000	800.0	1.60E-22	1.000	900.0	0.00E+00	1.000
Photolysis File = O3O1D														
280.0	3.97E-18	0.900	281.0	3.60E-18	0.900	282.0	3.24E-18	0.900	283.0	3.01E-18	0.900	284.0	2.73E-18	0.900
285.0	2.44E-18	0.900	286.0	2.21E-18	0.900	287.0	2.01E-18	0.900	288.0	1.76E-18	0.900	289.0	1.58E-18	0.900
290.0	1.41E-18	0.900	291.0	1.26E-18	0.900	292.0	1.10E-18	0.900	293.0	9.89E-19	0.900	294.0	8.59E-19	0.900
295.0	7.70E-19	0.900	296.0	6.67E-19	0.900	297.0	5.84E-19	0.900	298.0	5.07E-19	0.900	299.0	4.52E-19	0.900
300.0	3.92E-19	0.900	301.0	3.42E-19	0.900	302.0	3.06E-19	0.900	303.0	2.60E-19	0.900	304.0	2.37E-19	0.900
305.0	2.01E-19	0.888	306.0	1.79E-19	0.851	307.0	1.56E-19	0.803	308.0	1.38E-19	0.741	309.0	1.25E-19	0.661
310.0	1.02E-19	0.563	311.0	9.17E-20	0.454	312.0	7.88E-20	0.348	313.0	6.77E-20	0.257	314.0	6.35E-20	0.184
315.0	5.10E-20	0.128	316.0	4.61E-20	0.084	317.0	4.17E-20	0.051	318.0	3.72E-20	0.024	319.0	2.69E-20	0.003
320.0	3.23E-20	0.000												
Photolysis File = HONO														
311.0	0.00E+00	1.000	312.0	2.00E-21	1.000	313.0	4.20E-21	1.000	314.0	4.60E-21	1.000	315.0	4.20E-21	1.000
316.0	3.00E-21	1.000	317.0	4.60E-21	1.000	318.0	3.60E-20	1.000	319.0	6.10E-20	1.000	320.0	2.10E-20	1.000
321.0	4.27E-20	1.000	322.0	4.01E-20	1.000	323.0	3.93E-20	1.000	324.0	4.01E-20	1.000	325.0	4.04E-20	1.000
326.0	3.13E-20	1.000	327.0	4.12E-20	1.000	328.0	7.55E-20	1.000	329.0	6.64E-20	1.000	330.0	7.29E-20	1.000
331.0	8.70E-20	1.000	332.0	1.38E-19	1.000	333.0	5.91E-20	1.000	334.0	5.91E-20	1.000	335.0	6.45E-20	1.000
336.0	5.91E-20	1.000	337.0	4.58E-20	1.000	338.0	1.91E-19	1.000	339.0	1.63E-19	1.000	340.0	1.05E-19	1.000
341.0	8.70E-20	1.000	342.0	3.35E-19	1.000	343.0	2.01E-19	1.000	344.0	1.02E-19	1.000	345.0	8.54E-20	1.000
346.0	8.32E-20	1.000	347.0	8.20E-20	1.000	348.0	7.49E-20	1.000	349.0	7.13E-20	1.000	350.0	6.83E-20	1.000
351.0	1.74E-19	1.000	352.0	1.14E-19	1.000	353.0	3.71E-19	1.000	354.0	4.96E-19	1.000	355.0	2.46E-19	1.000
356.0	1.19E-19	1.000	357.0	9.35E-20	1.000	358.0	7.78E-20	1.000	359.0	7.29E-20	1.000	360.0	6.83E-20	1.000
361.0	6.90E-20	1.000	362.0	7.32E-20	1.000	363.0	9.00E-20	1.000	364.0	1.21E-19	1.000	365.0	1.33E-19	1.000
366.0	2.13E-19	1.000	367.0	3.52E-19	1.000	368.0	4.50E-19	1.000	369.0	2.93E-19	1.000	370.0	1.19E-19	1.000
371.0	9.46E-20	1.000	372.0	8.85E-20	1.000	373.0	7.44E-20	1.000	374.0	4.77E-20	1.000	375.0	2.70E-20	1.000
376.0	1.90E-20	1.000	377.0	1.50E-20	1.000	378.0	1.90E-20	1.000	379.0	5.80E-20	1.000	380.0	7.78E-20	1.000
381.0	1.14E-19	1.000	382.0	1.40E-19	1.000	383.0	1.72E-19	1.000	384.0	1.99E-19	1.000	385.0	1.90E-19	1.000
386.0	1.19E-19	1.000	387.0	5.65E-20	1.000	388.0	3.20E-20	1.000	389.0	1.90E-20	1.000	390.0	1.20E-20	1.000
391.0	5.00E-21	1.000	392.0	0.00E+00	1.000									
Photolysis File = H2O2														
250.0	8.30E-20	1.000	255.0	6.70E-20	1.000	260.0	5.20E-20	1.000	265.0	4.20E-20	1.000	270.0	3.20E-20	1.000
275.0	2.50E-20	1.000	280.0	2.00E-20	1.000	285.0	1.50E-20	1.000	290.0	1.13E-20	1.000	295.0	8.70E-21	1.000
300.0	6.60E-21	1.000	305.0	4.90E-21	1.000	310.0	3.70E-21	1.000	315.0	2.80E-21	1.000	320.0	2.00E-21	1.000
325.0	1.50E-21	1.000	330.0	1.20E-21	1.000	335.0	9.00E-22	1.000	340.0	7.00E-22	1.000	345.0	5.00E-22	1.000
350.0	3.00E-22	1.000	355.0	0.00E+00	1.000									

Table A-3. (continued)

WL (nm)	Abs (cm^2)	QY	WL (nm)	Abs (cm^2)	QY	WL (nm)	Abs (cm^2)	QY	WL (nm)	Abs (cm^2)	QY	WL (nm)	Abs (cm^2)	QY
Photolysis File = CO2H														
210.0	3.75E-19	1.000	220.0	2.20E-19	1.000	230.0	1.38E-19	1.000	240.0	8.80E-20	1.000	250.0	5.80E-20	1.000
260.0	3.80E-20	1.000	270.0	2.50E-20	1.000	280.0	1.50E-20	1.000	290.0	9.00E-21	1.000	300.0	5.80E-21	1.000
310.0	3.40E-21	1.000	320.0	1.90E-21	1.000	330.0	1.10E-21	1.000	340.0	6.00E-22	1.000	350.0	4.00E-22	1.000
360.0	0.00E+00	1.000												
Photolysis File = HCHONEWR														
280.0	2.49E-20	0.590	280.5	1.42E-20	0.596	281.0	1.51E-20	0.602	281.5	1.32E-20	0.608	282.0	9.73E-21	0.614
282.5	6.76E-21	0.620	283.0	5.82E-21	0.626	283.5	9.10E-21	0.632	284.0	3.71E-20	0.638	284.5	4.81E-20	0.644
285.0	3.95E-20	0.650	285.5	2.87E-20	0.656	286.0	2.24E-20	0.662	286.5	1.74E-20	0.668	287.0	1.13E-20	0.674
287.5	1.10E-20	0.680	288.0	2.62E-20	0.686	288.5	4.00E-20	0.692	289.0	3.55E-20	0.698	289.5	2.12E-20	0.704
290.0	1.07E-20	0.710	290.5	1.35E-20	0.713	291.0	1.99E-20	0.717	291.5	1.56E-20	0.721	292.0	8.65E-21	0.724
292.5	5.90E-21	0.727	293.0	1.11E-20	0.731	293.5	6.26E-20	0.735	294.0	7.40E-20	0.738	294.5	5.36E-20	0.741
295.0	4.17E-20	0.745	295.5	3.51E-20	0.749	296.0	2.70E-20	0.752	296.5	1.75E-20	0.755	297.0	1.16E-20	0.759
297.5	1.51E-20	0.763	298.0	3.69E-20	0.766	298.5	4.40E-20	0.769	299.0	3.44E-20	0.773	299.5	2.02E-20	0.776
300.0	1.06E-20	0.780	300.4	7.01E-21	0.780	300.6	8.63E-21	0.779	300.8	1.47E-20	0.779	301.0	2.01E-20	0.779
301.2	2.17E-20	0.779	301.4	1.96E-20	0.779	301.6	1.54E-20	0.778	301.8	1.26E-20	0.778	302.0	1.03E-20	0.778
302.2	8.53E-21	0.778	302.4	7.13E-21	0.778	302.6	6.61E-21	0.777	302.8	1.44E-20	0.777	303.0	3.18E-20	0.777
303.2	3.81E-20	0.777	303.4	5.57E-20	0.777	303.6	6.91E-20	0.776	303.8	6.58E-20	0.776	304.0	6.96E-20	0.776
304.2	5.79E-20	0.776	304.4	5.24E-20	0.776	304.6	4.30E-20	0.775	304.8	3.28E-20	0.775	305.0	3.60E-20	0.775
305.2	5.12E-20	0.775	305.4	4.77E-20	0.775	305.6	4.43E-20	0.774	305.8	4.60E-20	0.774	306.0	4.01E-20	0.774
306.2	3.28E-20	0.774	306.4	2.66E-20	0.774	306.6	2.42E-20	0.773	306.8	1.95E-20	0.773	307.0	1.58E-20	0.773
307.2	1.37E-20	0.773	307.4	1.19E-20	0.773	307.6	1.01E-20	0.772	307.8	9.01E-21	0.772	308.0	8.84E-21	0.772
308.2	2.08E-20	0.772	308.4	2.39E-20	0.772	308.6	3.08E-20	0.771	308.8	3.39E-20	0.771	309.0	3.18E-20	0.771
309.2	3.06E-20	0.771	309.4	2.84E-20	0.771	309.6	2.46E-20	0.770	309.8	1.95E-20	0.770	310.0	1.57E-20	0.770
310.2	1.26E-20	0.767	310.4	9.26E-21	0.764	310.6	7.71E-21	0.761	310.8	6.05E-21	0.758	311.0	5.13E-21	0.755
311.2	4.82E-21	0.752	311.4	4.54E-21	0.749	311.6	6.81E-21	0.746	311.8	1.04E-20	0.743	312.0	1.43E-20	0.740
312.2	1.47E-20	0.737	312.4	1.35E-20	0.734	312.6	1.13E-20	0.731	312.8	9.86E-21	0.728	313.0	7.82E-21	0.725
313.2	6.48E-21	0.722	313.4	1.07E-20	0.719	313.6	2.39E-20	0.716	313.8	3.80E-20	0.713	314.0	5.76E-20	0.710
314.2	6.14E-20	0.707	314.4	7.45E-20	0.704	314.6	5.78E-20	0.701	314.8	5.59E-20	0.698	315.0	4.91E-20	0.695
315.2	4.37E-20	0.692	315.4	3.92E-20	0.689	315.6	2.89E-20	0.686	315.8	2.82E-20	0.683	316.0	2.10E-20	0.680
316.2	1.66E-20	0.677	316.4	2.05E-20	0.674	316.6	4.38E-20	0.671	316.8	5.86E-20	0.668	317.0	6.28E-20	0.665
317.2	5.07E-20	0.662	317.4	4.33E-20	0.659	317.6	4.17E-20	0.656	317.8	3.11E-20	0.653	318.0	2.64E-20	0.650
318.2	2.24E-20	0.647	318.4	1.70E-20	0.644	318.6	1.24E-20	0.641	318.8	1.11E-20	0.638	319.0	7.70E-21	0.635
319.2	6.36E-21	0.632	319.4	5.36E-21	0.629	319.6	4.79E-21	0.626	319.8	6.48E-21	0.623	320.0	1.48E-20	0.620
320.2	1.47E-20	0.614	320.4	1.36E-20	0.608	320.6	1.69E-20	0.601	320.8	1.32E-20	0.595	321.0	1.49E-20	0.589
321.2	1.17E-20	0.583	321.4	1.15E-20	0.577	321.6	9.64E-21	0.570	321.8	7.26E-21	0.564	322.0	5.94E-21	0.558
322.2	4.13E-21	0.552	322.4	3.36E-21	0.546	322.6	2.39E-21	0.539	322.8	2.01E-21	0.533	323.0	1.76E-21	0.527
323.2	2.82E-21	0.521	323.4	4.65E-21	0.515	323.6	7.00E-21	0.508	323.8	7.80E-21	0.502	324.0	7.87E-21	0.496
324.2	6.59E-21	0.490	324.4	5.60E-21	0.484	324.6	4.66E-21	0.477	324.8	4.21E-21	0.471	325.0	7.77E-21	0.465
325.2	2.15E-20	0.459	325.4	3.75E-20	0.453	325.6	4.10E-20	0.446	325.8	6.47E-20	0.440	326.0	7.59E-20	0.434
326.2	6.51E-20	0.428	326.4	5.53E-20	0.422	326.6	5.76E-20	0.415	326.8	4.43E-20	0.409	327.0	3.44E-20	0.403
327.2	3.22E-20	0.397	327.4	2.13E-20	0.391	327.6	1.91E-20	0.384	327.8	1.42E-20	0.378	328.0	9.15E-21	0.372
328.2	6.79E-21	0.366	328.4	4.99E-21	0.360	328.6	4.77E-21	0.353	328.8	1.75E-20	0.347	329.0	3.27E-20	0.341
329.2	3.99E-20	0.335	329.4	5.13E-20	0.329	329.6	4.00E-20	0.322	329.8	3.61E-20	0.316	330.0	3.38E-20	0.310
330.2	3.08E-20	0.304	330.4	2.16E-20	0.298	330.6	2.09E-20	0.291	330.8	1.41E-20	0.285	331.0	9.95E-21	0.279
331.2	7.76E-21	0.273	331.4	6.16E-21	0.267	331.6	4.06E-21	0.260	331.8	3.03E-21	0.254	332.0	2.41E-21	0.248
332.2	1.74E-21	0.242	332.4	1.33E-21	0.236	332.6	2.70E-21	0.229	332.8	1.65E-21	0.223	333.0	1.17E-21	0.217
333.2	9.84E-22	0.211	333.4	8.52E-22	0.205	333.6	6.32E-22	0.198	333.8	5.21E-22	0.192	334.0	1.46E-21	0.186
334.2	1.80E-21	0.180	334.4	1.43E-21	0.174	334.6	1.03E-21	0.167	334.8	7.19E-22	0.161	335.0	4.84E-22	0.155
335.2	2.73E-22	0.149	335.4	1.34E-22	0.143	335.6	-1.62E-22	0.136	335.8	1.25E-22	0.130	336.0	4.47E-22	0.124
336.2	1.23E-21	0.118	336.4	2.02E-21	0.112	336.6	3.00E-21	0.105	336.8	2.40E-21	0.099	337.0	3.07E-21	0.093
337.2	2.29E-21	0.087	337.4	2.46E-21	0.081	337.6	2.92E-21	0.074	337.8	8.10E-21	0.068	338.0	1.82E-20	0.062
338.2	3.10E-20	0.056	338.4	3.24E-20	0.050	338.6	4.79E-20	0.043	338.8	5.25E-20	0.037	339.0	5.85E-20	0.031
339.2	4.33E-20	0.025	339.4	4.20E-20	0.019	339.6	3.99E-20	0.012	339.8	3.11E-20	0.006	340.0	2.72E-20	0.000
Photolysis File = HCHONEWM														
280.0	2.49E-20	0.350	280.5	1.42E-20	0.346	281.0	1.51E-20	0.341	281.5	1.32E-20	0.336	282.0	9.73E-21	0.332
282.5	6.76E-21	0.327	283.0	5.82E-21	0.323	283.5	9.10E-21	0.319	284.0	3.71E-20	0.314	284.5	4.81E-20	0.309
285.0	3.95E-20	0.305	285.5	2.87E-20	0.301	286.0	2.24E-20	0.296	286.5	1.74E-20	0.291	287.0	1.13E-20	0.287
287.5	1.10E-20	0.282	288.0	2.62E-20	0.278	288.5	4.00E-20	0.273	289.0	3.55E-20	0.269	289.5	2.12E-20	0.264
290.0	1.07E-20	0.260	290.5	1.35E-20	0.258	291.0	1.99E-20	0.256	291.5	1.56E-20	0.254	292.0	8.65E-21	0.252
292.5	5.90E-21	0.250	293.0	1.11E-20	0.248	293.5	6.26E-20	0.246	294.0	7.40E-20	0.244	294.5	5.36E-20	0.242
295.0	4.17E-20	0.240	295.5	3.51E-20	0.238	296.0	2.70E-20	0.236	296.5	1.75E-20	0.234	297.0	1.16E-20	0.232
297.5	1.51E-20	0.230	298.0	3.69E-20	0.228	298.5	4.40E-20	0.226	299.0	3.44E-20	0.224	299.5	2.02E-20	0.222
300.0	1.06E-20	0.220	300.4	7.01E-21	0.220	300.6	8.63E-21	0.221	300.8	1.47E-20	0.221	301.0	2.01E-20	0.221
301.2	2.17E-20	0.221	301.4	1.96E-20	0.221	301.6	1.54E-20	0.222	301.8	1.26E-20	0.222	302.0	1.03E-20	0.222
302.2	8.53E-21	0.222	302.4	7.13E-21	0.222	302.6	6.61E-21	0.223	302.8	1.44E-20	0.223	303.0	3.18E-20	0.223
303.2	3.81E-20	0.223	303.4	5.57E-20	0.223	303.6	6.91E-20	0.224	303.8	6.58E-20	0.224	304.0	6.96E-20	0.224
304.2	5.79E-20	0.224	304.4	5.24E-20	0.224	304.6	4.30E-20	0.225	304.8	3.28E-20	0.225	305.0	3.60E-20	0.225
305.2	5.12E-20	0.225	305.4	4.77E-20	0.225	305.6	4.43E-20	0.226	305.8	4.60E-20	0.226	306.0	4.01E-20	0.226
306.2	3.28E-20	0.226	306.4	2.66E-20	0.226	306.6	2.42E-20	0.227	306.8	1.95E-20	0.227	307.0	1.58E-20	0.227
307.2	1.37E-20	0.227	307.4	1.19E-20	0.227	307.6	1.01E-20	0.228	307.8	9.01E-21	0.228	308.0	8.84E-21	0.228
308.2	2.08E-20	0.228	308.4	2.39E-20	0.228	308.6	3.08E-20	0.229	308.8	3.39E-20	0.229	309.0	3.18E-20	0.229
309.2	3.06E-20	0.229	309.4	2.84E-20	0.229	309.6	2.46E-20	0.230	309.8	1.95E-20	0.230	310.0	1.57E-20	0.230
310.2	1.26E-20	0.233	310.4	9.26E-21	0.236	310.6	7.71E-21	0.239	310.8	6.05E-21	0.242	311.0	5.13E-21	0.245
311.2	4.82E-21	0.248	311.4	4.54E-21	0.251	311.6	6.81E-21	0.254	311.8	1.04E-20	0.257	312.0	1.43E-20	0.260
312.2	1.47E-20	0.263	312.4	1.35E-20	0.266	312.6	1.13E-20	0.269	312.8	9.86E-21	0.272	313.0	7.82E-21	0.275
313.2	6.48E-21	0.278	313.4	1.07E-20	0.281	313.6	2.39E-20	0.284	313.8	3.80E-20	0.287	314.0	5.76E-20	0.290
314.2	6.14E-20	0.293	314.4	7.45E-20	0.296	314.6	5.78E-20	0.299	314.8	5.59E-20	0.302	315.0	4.91E-20	0.305
315.2	4.37E-20	0.308	315.4	3.92E-20	0.311	315.6	2.89E-20	0.314	315.8	2.82E-20	0.317	316.0	2.10E-20	0.320
316.2	1.66E-20	0.323	316.4	2.05E-20	0.326	316.6	4.38E-20	0.329	316.8	5.86E-20	0.332	317.0	6.28E-20	0.335
317.2	5.07E-20	0.338	317.4	4.33E-20	0.341	317.6	4.17E-20	0.344	317.8	3.11E-20	0.347	318.0	2.64E-20	0.350
318.2	2.24E-20	0.353	318.4	1.70E-20	0.356	318.6	1.24E-20	0.359	318.8	1.11E-20	0.362	319.0	7.70E-21	0.365
319.2	6.36E-21	0.368	319.4	5.36E-21	0.371	319.6	4.79E-21	0.374	319.8	6.48E-21	0.377	320.0	1.48E-20	0.380
320.2	1.47E-20	0.386	320.4	1.36E-20	0.392	320.6	1.69E-20	0.399	320.8	1.32E-20	0.405	321.0	1.49E-20	0.411
321.2	1.17E-20	0.417	321.4	1.15E-20	0.423	321.6	9.64E-21	0.430	321.8	7.26E-21	0.436	322.0	5.94E-21	0.442

Table A-3. (continued)

WL (nm)	Abs (cm^2)	QY	WL (nm)	Abs (cm^2)	QY	WL (nm)	Abs (cm^2)	QY	WL (nm)	Abs (cm^2)	QY	WL (nm)	Abs (cm^2)	QY
322.2	4.13E-21	0.448	322.4	3.36E-21	0.454	322.6	2.39E-21	0.461	322.8	2.01E-21	0.467	323.0	1.76E-21	0.473
323.2	2.82E-21	0.479	323.4	4.65E-21	0.485	323.6	7.00E-21	0.492	323.8	7.80E-21	0.498	324.0	7.87E-21	0.504
324.2	6.59E-21	0.510	324.4	5.60E-21	0.516	324.6	4.66E-21	0.523	324.8	4.21E-21	0.529	325.0	7.77E-21	0.535
325.2	2.15E-20	0.541	325.4	3.75E-20	0.547	325.6	4.10E-20	0.554	325.8	6.47E-20	0.560	326.0	7.59E-20	0.566
326.2	6.51E-20	0.572	326.4	5.53E-20	0.578	326.6	5.76E-20	0.585	326.8	4.43E-20	0.591	327.0	3.44E-20	0.597
327.2	3.22E-20	0.603	327.4	2.13E-20	0.609	327.6	1.91E-20	0.616	327.8	1.42E-20	0.622	328.0	9.15E-21	0.628
328.2	6.79E-21	0.634	328.4	4.99E-21	0.640	328.6	4.77E-21	0.647	328.8	1.75E-20	0.653	329.0	3.27E-20	0.659
329.2	3.99E-20	0.665	329.4	5.13E-20	0.671	329.6	4.00E-20	0.678	329.8	3.61E-20	0.684	330.0	3.38E-20	0.690
330.2	3.08E-20	0.694	330.4	2.16E-20	0.699	330.6	2.09E-20	0.703	330.8	1.41E-20	0.708	331.0	9.95E-21	0.712
331.2	7.76E-21	0.717	331.4	6.16E-21	0.721	331.6	4.06E-21	0.726	331.8	3.03E-21	0.730	332.0	2.41E-21	0.735
332.2	1.74E-21	0.739	332.4	1.33E-21	0.744	332.6	2.70E-21	0.748	332.8	1.65E-21	0.753	333.0	1.17E-21	0.757
333.2	9.84E-22	0.762	333.4	8.52E-22	0.766	333.6	6.32E-22	0.771	333.8	5.21E-22	0.775	334.0	1.46E-21	0.780
334.2	1.80E-21	0.784	334.4	1.43E-21	0.789	334.6	1.03E-21	0.793	334.8	7.19E-22	0.798	335.0	4.84E-22	0.802
335.2	2.73E-22	0.798	335.4	1.34E-22	0.794	335.6	0.00E+00	0.790	335.8	1.25E-22	0.786	336.0	4.47E-22	0.782
336.2	1.23E-21	0.778	336.4	2.02E-21	0.773	336.6	3.00E-21	0.769	336.8	2.40E-21	0.764	337.0	3.07E-21	0.759
337.2	2.29E-21	0.754	337.4	2.46E-21	0.749	337.6	2.92E-21	0.745	337.8	8.10E-21	0.740	338.0	1.82E-20	0.734
338.2	3.10E-20	0.729	338.4	3.24E-20	0.724	338.6	4.79E-20	0.719	338.8	5.25E-20	0.714	339.0	5.85E-20	0.709
339.2	4.33E-20	0.703	339.4	4.20E-20	0.698	339.6	3.99E-20	0.693	339.8	3.11E-20	0.687	340.0	2.72E-20	0.682
340.2	1.99E-20	0.676	340.4	1.76E-20	0.671	340.6	1.39E-20	0.666	340.8	1.01E-20	0.660	341.0	6.57E-21	0.655
341.2	4.83E-21	0.649	341.4	3.47E-21	0.643	341.6	2.23E-21	0.638	341.8	1.55E-21	0.632	342.0	3.70E-21	0.627
342.2	4.64E-21	0.621	342.4	1.08E-20	0.616	342.6	1.14E-20	0.610	342.8	1.79E-20	0.604	343.0	2.33E-20	0.599
343.2	1.72E-20	0.593	343.4	1.55E-20	0.588	343.6	1.46E-20	0.582	343.8	1.38E-20	0.576	344.0	1.00E-20	0.571
344.2	8.26E-21	0.565	344.4	6.32E-21	0.559	344.6	4.28E-21	0.554	344.8	3.22E-21	0.548	345.0	2.54E-21	0.542
345.2	1.60E-21	0.537	345.4	1.15E-21	0.531	345.6	8.90E-22	0.525	345.8	6.50E-22	0.520	346.0	5.09E-22	0.514
346.2	5.15E-22	0.508	346.4	3.45E-22	0.503	346.6	3.18E-22	0.497	346.8	3.56E-22	0.491	347.0	3.24E-22	0.485
347.2	3.34E-22	0.480	347.4	2.88E-22	0.474	347.6	2.84E-22	0.468	347.8	9.37E-22	0.463	348.0	9.70E-22	0.457
348.2	7.60E-22	0.451	348.4	6.24E-22	0.446	348.6	4.99E-22	0.440	348.8	4.08E-22	0.434	349.0	3.39E-22	0.428
349.2	1.64E-22	0.423	349.4	1.49E-22	0.417	349.6	8.30E-23	0.411	349.8	2.52E-23	0.406	350.0	2.57E-23	0.400
350.2	0.00E+00	0.394	350.4	5.16E-23	0.389	350.6	0.00E+00	0.383	350.8	2.16E-23	0.377	351.0	7.07E-23	0.371
351.2	3.45E-23	0.366	351.4	1.97E-22	0.360	351.6	4.80E-22	0.354	351.8	3.13E-21	0.349	352.0	6.41E-21	0.343
352.2	8.38E-21	0.337	352.4	1.55E-20	0.331	352.6	1.86E-20	0.326	352.8	1.94E-20	0.320	353.0	2.78E-20	0.314
353.2	1.96E-20	0.309	353.4	1.67E-20	0.303	353.6	1.75E-20	0.297	353.8	1.63E-20	0.291	354.0	1.36E-20	0.286
354.2	1.07E-20	0.280	354.4	9.82E-21	0.274	354.6	8.66E-21	0.269	354.8	6.44E-21	0.263	355.0	4.84E-21	0.257
355.2	3.49E-21	0.251	355.4	2.41E-21	0.246	355.6	1.74E-21	0.240	355.8	1.11E-21	0.234	356.0	7.37E-22	0.229
356.2	4.17E-22	0.223	356.4	1.95E-22	0.217	356.6	1.50E-22	0.211	356.8	8.14E-23	0.206	357.0	0.00E+00	0.200
Photolysis File = CCHOR														
260.0	2.00E-20	0.310	270.0	3.40E-20	0.390	280.0	4.50E-20	0.580	290.0	4.90E-20	0.530	295.0	4.50E-20	0.480
300.0	4.30E-20	0.430	305.0	3.40E-20	0.370	315.0	2.10E-20	0.170	320.0	1.80E-20	0.100	325.0	1.10E-20	0.040
330.0	6.90E-21	0.000												
Photolysis File = RCHO														
280.0	5.26E-20	0.960	290.0	5.77E-20	0.910	300.0	5.05E-20	0.860	310.0	3.68E-20	0.600	320.0	1.66E-20	0.360
330.0	6.49E-21	0.200	340.0	1.44E-21	0.080	345.0	0.00E+00	0.020						
Photolysis File = ACET-93C														
250.0	2.37E-20	0.760	260.0	3.66E-20	0.800	270.0	4.63E-20	0.640	280.0	5.05E-20	0.550	290.0	4.21E-20	0.300
300.0	2.78E-20	0.150	310.0	1.44E-20	0.050	320.0	4.80E-21	0.026	330.0	8.00E-22	0.017	340.0	1.00E-22	0.000
350.0	3.00E-23	0.000	360.0	0.00E+00	0.000									
Photolysis File = KETONE														
210.0	1.10E-21	1.000	220.0	1.20E-21	1.000	230.0	4.60E-21	1.000	240.0	1.30E-20	1.000	250.0	2.68E-20	1.000
260.0	4.21E-20	1.000	270.0	5.54E-20	1.000	280.0	5.92E-20	1.000	290.0	5.16E-20	1.000	300.0	3.44E-20	1.000
310.0	1.53E-20	1.000	320.0	4.60E-21	1.000	330.0	1.10E-21	1.000	340.0	0.00E+00	1.000			
Photolysis File = GLYOXAL1 (used for aromatics and SAPRC-90 acetylene mechanisms)														
230.0	2.87E-21	1.000	235.0	2.87E-21	1.000	240.0	4.30E-21	1.000	245.0	5.73E-21	1.000	250.0	8.60E-21	1.000
255.0	1.15E-20	1.000	260.0	1.43E-20	1.000	265.0	1.86E-20	1.000	270.0	2.29E-20	1.000	275.0	2.58E-20	1.000
280.0	2.87E-20	1.000	285.0	3.30E-20	1.000	290.0	3.15E-20	1.000	295.0	3.30E-20	1.000	300.0	3.58E-20	1.000
305.0	2.72E-20	1.000	310.0	2.72E-20	1.000	312.5	2.87E-20	1.000	315.0	2.29E-20	1.000	320.0	1.43E-20	1.000
325.0	1.15E-20	1.000	327.5	1.43E-20	1.000	330.0	1.15E-20	1.000	335.0	2.87E-21	1.000	340.0	0.00E+00	1.000
Photolysis File = GLYOXAL2 (used for aromatics and SAPRC-90 acetylene mechanisms)														
355.0	0.00E+00	1.000	360.0	2.29E-21	1.000	365.0	2.87E-21	1.000	370.0	8.03E-21	1.000	375.0	1.00E-20	1.000
380.0	1.72E-20	1.000	382.0	1.58E-20	1.000	384.0	1.49E-20	1.000	386.0	1.49E-20	1.000	388.0	2.87E-20	1.000
390.0	3.15E-20	1.000	391.0	3.24E-20	1.000	392.0	3.04E-20	1.000	393.0	2.23E-20	1.000	394.0	2.63E-20	1.000
395.0	3.04E-20	1.000	396.0	2.63E-20	1.000	397.0	2.43E-20	1.000	398.0	3.24E-20	1.000	399.0	3.04E-20	1.000
400.0	2.84E-20	1.000	401.0	3.24E-20	1.000	402.0	4.46E-20	1.000	403.0	5.27E-20	1.000	404.0	4.26E-20	1.000
405.0	3.04E-20	1.000	406.0	3.04E-20	1.000	407.0	2.84E-20	1.000	408.0	2.43E-20	1.000	409.0	2.84E-20	1.000
410.0	6.08E-20	1.000	411.0	5.07E-20	1.000	411.5	6.08E-20	1.000	412.0	4.86E-20	1.000	413.0	8.31E-20	1.000
413.5	6.48E-20	1.000	414.0	7.50E-20	1.000	414.5	8.11E-20	1.000	415.0	8.11E-20	1.000	415.5	6.89E-20	1.000
416.0	4.26E-20	1.000	417.0	4.86E-20	1.000	418.0	5.88E-20	1.000	419.0	6.69E-20	1.000	420.0	3.85E-20	1.000
421.0	5.67E-20	1.000	421.5	4.46E-20	1.000	422.0	5.27E-20	1.000	422.5	1.05E-19	1.000	423.0	8.51E-20	1.000
424.0	6.08E-20	1.000	425.0	7.29E-20	1.000	426.0	1.18E-19	1.000	426.5	1.30E-19	1.000	427.0	1.07E-19	1.000
428.0	1.66E-19	1.000	429.0	4.05E-20	1.000	430.0	5.07E-20	1.000	431.0	4.86E-20	1.000	432.0	4.05E-20	1.000
433.0	3.65E-20	1.000	434.0	4.05E-20	1.000	434.5	6.08E-20	1.000	435.0	5.07E-20	1.000	436.0	8.11E-20	1.000
436.5	1.13E-19	1.000	437.0	5.27E-20	1.000	438.0	1.01E-19	1.000	438.5	1.38E-19	1.000	439.0	7.70E-20	1.000
440.0	2.47E-19	1.000	441.0	8.11E-20	1.000	442.0	6.08E-20	1.000	443.0	7.50E-20	1.000	444.0	9.32E-20	1.000
445.0	1.13E-19	1.000	446.0	5.27E-20	1.000	447.0	2.43E-20	1.000	448.0	2.84E-20	1.000	449.0	3.85E-20	1.000
450.0	6.08E-20	1.000	451.0	1.09E-19	1.000	451.5	9.32E-20	1.000	452.0	1.22E-19	1.000	453.0	2.39E-19	1.000
454.0	1.70E-19	1.000	455.0	3.40E-19	1.000	455.5	4.05E-19	1.000	456.0	1.01E-19	1.000	457.0	1.62E-20	1.000
458.0	1.22E-20	1.000	458.5	1.42E-20	1.000	459.0	4.05E-21	1.000	460.0	4.05E-21	1.000	460.5	6.08E-21	1.000
461.0	2.03E-21	1.000	462.0	0.00E+00	1.000									
Photolysis File = MEGLYOX1														
220.0	2.10E-21	1.000	225.0	2.10E-21	1.000	230.0	4.21E-21	1.000	235.0	7.57E-21	1.000	240.0	9.25E-21	1.000
245.0	8.41E-21	1.000	250.0	9.25E-21	1.000	255.0	9.25E-21	1.000	260.0	9.67E-21	1.000	265.0	1.05E-20	1.000

Table A-3. (continued)

WL (nm)	Abs (cm^2)	QY	WL (nm)	Abs (cm^2)	QY	WL (nm)	Abs (cm^2)	QY	WL (nm)	Abs (cm^2)	QY	WL (nm)	Abs (cm^2)	QY
270.0	1.26E-20	1.000	275.0	1.43E-20	1.000	280.0	1.51E-20	1.000	285.0	1.43E-20	1.000	290.0	1.47E-20	1.000
295.0	1.18E-20	1.000	300.0	1.14E-20	1.000	305.0	9.25E-21	1.000	310.0	6.31E-21	1.000	315.0	5.47E-21	1.000
320.0	3.36E-21	1.000	325.0	1.68E-21	1.000	330.0	8.41E-22	1.000	335.0	0.00E+00	1.000			
Photolysis File = MEGLYOX2														
350.0	0.00E+00	1.000	354.0	4.21E-22	1.000	358.0	1.26E-21	1.000	360.0	2.10E-21	1.000	362.0	2.10E-21	1.000
364.0	2.94E-21	1.000	366.0	3.36E-21	1.000	368.0	4.21E-21	1.000	370.0	5.47E-21	1.000	372.0	5.89E-21	1.000
374.0	7.57E-21	1.000	376.0	7.99E-21	1.000	378.0	8.83E-21	1.000	380.0	1.01E-20	1.000	382.0	1.09E-20	1.000
384.0	1.35E-20	1.000	386.0	1.51E-20	1.000	388.0	1.72E-20	1.000	390.0	2.06E-20	1.000	392.0	2.10E-20	1.000
394.0	2.31E-20	1.000	396.0	2.48E-20	1.000	398.0	2.61E-20	1.000	400.0	2.78E-20	1.000	402.0	2.99E-20	1.000
404.0	3.20E-20	1.000	406.0	3.79E-20	1.000	408.0	3.95E-20	1.000	410.0	4.33E-20	1.000	412.0	4.71E-20	1.000
414.0	4.79E-20	1.000	416.0	4.88E-20	1.000	418.0	5.05E-20	1.000	420.0	5.21E-20	1.000	422.0	5.30E-20	1.000
424.0	5.17E-20	1.000	426.0	5.30E-20	1.000	428.0	5.21E-20	1.000	430.0	5.55E-20	1.000	432.0	5.13E-20	1.000
434.0	5.68E-20	1.000	436.0	6.22E-20	1.000	438.0	6.06E-20	1.000	440.0	5.47E-20	1.000	441.0	6.14E-20	1.000
442.0	5.47E-20	1.000	443.0	5.55E-20	1.000	443.5	6.81E-20	1.000	444.0	5.97E-20	1.000	445.0	5.13E-20	1.000
446.0	4.88E-20	1.000	447.0	5.72E-20	1.000	448.0	5.47E-20	1.000	449.0	6.56E-20	1.000	450.0	5.05E-20	1.000
451.0	3.03E-20	1.000	452.0	4.29E-20	1.000	453.0	2.78E-20	1.000	454.0	2.27E-20	1.000	456.0	1.77E-20	1.000
458.0	8.41E-21	1.000	460.0	4.21E-21	1.000	464.0	1.68E-21	1.000	468.0	0.00E+00	1.000			
Photolysis File = BZCHO														
299.0	1.78E-19	1.000	304.0	7.40E-20	1.000	306.0	6.91E-20	1.000	309.0	6.41E-20	1.000	313.0	6.91E-20	1.000
314.0	6.91E-20	1.000	318.0	6.41E-20	1.000	325.0	8.39E-20	1.000	332.0	7.65E-20	1.000	338.0	8.88E-20	1.000
342.0	8.88E-20	1.000	346.0	7.89E-20	1.000	349.0	7.89E-20	1.000	354.0	9.13E-20	1.000	355.0	8.14E-20	1.000
364.0	5.67E-20	1.000	368.0	6.66E-20	1.000	369.0	8.39E-20	1.000	370.0	8.39E-20	1.000	372.0	3.45E-20	1.000
374.0	3.21E-20	1.000	376.0	2.47E-20	1.000	377.0	2.47E-20	1.000	380.0	3.58E-20	1.000	382.0	9.90E-21	1.000
386.0	0.00E+00	1.000												
Photolysis File = ACROLEIN														
250.0	1.80E-21	1.000	252.0	2.05E-21	1.000	253.0	2.20E-21	1.000	254.0	2.32E-21	1.000	255.0	2.45E-21	1.000
256.0	2.56E-21	1.000	257.0	2.65E-21	1.000	258.0	2.74E-21	1.000	259.0	2.83E-21	1.000	260.0	2.98E-21	1.000
261.0	3.24E-21	1.000	262.0	3.47E-21	1.000	263.0	3.58E-21	1.000	264.0	3.93E-21	1.000	265.0	4.67E-21	1.000
266.0	5.10E-21	1.000	267.0	5.38E-21	1.000	268.0	5.73E-21	1.000	269.0	6.13E-21	1.000	270.0	6.64E-21	1.000
271.0	7.20E-21	1.000	272.0	7.77E-21	1.000	273.0	8.37E-21	1.000	274.0	8.94E-21	1.000	275.0	9.55E-21	1.000
276.0	1.04E-20	1.000	277.0	1.12E-20	1.000	278.0	1.19E-20	1.000	279.0	1.27E-20	1.000	280.0	1.27E-20	1.000
281.0	1.26E-20	1.000	282.0	1.26E-20	1.000	283.0	1.28E-20	1.000	284.0	1.33E-20	1.000	285.0	1.38E-20	1.000
286.0	1.44E-20	1.000	287.0	1.50E-20	1.000	288.0	1.57E-20	1.000	289.0	1.63E-20	1.000	290.0	1.71E-20	1.000
291.0	1.78E-20	1.000	292.0	1.86E-20	1.000	293.0	1.95E-20	1.000	294.0	2.05E-20	1.000	295.0	2.15E-20	1.000
296.0	2.26E-20	1.000	297.0	2.37E-20	1.000	298.0	2.48E-20	1.000	299.0	2.60E-20	1.000	300.0	2.73E-20	1.000
301.0	2.85E-20	1.000	302.0	2.99E-20	1.000	303.0	3.13E-20	1.000	304.0	3.27E-20	1.000	305.0	3.39E-20	1.000
306.0	3.51E-20	1.000	307.0	3.63E-20	1.000	308.0	3.77E-20	1.000	309.0	3.91E-20	1.000	310.0	4.07E-20	1.000
311.0	4.25E-20	1.000	312.0	4.39E-20	1.000	313.0	4.44E-20	1.000	314.0	4.50E-20	1.000	315.0	4.59E-20	1.000
316.0	4.75E-20	1.000	317.0	4.90E-20	1.000	318.0	5.05E-20	1.000	319.0	5.19E-20	1.000	320.0	5.31E-20	1.000
321.0	5.43E-20	1.000	322.0	5.52E-20	1.000	323.0	5.60E-20	1.000	324.0	5.67E-20	1.000	325.0	5.67E-20	1.000
326.0	5.62E-20	1.000	327.0	5.63E-20	1.000	328.0	5.71E-20	1.000	329.0	5.76E-20	1.000	330.0	5.80E-20	1.000
331.0	5.95E-20	1.000	332.0	6.23E-20	1.000	333.0	6.39E-20	1.000	334.0	6.38E-20	1.000	335.0	6.24E-20	1.000
336.0	6.01E-20	1.000	337.0	5.79E-20	1.000	338.0	5.63E-20	1.000	339.0	5.56E-20	1.000	340.0	5.52E-20	1.000
341.0	5.54E-20	1.000	342.0	5.53E-20	1.000	343.0	5.47E-20	1.000	344.0	5.41E-20	1.000	345.0	5.40E-20	1.000
346.0	5.48E-20	1.000	347.0	5.90E-20	1.000	348.0	6.08E-20	1.000	349.0	6.00E-20	1.000	350.0	5.53E-20	1.000
351.0	5.03E-20	1.000	352.0	4.50E-20	1.000	353.0	4.03E-20	1.000	354.0	3.75E-20	1.000	355.0	3.55E-20	1.000
356.0	3.45E-20	1.000	357.0	3.46E-20	1.000	358.0	3.49E-20	1.000	359.0	3.41E-20	1.000	360.0	3.23E-20	1.000
361.0	2.95E-20	1.000	362.0	2.81E-20	1.000	363.0	2.91E-20	1.000	364.0	3.25E-20	1.000	365.0	3.54E-20	1.000
366.0	3.30E-20	1.000	367.0	2.78E-20	1.000	368.0	2.15E-20	1.000	369.0	1.59E-20	1.000	370.0	1.19E-20	1.000
371.0	8.99E-21	1.000	372.0	7.22E-21	1.000	373.0	5.86E-21	1.000	374.0	4.69E-21	1.000	375.0	3.72E-21	1.000
376.0	3.57E-21	1.000	377.0	3.55E-21	1.000	378.0	2.83E-21	1.000	379.0	1.69E-21	1.000	380.0	8.29E-24	1.000
381.0	0.00E+00	1.000												
Photolysis File = GLYR-A [a]														
230.0	2.87E-21	0.400	235.0	2.87E-21	0.400	240.0	4.30E-21	0.400	245.0	5.73E-21	0.400	250.0	8.60E-21	0.400
255.0	1.15E-20	0.400	260.0	1.43E-20	0.400	265.0	1.86E-20	0.400	270.0	2.29E-20	0.400	275.0	2.58E-20	0.400
280.0	2.87E-20	0.400	285.0	3.30E-20	0.400	290.0	3.15E-20	0.400	295.0	3.30E-20	0.400	300.0	3.58E-20	0.400
305.0	2.72E-20	0.400	310.0	2.72E-20	0.400	312.5	2.87E-20	0.400	315.0	2.29E-20	0.400	320.0	1.43E-20	0.400
325.0	1.15E-20	0.400	327.5	1.43E-20	0.400	330.0	1.15E-20	0.400	335.0	2.87E-21	0.400	340.0	0.00E+00	0.400
345.0	0.00E+00	0.400	350.0	0.00E+00	0.400	355.0	0.00E+00	0.392	360.0	2.29E-21	0.360	365.0	2.87E-21	0.328
370.0	8.03E-21	0.297	375.0	1.00E-20	0.265	380.0	1.72E-20	0.234	382.0	1.58E-20	0.221	384.0	1.49E-20	0.208
386.0	1.49E-20	0.196	388.0	2.87E-20	0.183	390.0	3.15E-20	0.171	391.0	3.24E-20	0.164	392.0	3.04E-20	0.158
393.0	2.23E-20	0.152	394.0	2.63E-20	0.145	395.0	3.04E-20	0.139	396.0	2.63E-20	0.133	397.0	2.43E-20	0.126
398.0	3.24E-20	0.120	399.0	3.04E-20	0.114	400.0	2.84E-20	0.107	401.0	3.24E-20	0.101	402.0	4.46E-20	0.095
403.0	5.27E-20	0.088	404.0	4.26E-20	0.082	405.0	3.04E-20	0.076	406.0	3.04E-20	0.069	407.0	2.84E-20	0.063
408.0	2.43E-20	0.057	409.0	2.84E-20	0.051	410.0	6.08E-20	0.044	411.0	5.07E-20	0.038	411.5	6.08E-20	0.035
412.0	4.86E-20	0.032	413.0	8.31E-20	0.025	413.5	6.48E-20	0.022	414.0	7.50E-20	0.019	414.5	8.11E-20	0.016
415.0	8.11E-20	0.013	415.5	6.89E-20	0.009	416.0	4.26E-20	0.006	417.0	4.86E-20	0.000			
Photolysis File = GLYR-B [b]														
230.0	2.87E-21	0.400	235.0	2.87E-21	0.400	240.0	4.30E-21	0.400	245.0	5.73E-21	0.400	250.0	8.60E-21	0.400
255.0	1.15E-20	0.400	260.0	1.43E-20	0.400	265.0	1.86E-20	0.400	270.0	2.29E-20	0.400	275.0	2.58E-20	0.400
280.0	2.87E-20	0.400	285.0	3.30E-20	0.400	290.0	3.15E-20	0.400	295.0	3.30E-20	0.400	300.0	3.58E-20	0.400
305.0	2.72E-20	0.400	310.0	2.72E-20	0.400	312.5	2.87E-20	0.400	315.0	2.29E-20	0.400	320.0	1.43E-20	0.400
325.0	1.15E-20	0.400	327.5	1.43E-20	0.400	330.0	1.15E-20	0.400	335.0	2.87E-21	0.400	340.0	0.00E+00	0.400
345.0	0.00E+00	0.400	350.0	0.00E+00	0.400	355.0	0.00E+00	0.400	360.0	2.29E-21	0.400	365.0	2.87E-21	0.400
370.0	8.03E-21	0.400	375.0	1.00E-20	0.400	380.0	1.72E-20	0.400	382.0	1.58E-20	0.400	384.0	1.49E-20	0.400
386.0	1.49E-20	0.386	388.0	2.87E-20	0.361	390.0	3.15E-20	0.336	391.0	3.24E-20	0.324	392.0	3.04E-20	0.311
393.0	2.23E-20	0.299	394.0	2.63E-20	0.286	395.0	3.04E-20	0.274	396.0	2.63E-20	0.261	397.0	2.43E-20	0.249
398.0	3.24E-20	0.236	399.0	3.04E-20	0.224	400.0	2.84E-20	0.212	401.0	3.24E-20	0.199	402.0	4.46E-20	0.187
403.0	5.27E-20	0.174	404.0	4.26E-20	0.162	405.0	3.04E-20	0.149	406.0	3.04E-20	0.137	407.0	2.84E-20	0.124
408.0	2.43E-20	0.112	409.0	2.84E-20	0.100	410.0	6.08E-20	0.087	411.0	5.07E-20	0.075	411.5	6.08E-20	0.068

Table A-3. (continued)

WL (nm)	Abs (cm^2)	QY	WL (nm)	Abs (cm^2)	QY	WL (nm)	Abs (cm^2)	QY	WL (nm)	Abs (cm^2)	QY	WL (nm)	Abs (cm^2)	QY
412.0	4.86E-20	0.062	413.0	8.31E-20	0.050	413.5	6.48E-20	0.044	414.0	7.50E-20	0.037	414.5	8.11E-20	0.031
415.0	8.11E-20	0.025	415.5	6.89E-20	0.019	416.0	4.26E-20	0.012	417.0	4.86E-20	0.000	418.0	5.88E-20	0.000
Photolysis File = GLYR-C [c]														
230.0	2.87E-21	0.400	235.0	2.87E-21	0.400	240.0	4.30E-21	0.400	245.0	5.73E-21	0.400	250.0	8.60E-21	0.400
255.0	1.15E-20	0.400	260.0	1.43E-20	0.400	265.0	1.86E-20	0.400	270.0	2.29E-20	0.400	275.0	2.58E-20	0.400
280.0	2.87E-20	0.400	285.0	3.30E-20	0.400	290.0	3.15E-20	0.400	295.0	3.30E-20	0.400	300.0	3.58E-20	0.400
305.0	2.72E-20	0.400	310.0	2.72E-20	0.400	312.5	2.87E-20	0.400	315.0	2.29E-20	0.400	320.0	1.43E-20	0.400
325.0	1.15E-20	0.400	327.5	1.43E-20	0.400	330.0	1.15E-20	0.400	335.0	2.87E-21	0.400	340.0	0.00E+00	0.400
345.0	0.00E+00	0.400	350.0	0.00E+00	0.400	355.0	0.00E+00	0.400	360.0	2.29E-21	0.400	365.0	2.87E-21	0.400
370.0	8.03E-21	0.400	375.0	1.00E-20	0.400	380.0	1.72E-20	0.400	382.0	1.58E-20	0.381	384.0	1.49E-20	0.359
386.0	1.49E-20	0.337	388.0	2.87E-20	0.316	390.0	3.15E-20	0.294	391.0	3.24E-20	0.283	392.0	3.04E-20	0.272
393.0	2.23E-20	0.261	394.0	2.63E-20	0.250	395.0	3.04E-20	0.239	396.0	2.63E-20	0.229	397.0	2.43E-20	0.218
398.0	3.24E-20	0.207	399.0	3.04E-20	0.196	400.0	2.84E-20	0.185	401.0	3.24E-20	0.174	402.0	4.46E-20	0.163
403.0	5.27E-20	0.152	404.0	4.26E-20	0.141	405.0	3.04E-20	0.131	406.0	3.04E-20	0.120	407.0	2.84E-20	0.109
408.0	2.43E-20	0.098	409.0	2.84E-20	0.087	410.0	6.08E-20	0.076	411.0	5.07E-20	0.065	411.5	6.08E-20	0.060
412.0	4.86E-20	0.054	413.0	8.31E-20	0.044	413.5	6.48E-20	0.038	414.0	7.50E-20	0.033	414.5	8.11E-20	0.027
415.0	8.11E-20	0.022	415.5	6.89E-20	0.016	416.0	4.26E-20	0.011	417.0	4.86E-20	0.000	418.0	5.88E-20	0.000
Photolysis File = GLYM [d]														
230.0	2.87E-21	0.450	235.0	2.87E-21	0.450	240.0	4.30E-21	0.450	245.0	5.73E-21	0.450	250.0	8.60E-21	0.450
255.0	1.15E-20	0.450	260.0	1.43E-20	0.450	265.0	1.86E-20	0.450	270.0	2.29E-20	0.450	275.0	2.58E-20	0.450
280.0	2.87E-20	0.450	285.0	3.30E-20	0.450	290.0	3.15E-20	0.450	295.0	3.30E-20	0.450	300.0	3.58E-20	0.450
305.0	2.72E-20	0.450	310.0	2.72E-20	0.450	312.5	2.87E-20	0.450	315.0	2.29E-20	0.450	320.0	1.43E-20	0.450
325.0	1.15E-20	0.450	327.5	1.43E-20	0.450	330.0	1.15E-20	0.450	335.0	2.87E-21	0.450	340.0	0.00E+00	0.450
355.0	0.00E+00	0.304	360.0	2.29E-21	0.255	365.0	2.87E-21	0.206	370.0	8.03E-21	0.157	375.0	1.00E-20	0.108
380.0	1.72E-20	0.059	382.0	1.58E-20	0.040	384.0	1.49E-20	0.020	386.0	1.49E-20	0.001	388.0	2.87E-20	0.000

[a] Adjusted so that radical quantum yield is equal to upper limit value which is consistent with data of Plum et al. (1983). λ_1^{gly} = 356 nm.
[b] Adjusted so that radical quantum yield gave best fit to the acetylene - NO_x and acetylene reactivity chamber data using acetylene model B. λ_1^{gly} = 385 nm.
[c] Adjusted so that radical quantum yield gave best fit to the acetylene - NO_x and acetylene reactivity chamber data using acetylene model C. λ_1^{gly} = 300 nm.
[d] The quantum yield assumed for the lower wavlength band is based on Langford and Moore (1984). Quantum yields in the longer wavelength band are assumed to decline linearly, with the wavelength where they become zero being adjusted to be consistent with the overall formaldehyde yield reported by Plum et al. (1983).

Table A-4. Values of chamber-dependent parameters used in the model simulations of the environmental chamber experiments for this study.

Parm.	Value(s)	Discussion
k(O3W)	8.5×10^{-4} min^{-1}	k(O3W) is rate constant for unimolecular wall loss of O_3. The value used runs is based on the results of runs CTC053 and CTC106, which are reasonably consistent with each other.
k(N25I) k(N25S)	2.8×10^{-3} min^{-1}, 1.5×10^{-6} - k_g ppm^{-1} min^{-1}	k(N25I) is unimolecular decay of N_2O_5 to the walls. K(N25S) is the rate constant for bimolecular reaction with H_2O, forming 2 HNO3. The value used is based on the N_2O_5 decay rate measurements in a similar chamber reported by Tuazon et al. (1983). The same rate constants are used for all Teflon bag chambers (Carter et al., 1995b).
k(NO2W) yHONO	1.6×10^{-4} min^{-1} 0.2	k(NO2W) is the rate constant for a unimolecular decay of NO_2 to the walls, forming HONO with a yield of yHOHO. The values used are based on dark NO_2 decay and HONO formation measured in a similar chamber by Pitts et al. (1984). This is assumed to be the same in all Teflon bag chambers (Carter et al. 1995b).
k(XSHC)	250 min^{-1}	k(XSHC) is the rate constant for a unimolecular conversion of HO to HO_2, which is used to represent the effect of background VOC reactants. It is estimated by modeling pure air irradiations carried out in this reactor. This is an important parameter affecting model predictions except for pure air or NO_x-air runs.
RS/K1	0.07 ppb	The continuous chamber radical source is represented as a light-dependent flux of OH radicals, whose rate is given by the NO_2 photolysis rate (k_1) multiplied by the parameter RS/K1. This parameter is derived from model simulations of n-butane - NO_x and CO - NO_x experiments as discussed by Carter et al. (1995b,c). The values used are based on averages which fit the n-butane - NO_x experiments as discussed by Carter et al. (1997).
E-NO2/K1	0.04 ppb	The rate of NO_2 offgasing from the chamber walls is obtained by multiplying the parameter E-NO2/K1 by the NO_2 photolysis rate. Model simulations of acetaldehyde - air runs are used to derive this parameter. For the CTC, the value used is based on the results of CTC019.
HONO-F	0.0	HONO-F is the fraction of initially present NO_2 which is assumed to be converted to HONO prior to the start of the run. When the light-induced radical source is represented by a continuous OH flux, best fits to most n-butane - NO_x experiments are obtained if this is assumed to be negligible.